1-1-1992

The determination of stresses and material properties of polyimide coatings and films using real time holographic interferometry/

Michele A. Maden

University of Massachusetts Amherst

THE DETERMINATION OF STRESSES AND MATERIAL PROPERTIES OF

POLYIMIDE COATINGS AND FILMS USING REAL TIME HOLOGRAPHIC

INTERFEROMETRY

A Dissertation Presented

by

MICHELE A. MADEN

Submitted to the Graduate School of the
University of Massachusetts in partial fulfillment
of the requirements for the degree of

DOCTOR OF PHILOSOPHY

May 1992

Department of Polymer Science and Engineering

THE DETERMINATION OF STRESSES AND MATERIAL PROPERTIES OF

POLYIMIDE COATINGS AND FILMS USING REAL TIME HOLOGRAPHIC

INTERFEROMETRY

A Dissertation Presented

by

MICHELE A. MADEN

Approved as to style and content by:

_____
Richard J. Farris, Chair

_____
Marion Rhodes, Member

_____
David Hoagland, Member

_____
William J. MacKnight, Department Head
Polymer Science and Engineering Department

"It would be an unsound fancy ... to expect that things which have never yet been done can be done except by means which have never yet been tried." - Francis Bacon; *The New Organon (Aphorisms: Book I (VI))*

To my parents, for giving me the opportunity to do the "things which have never yet been done".

ACKNOWLEDGEMENTS

ABSTRACT

THE DETERMINATION OF STRESSES AND MATERIAL PROPERTIES OF POLYIMIDE COATINGS AND FILMS USING REAL-TIME HOLOGRAPHIC INTERFEROMETRY
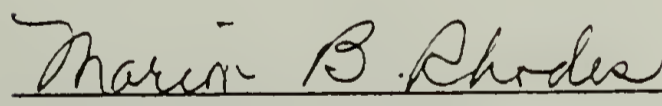
MAY 1992

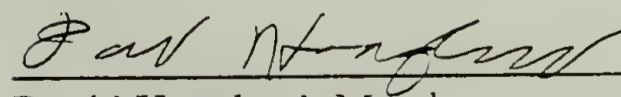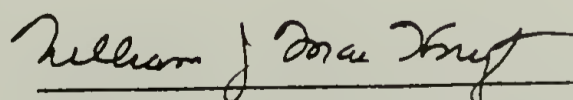MICHELE A. MADEN, Sc.B., BROWN UNIVERSITY

Ph.D., UNIVERSITY OF MASSACHUSETTS

Directed by: Professor Richard J. Farris

This dissertation presents a new technique for determining the residual stresses and material properties of polyimide coatings. The primary materials studied are polyimides, pyromellitic dianhydride - oxydianiline (PMDA-ODA) and poly[N,N'(phenylene)-3,3'4,4'-biphenyl tetracarboxylic diimide] (BPDA-PDA). The determination of the internal stresses which develop during processing in these coatings is critical for reliability prediction and material selection for the microelectronics industry.

For any given coating on a rigid substrate, the shear and normal tractions between the two materials goes to zero away from the edges. A portion of the substrate can therefore be removed leaving a simply supported membrane (coating) with its original state of stress intact. Classical vibration theory states that the square of the resonant frequency of a membrane is proportional to its biaxial stress. Real-time holographic interferometry is used to identify the resonant modes of vibration. It is also shown that using this technique the orthotropic axes of polymer films can be identified, thus simplifying the determination of all nine orthotropic elasticity coefficients.

TABLE OF CONTENTS

LIST OF TABLES

LIST OF FIGURES

CHAPTER 1

INTRODUCTION

1.1   Stresses in Coatings

The primary objective of the work described in this thesis is to develop a new technique for measuring the biaxial stresses in coatings. Such a technique should require little knowledge of material properties and none of the linear elastic assumptions required for existing stress measurement methods. The measurement of stresses in coatings is a topic of great interest to those responsible for the production of microelectronic components, paints, and any other type of coating. This chapter gives an overview of the importance of quantifying stresses in coatings, discusses the materials and systems studied in this work, and introduces the content of the thesis.

1.1.1   Mechanisms

Coatings are used in many different applications. They are used as passivation layers, to prevent corrosion of a substrate, as insulating layers between the metallization on integrated circuits, as decorative finishes, and as sealants for wood or tiles. In all cases a coating must be continuous to function effectively. One of the most undesirable problems that a coating can exhibit is a tendency to crack and/or peel. Cracking and peeling are directly related to the state of stress in the coating which is a consequence of a combination of the material properties of the coating and the processing conditions to which it has been subjected. The primary system of interest in this thesis is that in which a polyimide coating is spin coated onto a substrate, cured at some elevated temperature (200 - 400 °C) and upon cooling to room temperature, is under a tensile stress. It is this

state of stress which causes cracking and delamination of coatings, although coatings under compressive stresses can also buckle and delaminate from the substrate under certain conditions [1, 2].

There are three primary mechanisms that lead to the development of stress in coatings. The most commonly discussed is the mismatch in coefficient of thermal expansion (CTE), $\Delta\alpha$, between the substrate and coating which may subject the coating to either a tensile or a compressive stress. If the CTE of the substrate is greater than that of the coating, upon cooling from above the coatings glass transition temperature, the coating will be placed under a compressive stress because the substrate wants to shrink more than the coating. If on the other hand, the CTE of the coating is greater than that of the substrate, the coating would be in tension with respect to the substrate which constrains the coating from shrinking. This behavior is illustrated in Figure 1.1. Another factor which causes stress build-up in polymer films is the volume change of the film upon curing or solvent loss. The coating is constrained by the substrate in the lateral direction, therefore the volume change will occur predominantly in the out of plane direction. Any tendency towards shrinkage in the in-plane direction causes tensile stresses in the plane of the coating because it is constrained by the rigid substrate. A state of tensile stress is the most common case for a polymer coating applied to a rigid substrate such as a metal or a ceramic. The exception would be if there were a high degree of swelling in the coating after complete solidification. The third factor which could cause biaxial stress changes in coatings is the rearrangement or relaxation of molecules over time, or aging. These effects have been discussed in detail by other authors [3, 4, 5, 6, 7, 8, 9, 10, 11]. There have also been several excellent papers written on the theoretical analysis of stresses in bilayer and multilayer coating systems [12, 13, 14]. These will not be discussed in detail in this thesis, but are useful for understanding these mechanisms.
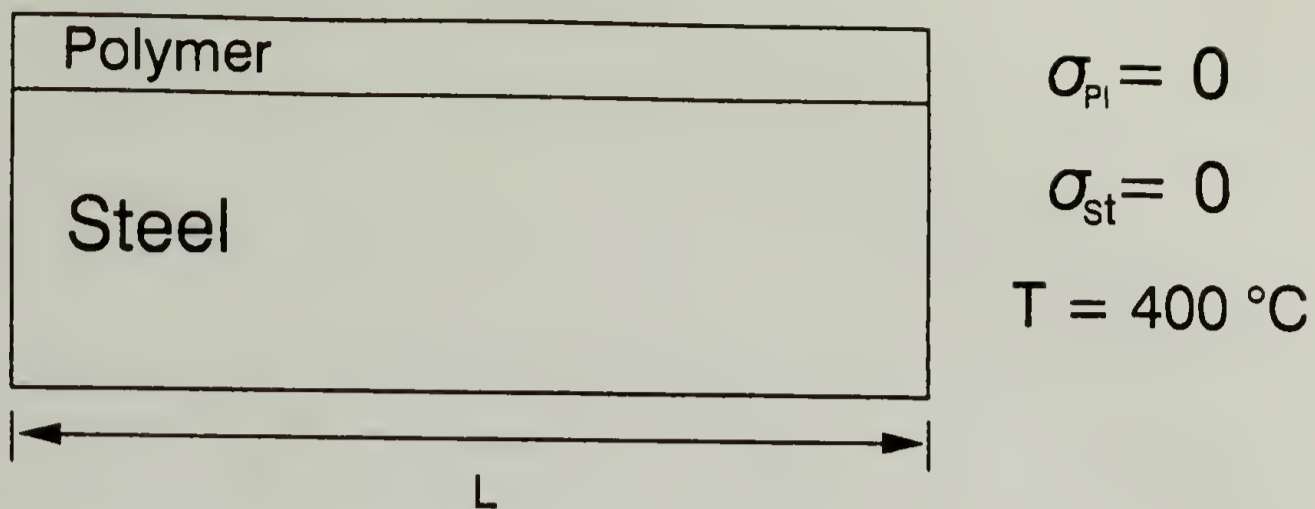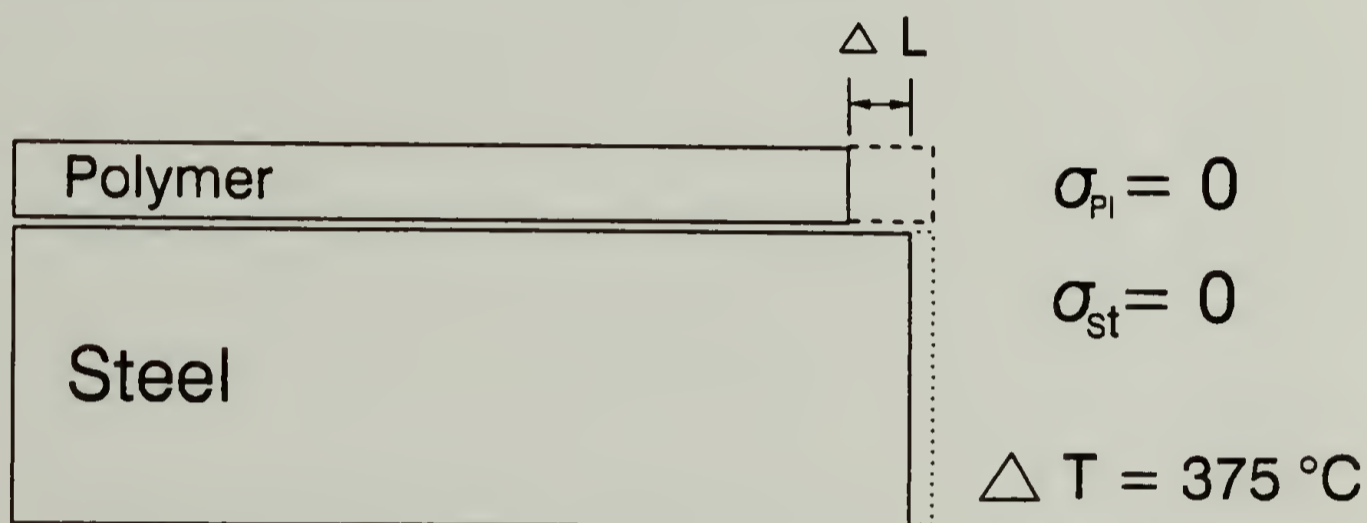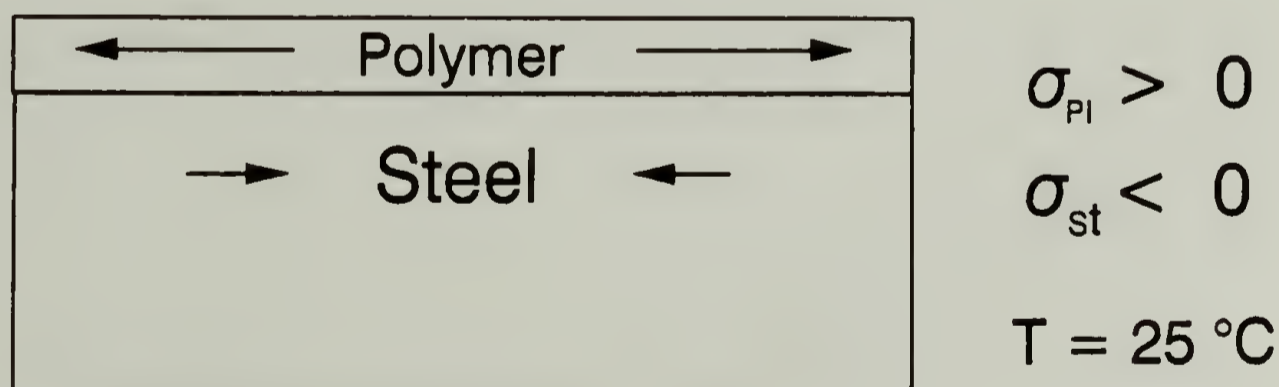
Figure 1.1   Schematic of how the build-up of thermally induced stresses occurs in systems with large mismatch in coefficients of thermal expansion. For the systems studied in this work, the curing temperatures may be as high as 400 °C, causing tensile stresses in the plane of the polymer film (which has a higher coefficient of thermal expansion than the steel or silicon substrate).

1.1.2 Coating Failure

When a coating fails, the failure will most likely occur as cracking, delamination or buckling. The first of these failures is generally attributed to tensile stresses in the plane of the coating which exceed the ultimate tensile strength of the material. Delamination occurs when the elastic energy stored in the coating is greater than the energy of adhesion. This is often the case for thicker coatings since the elastic energy is proportional to the thickness of the coating and the square of its biaxial stress. [7, 8, 9, 15, 16]. The last form of failure which may occur is delamination by buckling in coatings under compressive stresses. Such buckling is commonly observed in coatings which are heated locally or in coatings which develop compressive stresses upon exposure to higher temperatures and/or humidity [1, 2].

1.1.3 Measurement Techniques

This section will describe the main classes of stress measurement techniques and discuss the advantages, disadvantages and variations of each. Several older review articles give good summaries of these methods [17, 18], and new methods will be outlined in this introduction. The measurement techniques currently used for determining the stress in a coating can be divided into three main categories, 1.) those which measure the radius of curvature induced in a substrate due to the stress in the coating; 2.) those which measure the displacement in a coating or coating/substrate system due to an applied force, and 3.) those which measure the vibrational response of a coating or coating/substrate system. The technique developed in this thesis falls into the latter category, and will be discussed in great detail in the chapter to follow. Here, I will briefly highlight the salient features of other methods.

The substrate bending stress measurements, involve the determination of the radius of curvature of a substrate before and after deposition of a coating. The curvature induced in the substrate is related to the stress in the coating according to the general relation first proposed by Timoshenko [12],

$$\sigma \sim \frac{E\,h_s^3}{\rho(1-\nu)\,h_c} \tag{1.1}$$

where E and ν are the Young's modulus and Poisson's ratio of the substrate, h_s and h_c are the thicknesses of the substrate and the coating respectively, and ρ is the curvature of the substrate due to the stress in the coating.

Variations in substrate bending methods most often occur in the geometry of the sample (either cantilever beam or wafer type substrates) or in the method used to measure the curvature. The curvature is measured using various interferometry techniques, detection of movement by optical fibers which send and receive a beam of reflected light from the sample [19, 20], electromagnetic methods which detect the movement of a cantilever between two electrodes, mechanical displacement measurements [5, 6, 7, 9, 21], or X-ray methods [11]. The advantages of this type of technique are that the Young's modulus of the coating does not in general need to be known to calculate the stress, provided the substrate is thick and rigid compared to the coating. Disadvantages of the wafer curvature method are that the coating and substrate thicknesses, and the substrate Young's modulus and Poisson's ratio must be known. Because typical radii of curvature are on the order of 400 m, highly sensitive equipment is usually required for such measurements. This analysis also assumes uniform curvature of the substrate which may not always be accurate, especially in cases of non-uniform biaxial stresses.

The methods which rely on the response of a coating or coating/substrate system to an applied load, vary primarily in the method of applying and detecting the load and material response. A method developed by Allen and Senturia [22, 23, 24] uses air pressure on one side of a sealed membrane (a coating with a portion of the substrate removed) and measures the maximum deflection of the membrane on a microscope stage. The displacement is measured by adjusting the microscope stage so that the highest point on the membrane stays in focus. The stress is related to the applied pressure using the equation,

$$p = \frac{4hd}{a^2}\left[\sigma_o + \frac{2K}{3}\frac{d^2}{a^2}\right] \tag{1.2}$$

where a, h and d are the radius, thickness and displacement of the membrane, p is the applied pressure, σ_o is the residual stress in the coating, and K is the biaxial modulus, $E/(1 - v)$. A similar method has also been developed recently in which the response of a polymeric coating to a small probe deflecting the center of the sample is measured, [25]. Techniques where the stress in the coating is determined by deforming the entire substrate/coating system have also been reported [3, 17, 26]. The deformation techniques have an advantage in that the material properties such as Young's modulus and Poisson's ratio can be determined. However, excepting work done by Gruninger, et al. [21], the methods are not generally sensitive to non-uniform biaxial stresses and require knowledge of the thicknesses of the coating, substrate and the material properties of the substrate. The only material parameter required for the holographic vibrational technique described in this dissertation is the density of the coating.

Rayleigh first proposed in 1866 that the stress (or tension) in a vibrating membrane is directly proportional to the square of its natural frequency [27]. Most vibration methods used in the past to measure the stress in fibers or in membranes have

used only the first resonant mode of vibration or the natural frequency to calculate the stress [28, 29]. Others have used methods which allowed them to measure the circularly symmetric modes of vibrations and resonant frequencies [30, 31]. A string or a membrane held at the ends or around the circumference will resonate at specific frequencies in response to a forced vibration of steadily increasing frequency. The above methods use various tools for the excitation and detection of resonant frequencies which include: a speaker driven at increasing sinusoidal frequencies placed behind a membrane to cause it to resonate at its resonant frequencies; passing current through electrodes placed at the center of a membrane for both excitation and detection of the circularly symmetric modes of vibration [30]; mechanical vibration with a piezoelectric transducer and detection of out of plane motion using a photonics detector [32]; and passing current through whiskers and measuring the frequency at which the amplitude of the vibrational response of the fiber is at a maximum [28].

The stress measurement method developed in this thesis combines the membrane vibration theory first proposed by Rayleigh and the more modern method of real time holographic interferometry. The coatings used for these studies are spin-coated onto a substrate and then cured, developing in-plane residual stresses. Membranes can be made from these coatings without changing their state of stress by removing a portion of the substrate or by mounting a washer to the top of the coating and removing the entire substrate. For a coating/substrate system in which the substrate is sufficiently thicker and stiffer (high Young's modulus) than the coating, there are no shear or normal tractions between the coating and the substrate beyond a few film thicknesses from the edge of the film. This is shown schematically in Figure 1.2. Therefore, a constrained coating does not "feel" the removal of a portion of the substrate, and the original state of stress is preserved. This analysis has been discussed by several authors, and finite element

analyses performed to support the theory [33, 33]. A more detailed discussion in light of sample preparation techniques will be given in chapter 2.
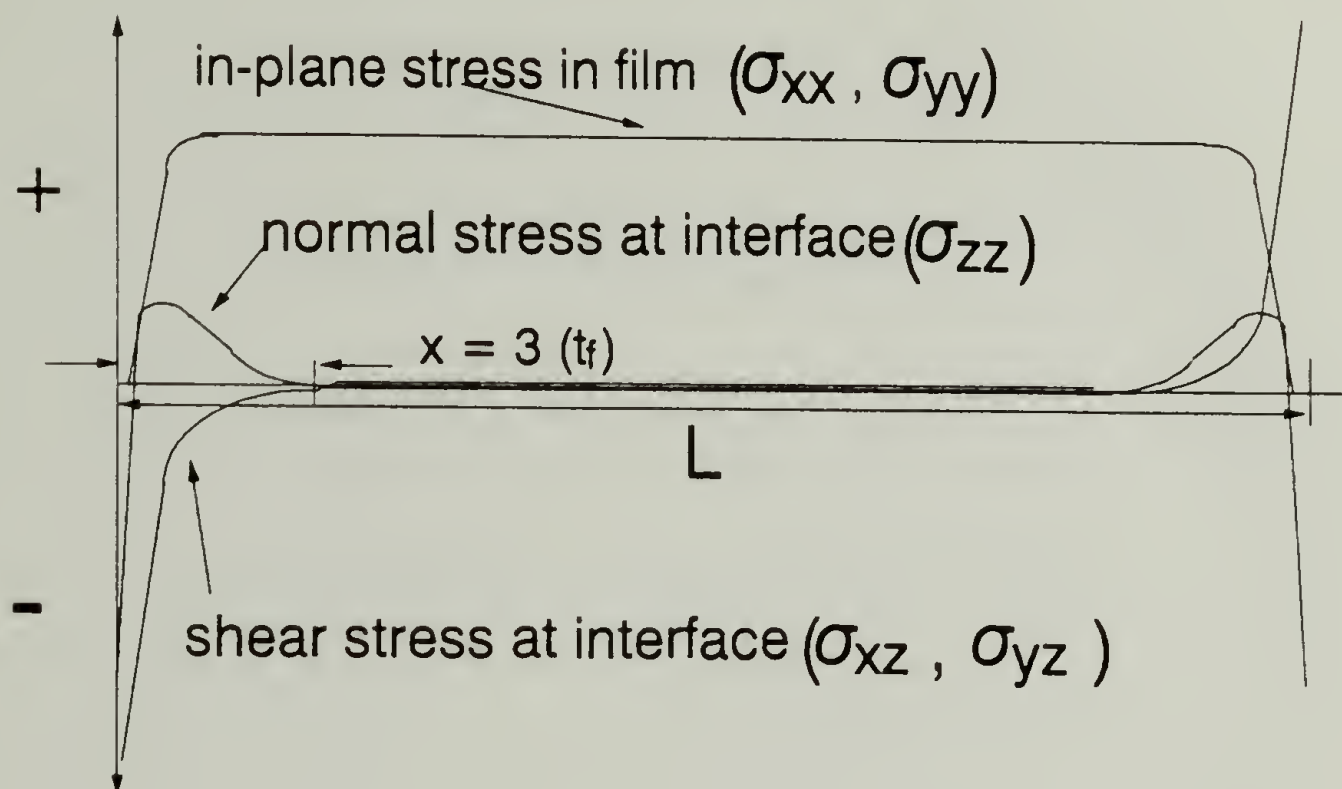
Figure 1.2   Schematic representation of the stresses at the edges and through the width of a coating. This analysis assumes that the thickness and Young's modulus of the substrate are much larger than that of the coating. It can be seen that at a distance of no more than three film thicknesses from the edge of the coating all shear and normal stresses between the coating and the substrate go to zero (after Hess [34]). This is an important consideration in the sample fabrication techniques developed as part of this work to make membranes for testing, without disturbing the state of stress in the plane of the film.

The real-time holographic interferometry method images the vibration patterns of all resonant modes of vibration in the form of a contour map of the out-of-plane displacement. Observing the membrane vibration holographically allows one to observe many resonant frequencies for each membrane and to assign each frequency to the appropriate order of the Bessel function which describes its vibration. This is a significant advantage over methods which measure the displacement only at the center of

the membrane. Another equally important advantage is that the holographic interferometry method can be used to determine the biaxial stresses for a non-uniformly stressed material. The versatility and application of the vibrating membrane/holographic interferometry technique for stress measurement will be discussed in much greater detail in the remainder of this dissertation.

1.2 Material Properties of Orthotropic Films

An orthotropic material has different material properties in three orthogonal directions. During the commercial manufacture of polymer films, a shear stress gradient commonly exists across the width of the film line. As the film is cooled, residual orientation is frozen in the plane of the film. The principal directions of stress do not necessarily coincide with the machine and transverse directions. In fact, the direction of orientation due to shear stress during processing will vary across the width of a film line. For instance, at the center of the film, the material properties in the plane of the film in all directions can be isotropic, but will become increasingly anisotropic for samples taken closer to the outside edge of the film line [34]. To fully characterize an orthotropic material, 21 material constants are required. However, if the orthotropic axes can be identified, the number of independent material constants reduces to nine. The ability to characterize the orthotropic nature of commercially made films is critical for the prediction of film reliability.

Very little work has been done in the characterization of orthotropic polymer films. One of the difficulties has been the inability to discern the directions of the orthotropic axes. The work that has been done in this area has been on polymer single crystals of polydiacetylene [35, 36], on paper sheets with fibers oriented in known directions [37, 38] and also on composites with specific fiber orientations [39]. The

predominant technique used in these measurements was that of sonic reflectance to measure the velocity of a sound wave through a material which can then be related to the moduli.

This dissertation presents a method for determining the orthotropic axes of commercially made polymer films, as well as a comprehensive series of mechanical tests which may be used to determine the orthotropic material constants. A holographic technique to measure biaxial stresses in films [40] can be used as a tool to determine the orthotropic axes of a polymer film. By knowing the orthotropic axes, the material properties such as shear moduli, Poisson's ratios and Young's moduli in these directions can be calculated using special tests we have developed to obtain the nine orthotropic elasticity constants. Determination of the state of stress and the elastic constants are required to predict the stress behavior in complex coating geometries and around holes. This set of experiments will be described in detail in chapter 5.

1.3 Materials Studied

This section introduces the materials studied as part of this work. It will be divided into two sections, one which describes materials used in the development of the holographic interferometry stress measurement studies, and the second which discusses commercial films used for material property measurements. Four different types of materials were studied in the stress measurement experiments. Our main interest was in the spin-coated polyimides materials. Studies conducted on silver films, epoxy coatings, and filled and unfilled poly(tetrafluoroethylene) (PTFE) materials allowed the study of geometry effects on air-damping, stiffness effects and the effects of fillers on stresses in films. Table 1.1 below lists the materials studied, and the experiments conducted in each case.

Table 1.1   Materials studied in this dissertation and the information obtained from each.

Material	Property Studied
PMDA-ODA (spin-coated polyimide)	In-plane stresses, Air damping effects
Silver Films	Stresses, Air Damping and geometry effects
Epoxy Paint Base Coatings	Stresses, Air damping and geometry effects
Filled/Unfilled PTFE	Stress difference between filled and unfilled samples
Kapton™	Orthotropic nature and material properties of free-standing films
Upilex R™	Orthotropic nature and material properties of free-standing films
Poly(vinyl alcohol)	Highly oriented material, stretch ratio of 3.6:1 in orthogonal directions - Studied orthotropic nature and material properties

1.3.1   Stress Measurement

The impetus behind this work was to determine the values of the biaxial stresses in polyimide materials used as passivation layers in microelectronic devices. These materials have been selected for use based on their high thermal stability, low dielectric constants, and the ability to be spin-coated from solution. Spin-coating gives greater coating planarization on devices, thus reducing sharp corners between layers which are

sources of high stress concentration. Polyimides are made via condensation reactions between diamines and diacids. The two particular polyimides studied in this work are PMDA-ODA (poly[N,N'-(p,p'-oxydiphenylene)-pyromellitimide]) also known as pyromellitic dianhydride oxydianiline and BPDA-PDA, poly[N,N'(phenylene)-3,3'4,4'-biphenyl tetracarboxylic diimide]. Both of these polymers are spin coated from ~ 20% solid solutions of the polyamic acid precursors in NMP (N-methyl pyrolidinone). The reaction schemes of these two materials are shown in Figures 1.3 and 1.4. Upon curing, solvent removal and condensation reactions lead to volume decreases in the polymer coating which can bring about large in-plane tensile stresses. If the stresses are high enough, delamination and cracking will occur.

PMDA   ODA

Polyamic acid   Polyimide

PMDA: pyromellitic dianhydride
ODA: oxydianiline
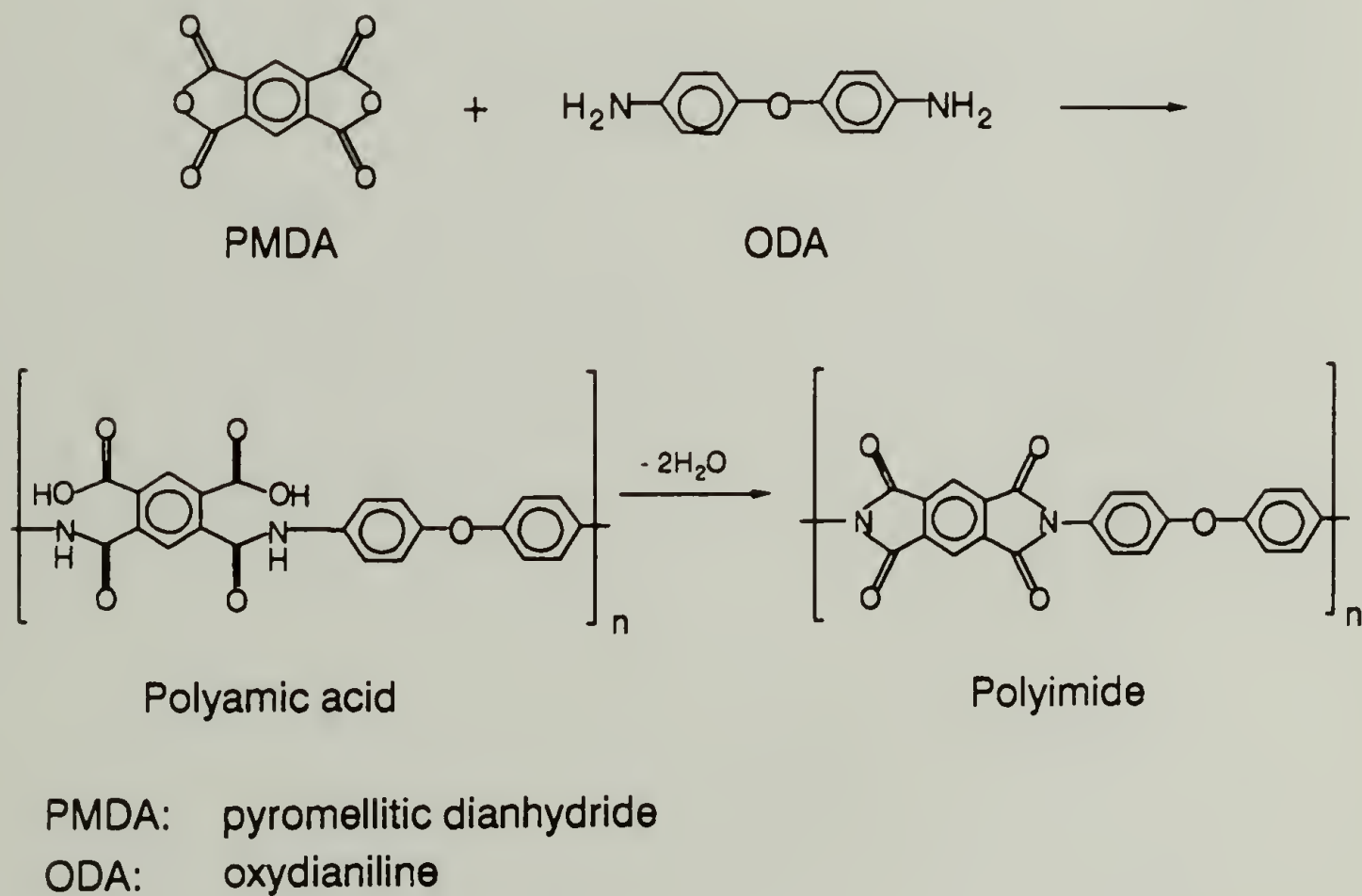
Figure 1.3   Reaction scheme for pyromellitic dyanhydride - oxydianiline (PMDA-ODA). The polyamic acid is formed in a solution of N-methyl pyrrolidinone (NMP) and upon curing to 200 °C undergoes a condensation reaction, giving off water and completes its imidization reaction. Upon further heating, molecular rearrangement occurs and the stress in the film continues to increase.

BPDA

PDA

Polyamic acid

Polyimide
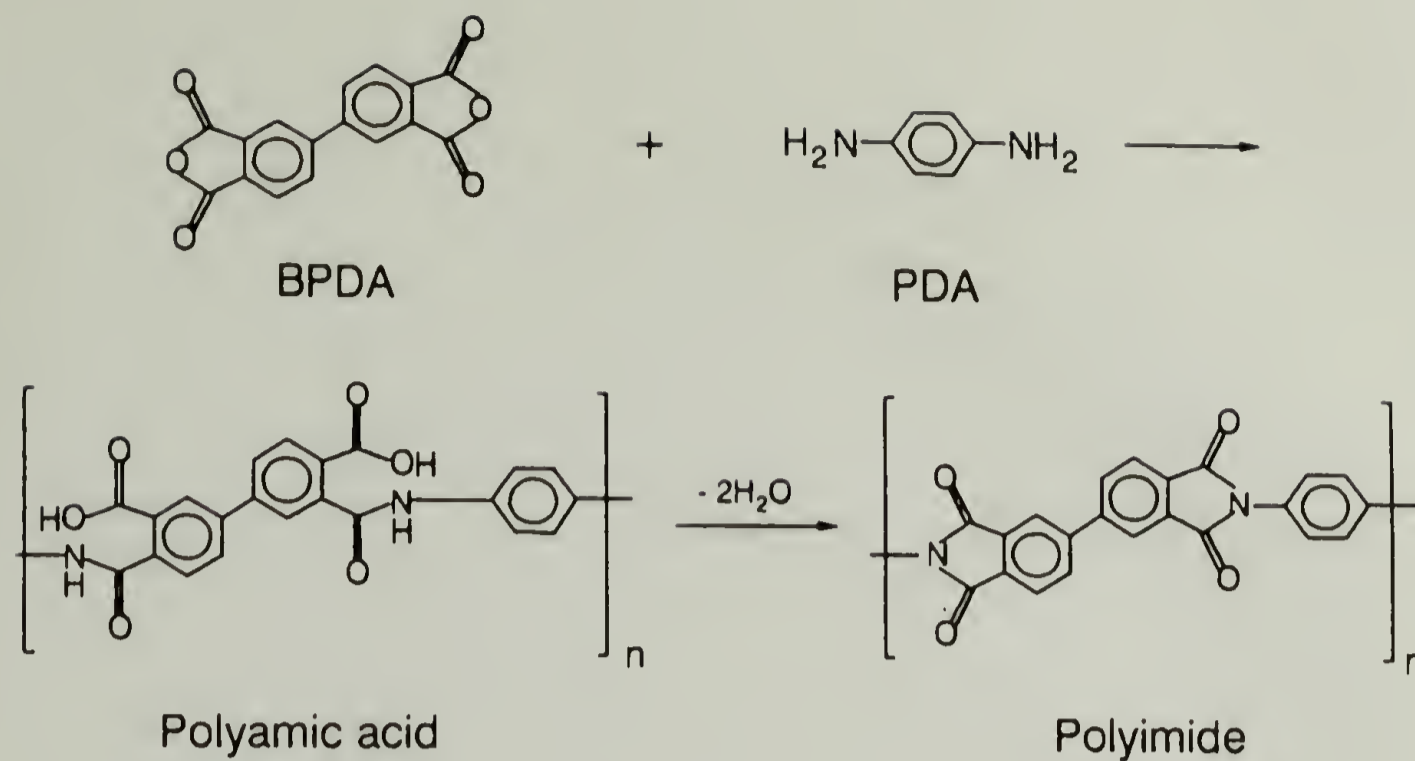
BPDA: 3,3'4,4' - biphenyl tetracarboxylic dianhydride
PDA: p - phenylenediamine

Figure 1.4   Reaction scheme for 3,3'4,4'-biphenyl tetracarboxylic dianhydride and p-phenylenediamine. A similar condensation reaction occurs as with the PMDA-ODA material.

The PMDA-ODA materials are desirable primarily for their high thermal stability, and the BPDA-PDA material has been developed with a low coefficient of thermal expansion. The smaller the mismatch in coefficient of thermal expansion between a coating and substrate, the lower the stresses in the coating will be (assuming the coatings have similar values of $E/(1-v)$). The two most important parameters to control when designing spin-on dielectrics such as these are the coefficient of thermal expansion and the Young's modulus. It is desirable to have the coefficient of thermal expansion low so that the mismatch between the coefficients of thermal expansion of the coating and the substrate is small and large thermal stresses do not develop. However, as the coefficient of thermal expansion of a material is lowered, the Young's modulus increases (increased stiffness). The biaxial stress in a coating is directly proportional to

the Young's modulus, so one must find the optimal values of CTE and modulus which yield the lowest curing stresses.

Stress measurement experiments are also conducted on epoxy materials used as paint base coats. These samples are made by constraining the coating on a washer and then removing the substrate. They vary in thickness, but all have the same radius. This allows a study of the effects of sample geometry on the air damping of a vibrating membrane.

Other samples tested include silver films of various thicknesses and diameters mounted in ceramic sample holders and heated to above their yield point, clamped and then cooled, causing a tensile stress in the plane of the film. These samples range from membrane-like to plate-like in their vibration behavior and allow conclusions to be drawn as to the critical values of air damping and stiffness parameters.
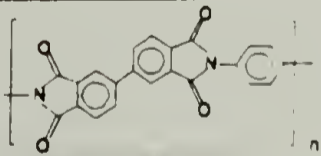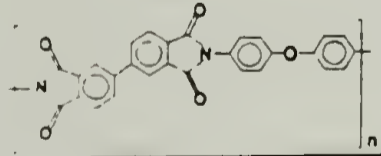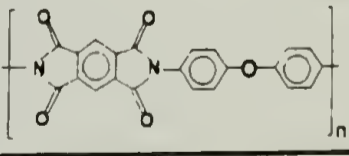
Filled and unfilled poly(tetrafluoroethylene) (PTFE) materials sandwiched between copper sheet under high pressures and temperatures are of potential use in the electronics industry as flexible circuit materials. The copper outer layers can be removed and stress measurements done to determine the effect of filler on the stresses in these films.

These last three sets of experiments enable us to study the effects of specimen geometry and material properties on the results of the holographic stress measurement technique, and in some cases gave an indication of what happens to a membrane sample as it approaches and adopts plate-like behavior. The restoring force for the vibration of a membrane is completely due to the tension in the membrane. However, as the thickness increases, the radius of the sample decreases, and/or the mode of vibration increases, the behavior becomes more plate-like and is increasingly dominated by bending moments. This complication will be discussed further in chapter 3.

1.3.2 Material Property Measurements

Materials used in the studies of material properties included the free-standing film materials which closely correspond to the coating materials used in the above experiments. The tradenames are Kapton ™ (DuPont) which is the commercial film version of PMDA-ODA and Upilex™ (Ube Corp.) which is the commercial film version of BPDA-PDA or BPDA-ODA. The reported properties of these materials are tabulated below. (MD and TD stand for the machine and transverse directions of a commercially made film.)

Table 1.2   Properties of commonly used commercially made polyimide films.

Property	Material		
	Upilex®R [41]	Upilex®S [41]	Kapton® H [42]
Young's Modulus (25°C)	3.72 GPa	8.83 GPa	3.0 GPa
Tensile Strength (25°C)	245 MPa	392 MPa	172 MPa
Density (kg/m^3)	1390	1470	1420
T_g (Glass Transition)	285 °C	> 500 °C	360 - 410 °C
Coefficient of Thermal Expansion (20 - 100) cm/cm/°C	MD 15 x 10^{-6} TD 17 x 10^{-6}	MD 8 x 10^{-6} TD 8 x 10^{-6}	18 - 20 x 10^{-6}
Dielectric Constant (25 mm)	3.5	3.5	3.5
Chemical Structure			

1.4   Dissertation Overview

Chapter 1 has given an introduction to stresses in coatings - why they are important and how they have been quantified in the past. Several dielectric coating materials have also been introduced, along with their commercial counterparts. Commercially made films are used for experiments in which the nine orthotropic elasticity coefficients can be determined. In chapter 2, the real time holographic interferometry technique, will be explained. This chapter will include a discussion of how the resonant frequency of a membrane is related to the stress in the membrane. Some background on holographic interferometry will be presented along with the theory of real time holographic interferometry and how it can be applied to the measurement of stresses in coatings. Preliminary results on stress measurements will be presented, and the implications of the results discussed.

Chapter 3 is a presentation of the complicating effects of air damping and stiffness. The primary focus in this chapter is on the air damping effect (the lowering of the resonant frequency due to the pressure exerted on the membrane by air). Corrections for this effect proposed by Lax [43] and Karnezos [44] will be applied to the data from PMDA-ODA coatings and compared to stress values measured in vacuum. We have written a FORTRAN program to analyze our data using Lax's correction and analysis by Gottleib and Aebischer [45], this is included as an Appendix. Chapter 4 presents experiments in which the stress in a coating is measured as a function of temperature. Chapter 5 focuses on the analysis of orthotropic material properties of commercially made polymer films, the identification of their orthotropic axes using holographic interferometry and the measurement of material properties using several other complementary techniques. Chapter 6 is a summary of the work done and an evaluation of which directions this work should take in the future.

REFERENCES

1. P. Buchwalter, in discussion at IBM T. J. Watson Research Center, Yorktown Heights, NY, April 1991.

2. M. A. Nkansah and K. E. Evans, "Thermal Stresses in Multilayer Optical Storage Media," *Journal of Applied Physics*, **66**(1), 50 (1989).

3. I. C. Noyan, and L. T. Nguyen, "Residual Stresses in Polymeric Passivation and Encapsulation Materials," *Polymer Engineering and Science*, **28**(16), 1026 (1988).

4. K. Sato, "The Internal Stress of Coating Films," *Progress in Organic Coatings*, **8**(2), 143 (1980).

5. D. Y. Perera, "Internal Stress in Latex Coatings," *Journal of Coatings Technology*, **56**(716), 111 (1984).

6. D. Y. Perera, and D. V. Eynde, "Moisture and Temperature Induced Stresses (Hygrothermal Stresses) in Organic Coatings," *Journal of Coatings Technology*, **59**(748), 55 (1987).

7. S. G. Croll, "Internal Stress in a Solvent-Cast Thermoplastic Coating," *Journal of Coatings Technology*, **50** (638), 33 (1978).

8. S. G. Croll, "The Origin of Residual Internal Stress in Solvent-Cast Thermoplastic Coatings," *Journal of Applied Polymer Science*, **23**(3), 847 (1979).

9. S. G. Croll, "Internal Strain in Solvent-Cast Coatings," *Journal of Coatings Technology*, **51**(648), 64 (1979).

10. G. Elsner, "Residual Stress and Thermal Expansion of Spun-on Polyimide Films," *Journal of Applied Polymer Science*, **34**(2), 815 (1987).

11. C. Goldsmith, P. Geldermans, F. Bedetti, G. A. Walker, "Measurement of Stresses Generated in Cured Polyimide Films," *Journal of Vacuum Science Technology*, **A1**(2), 407 (1983).

12. S. Timoshenko, "Analysis of Bi-Metal Thermostats," *Journal of the Optical Society of America*, **11**(9), 233 (1925).

13. K. Röll, "Analysis of Stress and Strain Distribution in Thin Films and Substrates," *Journal of Applied Physics*, **47**(7), 3224 (1976).

14. E. Suhir, "An Approximate Analysis of Stresses in Multilayered Elastic Thin Films," *Journal of Applied Mechanics*, **55**(3), 143 (1988).

15. E. Klokholm, "Delamination and Fracture of Thin Films," *IBM Journal of Research and Development*, 31(5), 585 (1987).

16. F. Faupel, C. H. Yang, S. T. Chen, P. S. Ho, "Adhesion and Deformation of Metal/Polyimide Layered Structures," *Journal of Applied Physics*, **65**(5), 1911 (1991).

17. D. S. Campbell, "Mechanical Properties of Thin Films," *Handbook of Thin Film Technology*, Chapter 12, ed. L. I. Maissel and R. Glang (New York: McGraw-Hill Book Company, 1970).

18. R. W. Hoffman, "The Mechanical Properties of Thin Condensed Films," *Physics of Thin Films: Advances in Research and Development*, Vol. 3, p. 211, ed. G. Haas, and R. Thun, (New York: Academic Press, 1966).

19. D. S. Soane, "Stresses In Packaged Semiconductor Devices," *Solid State Technology*, **32**(5) 165 (1989).

20. R. E. Cuthrell, F. P Gerstle, Jr., and D. M. Mattox, "Measurement of Residual Stresses in Films of Unknown Elastic Modulus," *Review of Scientific Instruments*, **60**(6), 1018 (1989).

21. M. F. Gruninger, B. R. Lawn, E. N. Farabaugh, J. B. Wachtman, Jr., "Measurement of Residual Stresses in Coatings on Brittle Substates by Indentation Fracture," *Journal of the American Ceramic Society*, **70**(5), 344 (1987).

22. M. G. Allen, *Measurement of Adhesion and Mechanical Properties of Thin Films Using Microfabricated Structures*, Ph.D. Dissertation, Massachusetts Institute of Technology, (1989).

23. M. G. Allen, M. Mehregany, R. T. Howe, and S. D. Senturia, "Microfabricated Structures for the in-situ Measurement of Residual Stress, Young's Modulus, and Ultimate Strain in Thin Films," *Applied Physics Letters*, **51**(4), 241 (1987).

24. P. Lin and S. Senturia, "The In-situ Measurement of Biaxial Modulus and Residual Stress of Multi-Layer Polymeric Thin Films," in *Thin Films: Stresses and Mechanical Properties II*, (Philadelphia, PA: Materials Research Society, 1990).

25. J. F. Taylor, R. M. Jennings, and R. J. Farris, "A Deflection Technique for the Determination of Residual Stresses in Coatings," in preparation (1991).

26. S. Tiitto, "Magnetoelastic Testing of Biaxial Stresses," *Experimental Techniques*, **15**(1), 17 (1991).

27. J. W. Strutt, 3rd Baron Rayleigh, *The Theory of Sound*, (New York: Dover Publications, 1945; London: 1867).

28. B. Ya. Pines, V. M. Andronov, and V. B. Rabukhin, "Device For Investigating the Mechanical Properties of Whiskers and Thin Films," trans. from *Zavodskaya Laboratoriya*, **35**(6), 741 (1969).

29. M. Karnezos, "Effects of Stress on the Stability of X-ray Masks," *Journal of Vacuum Science and Technology*, **B4**(1), 226 (1986).

30. B. S. Berry, W. C. Pritchet and C. E. Uzoh, "Dynamical Method for the Thermomechanical Study of Thin Membranes," *Journal of Vacuum Science Technology*, **B7**(6), 1565 (1989).

31. B. S. Berry and W. C. Pritchet, "Internal Stress and Internal Friction in Thin-Layer Microelectronic Materials," *Journal of Applied Physics*, **67**(8), 3661 (1990).

32. M. A. Maden, A. Jagota, R. J. Farris, Q. K. Tong, and S. Mazur, "Vibrational Technique for Stress Measurement in Films - 1. Ideal Membrane Behavior," submitted for publication, *Journal of Materials Research*, (1991).

33. M. S. Hess, "The End Problem for a Laminated Elastic Strip - II. Differential Expansion Stresses," *Journal of Composite Materials*, **3**(10), 630 (1969).

34. R. M. Jennings and R. J. Farris, "Analysis of Stresses Arising During the Processing of Polymeric Films on Tentering Frames," in press *Polymer Engineering and Science*, (1992).

35. W. Rehwald, A. Vonlanthen and W. Meyer, "Single Crystal 2,4-Hexadiynylene-Bis(p-Toluenesulfonate): Elastic Properties and Phase Transitions in the Monomer and Polymer," *Physica Status Solidi (A)* **75**(1), 219 (1983).

36. R. J. Young, "Polymer Single Crystal Fibres," *Developments in Oriented Polymers II*, ed. E. M. Ward, (New York: Elsevier Applied Science Publishers, 1987).

37. G. A. Baum, D. C. Brennan, and C. C. Habeger, "Orthotropic Elastic Constants of Paper," *Tappi*, **64**(8), 97 (1981).

38. R. W. Mann, G. A. Baum, and C.C. Habeger, "Determination of All Nine Orthotropic Elastic Constants for Machine-Made Paper," *Tappi*, **63**(2), 163 (1980).

39.   H.M. Ledbetter, "Orthotropic Elastic Stiffness of a Boron-Aluminum Composite," *Journal of Applied Physics*, **50**(12), 8247 (1979).

40.   Q. K. Tong and R. J. Farris, "Measurement of Two-Dimensional Stresses in Thin Polymer Films Using Holographic Interferometry," submitted for publication, (1990).

41.   *Upilex Polyimide Films: Technical Data*, (Wilmington: ICI Americas, Inc., 1989).

42.   *Kapton Polyimide Film: Summary of Properties*, (Wilmington: DuPont Company, 1986).

43.   M. Lax, "The Effect of Radiation on the Vibrations of a Circular Diaphragm," *The Journal of the Acoustical Society of America*, **16**(1), 5 (1944).

44.   M. Karnezos, "Effects of Stress on the Stability of X-ray Masks," *Journal of Vacuum Science and Technology*, **B4**(1), 226 (1986).

45.   H. P. W. Gottlieb, and H. A. Aebischer, "Eigenfrequency Shifts of a Baffled Circular Membrane in a Fluid Medium," *Acustica*, **61**(4), 223 (1986).

CHAPTER 2

VIBRATING MEMBRANES AND HOLOGRAPHIC INTERFEROMETRY

2.1   Introduction

An introduction to the real-time holographic interferometry technique for the

measurement of biaxial stresses in coatings is presented in this chapter. The new method

of stress measurement developed in this work is a synthesis of the theory of a vibrating

membrane, which dates from as early as the 1800's, and the modern technique of

holographic interferometry which was first used in the mid-1960's. The basic idea is

founded on the observation that the head of a drum when placed under different degrees

of tension, will resonate with different characteristic frequencies. For drummers,

especially timpanists, this is part of their practical knowledge. Drums are tuned by

adjusting screws around the head of the instrument to either loosen or tighten the drum

head and change its pitch. An analogy can be made here to the vibration of a string (see

Figure 2.1). If a string is held under tension and excited at various resonant frequencies,

it will have a specific number of nodes (points of zero displacement) along its length

depending upon the resonant frequency used to excite the string. The vibration of the

membrane is essentially a two dimensional analog to the vibration of a string. A

schematic of the vibrational nodes of a circular membrane is shown in Figure 2.2.

The mathematical solution to this observed behavior is described by the solution

of a second order differential equation of motion which relates the tension in a membrane

to its radius, density, and to the square of its resonant frequencies. In order to use this

relation, one must know the mode of vibration at which the membrane is resonating.

This is accomplished using real-time holographic interferometry which images the out-
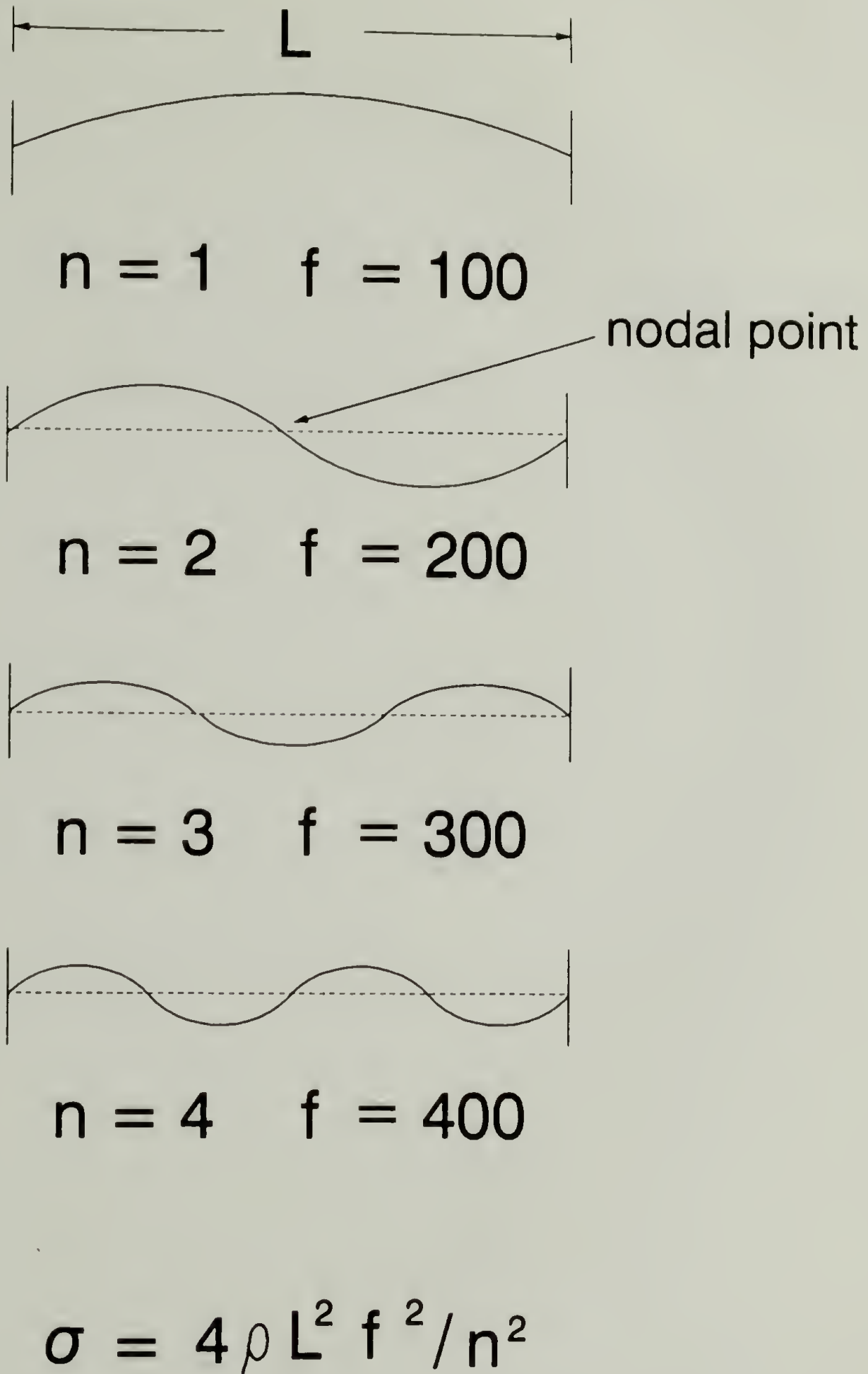
Figure 2.1   Vibration of a string under forced sinusoidal vibration. The nodal points are those at which the string is at a point of zero displacement over an average of all time. The equation for stress is given in the figure, f is the measured frequency in Hz ($\omega = 2\pi f$), and ρ is the density of the string.

radial node
(m)

tangential node
(n)

$m = 0$
$n = 1$

$m = 1$
$n = 1$

$m = 2$
$n = 1$

$m = 0$
$n = 2$
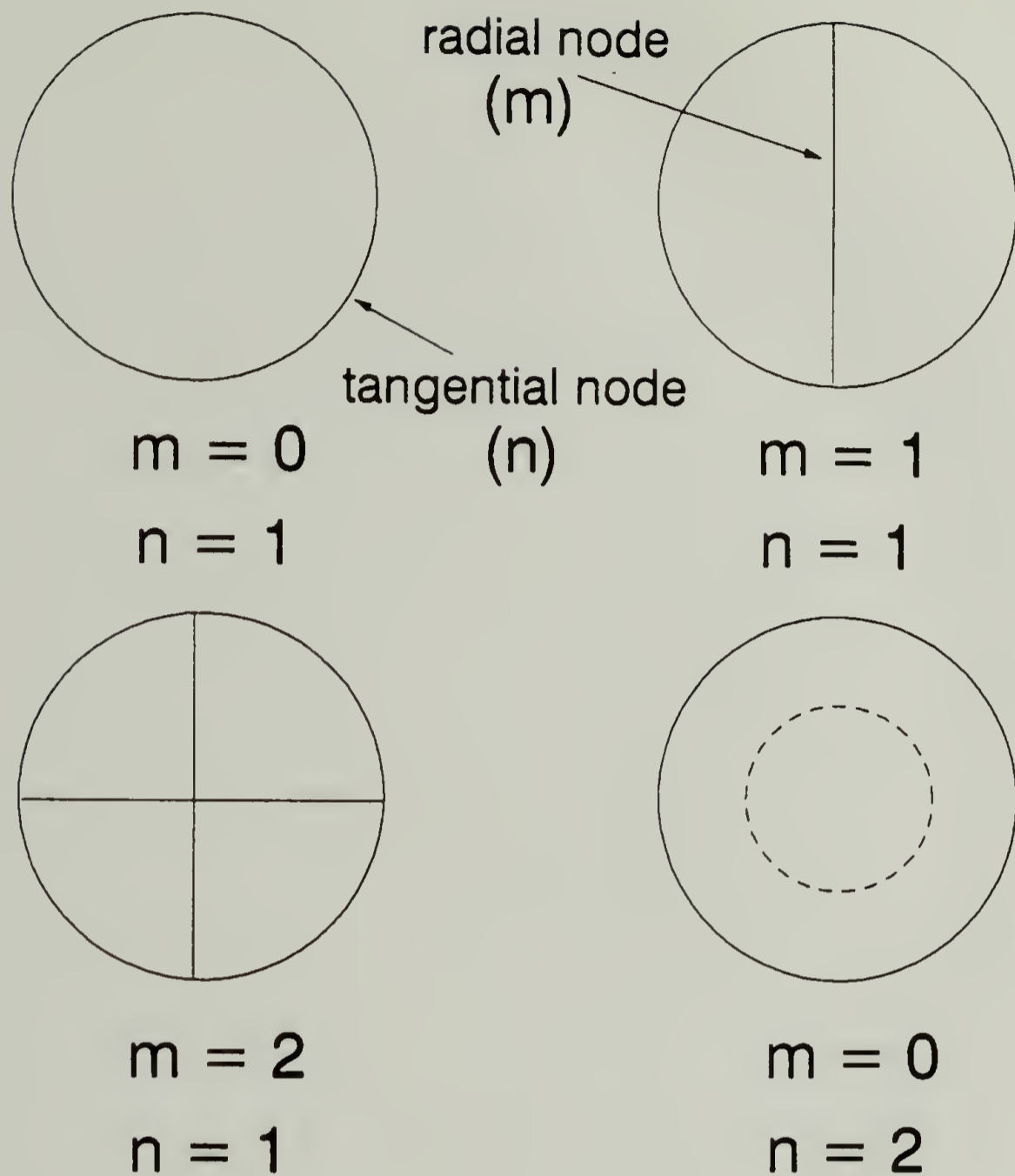
$$\sigma = \rho \, \omega^2 R^2 / Z_{mn}^2$$

Figure 2.2   Schematic representation of the vibration of a circular membrane, where the nodes in the radial and tangential directions are indicated. The number of each type of node identifies the value of the indices n and i respectively which denote the order of the Bessel function and the number of the zero of that Bessel function. The equation for stress is given in the figure above, where ω is the angular frequency in sec^{-1}, and Z_{mn} is the value of the nth zero of the mth order Bessel function.

of-plane motion of a vibrating membrane relative to a hologram of the stationary membrane. The mode of vibration is directly related to a specific zero of a particular order Bessel function (determined from the shape of the vibration pattern) and this also enters into the equation for stress in a vibrating membrane. While the focus of this work will be on thin polymer coatings (specifically polyimides of thicknesses in the 10 μm range), it should be emphasized that the method described herein is also applicable to the measurement of in-plane stresses in metal or ceramic films (provided the films are under tension).

Descriptions of the vibrating membrane analysis and holographic interferometry, including their historical context, various applications of each, as well as theoretical considerations pertinent to the stress measurement technique, are presented in the following sections. The development of the stress measurement technique based upon the union of these two ideas will also be discussed and the preliminary results reported. Membrane sample preparation techniques which allow a portion of the substrate or the entire substrate to be removed without affecting the state of stress in the coating are also described.

2.2   Vibrating Membrane

The following sections provide an introduction to the study of vibrating membranes. A brief history of the study of vibrating objects is given, followed by the theoretical basis for the determination of stress in a membrane.

2.2.1   Background

The history of the study of vibrating bodies is quite fascinating, and extends as far back as Pythagoras in the 6th Century. Robert Bruce Lindsay in his introduction to the

1945 edition of Rayleigh's *Theory of Sound* [1] and in his book *Acoustics* [2] gives a useful overview of the developments in this field. Some of the highlights will be presented here as an introduction to this discussion of the vibration of membranes. As mentioned above, the first recorded observations of vibrations related to sound were made by Pythagoras who noted that of two strings, fixed at both ends, one twice as long as the other, the shorter string when plucked, makes a sound one octave higher than the other. Galileo Galilei (1564 - 1642) also wrote on this topic (1683) [3] and seemed to have a clear understanding of the interrelation between the frequency, density, and length of a stretched string. He was most interested in these ideas as they related to the oscillation of pendulums. The first dynamical solution for the vibration of a string was derived by Brook Taylor in 1713 [4].

The earliest recorded studies of the two-dimensional vibration problem are those of the German scientist E. F. F. Chladni (1756-1824) in his book *Die Akustik*, (1802) [5]. He used sand sprinkled on vibrating plates to observe their nodes of vibration. In the early 1800's Napoleon offered a prize of 3000 francs to the person who could derive a "satisfactory theory for the vibration of plates." This prize was awarded to a Mlle. Sophie Germain in 1815 who came up with the correct fourth order differential equation describing this motion. The problem for membrane vibrations was not solved until 1829, by Poisson for a square membrane [6], followed by Clebsch in 1862 who solved the problem for a circular membrane [7]. In 1866, the first experiments to determine the vibration patterns of a membrane in tension were done by M. Bourget. He used the technique introduced earlier by Chladni (sand sprinkled on top of a membrane) to observe their resonant vibration patterns. To make his membranes Bourget immersed a sheet of paper in water and glued it to a wooden frame which upon drying, induced biaxial stresses in the membrane. Organ pipes were then used to excite the membrane to its resonant frequencies [8]. This method was crude at best, and did not work well past the first two resonance patterns due to their increased complexity. It did, however,

enable Bourget to roughly determine the lower resonant frequencies of a given membrane. He also found that if the tension in the membrane was unequal in different directions, oval shaped vibration patterns occurred. He made another observation which is connected to what was seen in our first experiments, that the resonant frequencies measured, did not follow the ratios predicted by the theory. This will be discussed in detail in chapter 3.

The work described in this proposal makes use of classical vibration theory in an innovative way to determine the biaxial stresses in coatings. Membrane vibrations have long been an intriguing subject for mathematicians and physicists alike.

Mathemeticians have puzzled for years over one's ability to "hear the shape of a drum" [9, 10, 11]. In other words, knowing the normal modes of vibration of a membrane, can one unequivocably determine its shape, size, and tension. Furthermore, the question has been asked, are there more than one combination of tension and area and drum head shape that will resonate at the same fundamental frequency? [12, 13].

2.2.2 Theory

Our technique builds on the accumulated knowledge of physicists and mathematicians, applying what is known to the solution of an engineering stress measurement problem. Both of the above analyses as well as our method for determining the state of stress in a membrane begin with the most fundamental equation of motion. The free vibration of a membrane in vacuum is described by the differential equation,

$$T \nabla^2 u = \rho_A \frac{\partial^2 u}{\partial t^2} \tag{2.1}$$

where,

$$T \quad = \text{biaxial tension in the membrane (N/m)}$$

$$u \quad = \text{out of plane displacement (m)}$$

$$\rho_A \quad = \text{areal density (kg/m}^2\text{)}$$

$$\frac{\partial^2 u}{\partial t^2} \quad = \text{second time derivative (acceleration) of}$$

$$\text{the out of plane displacement (m/sec}^2\text{)}$$

If we divide both sides by the thickness of the film, h, the differential equation for a circular membrane in cylindrical coordinates becomes,

$$\frac{\partial^2 u}{\partial r^2} + \frac{1}{r}\frac{\partial u}{\partial r} + \frac{1}{r^2}\frac{\partial^2 u}{\partial \theta^2} = k^2 \frac{\partial^2 u}{\partial t^2} \qquad (2.2)$$

where,

$$u = f(r,\theta,t) \quad = \text{out of plane deflection (m)}$$

$$\theta \quad = \text{tangential coordinate}$$

$$r \quad = \text{radial coordinate(m)}$$

$$k^2 \quad = \rho/\sigma$$

$$\rho \quad = \text{mass per unit volume (kg/m}^3\text{)}$$

$$\sigma \quad = \text{biaxial stress (N/m}^2\text{)}$$

$$t \quad = \text{time (seconds)}$$

If the membrane is attached at its circumference to a rigid support, the boundary condition at r = R (where R is the outer radius) is u = 0. The solution of this equation is of the form,

$$u_{mn}(r,\theta,t) = A_m J_m(\omega_{mn}kr) \sin(\omega_{mn}t + a) \cos(m\theta + b) \qquad (2.3)$$

where u_{mn} is the out of plane displacement of a membrane of which the vibration is described by the nth zero of the mth order Bessel function, A_m is a constant and $J_m(\omega_{mn}kr)$ is a Bessel function of the first kind of order m. At the critical frequencies, ω_{mn}, (i.e. where the membrane resonates) the deflection at the outer radius, $u_{mn}(r = R)$ must equal zero. Therefore, the nontrivial solution to this equation demands that the Bessel function must also be exactly equal to zero at the boundary, i.e.,

$$J_m(\omega_{mn}kR) = 0 \qquad (2.4)$$

The zeroes of integer order Bessel functions have been tabulated in the literature [14]. A table of the first twenty zeroes of the Bessel functions in order of appearance is given in Table 2.1. If the argument of the Bessel function is set equal to Z_{mn}, the tabulated value of the nth zero of the mth order Bessel function, then the stress in the film can be related to the frequency at which it vibrates, as follows:

$$\omega_{mn}kR = Z_{mn} \qquad (2.5)$$

and

$$\sigma = \rho(R\omega/Z_{mn})^2 \qquad (2.6)$$

Table 2.1   Mode numbers, mode shape indices (m, n), and zeros of the Bessel function, $J_m(Z_{mn}) = 0$.

Mode Number	m, n	Z_{mn}
1	0, 1	2.405
2	1, 1	3.831
3	2, 1	5.136
4	0, 2	5.520
5	3, 1	6.380
6	1, 2	7.016
7	4, 1	7.586
8	2, 2	8.417
9	0, 3	8.654
10	5, 1	8.708
11	3, 2	9.760
12	6, 1	9.953
13	1, 3	10.173
14	4, 2	11.064
15	7, 1	11.115
16	2, 3	11.620
17	0, 4	11.792
18	8, 1	12.270
19	5, 2	12.339
20	3, 3	13.017

The order of the Bessel function is determined from the observed vibration pattern at a given frequency. Vibrations of the zeroth order will have no lines of axial symmetry and should produce a circular vibration pattern. Vibrations of the first order will have one line of symmetry, etc.. (see Figure 2.2).

This type of analysis has also been done for thin plates taking into account the flexural rigidity and bending moments [15]. These factors should not play a significant

role in our results as the thickness of the membrane is much less than the diameter, and the flexural rigidity is low compared to the magnitude of the stress in the membrane. The holographic interferometry technique may be used to determine the stress in plates under tension, provided that a term containing the flexural rigidity, D, is included in the analysis. When the rigidity term is accounted for, the modulus and Poisson's ratio may also be determined from redundant stress measurements [16]. The above treatment assumes that the stresses in the film are isotropic, that there is no air damping as the membrane vibrates, and that out of plane stresses in the film disappear a few film thicknesses from the edge [17, 18]. The assumption of isotropic stress is not necessary for the solution of the vibrating membrane equation. It can be shown that two independent planar normal stresses and the inplane shear stress can be resolved if square membranes and higher order frequencies are used [16].

2.3   Real - Time Holographic Interferometry

In the following sections, the principles of holography will be introduced, and some discussion of its history and applications presented along with the rudimentary theory behind its use. The concept of holographic imaging was first proposed by Dennis Gabor in 1947 [19]. At the time, he was working in the field of electron microscopy at the Thomsom-Houston Company in England. He was interested in improving the resolution of the electron microscope which was limited to about 12 Angstroms by aberrations inherent in the electron objective lens. He came up with the idea that if one could record the phase of the electron beams instead of just their intensity, then reconstruct the image optically, the resolution would be improved. This is directly related to the construction of a diffraction grating, where two sources of light interact to form an interference pattern of maxima and minima. In the case presented by Gabor, one of the light (or electron) sources is collimated and the other reflects from an object onto

the recording plate. When the two beams interfere at the plate, a complex pattern is produced which upon re-illumination with collimated light, recreates an image of the original object that contains both phase and amplitude information, thus creating a three dimensional image. He called this image a hologram from the Greek *holos* (meaning "whole") and *gram* (meaning "picture") [20].

Gabor's efforts were limited by the lack of a good coherent light source and by the in-line nature of his electron microscope set-up which allowed him to image only two dimensional objects. Thus, the full effect of the phase recording properties (i.e. the ability to recreate a three-dimensional image) could not be fully appreciated. However, upon the invention of the laser in 1960, the door was opened to many researchers in this field and a bevy of researchers quickly began work on taking advantage of its applications. Among the first developers of this technique were Emmett Leith and Juris Upatnieks from the University of Michigan [21]. Their work focused on obtaining high quality three dimensional images of objects and the exploration of parallax. This enables one to see objects hidden behind other objects in a hologram by viewing the hologram from a different angle. Another interesting property of holograms is that any small fragment of the hologram has the ability to reproduce the entire image. This is due to the fact that each point on a hologram receives light reflected from all parts of an object, and therefore contains the whole image. The only limitation of this effect is that the smaller the portion of the hologram that is used, the poorer the resolution of the reconstructed image. This work was followed by that of Powell and Stetson [22], and Heflinger, Wuerker, and Brooks [23] in 1966 who worked on the use of holography as an interferometric method capable of imaging the out of plane displacement of objects, and also of imaging the vibrations of objects. A good review of early holographic developments was written by Pennington in 1968 [24].

There are many different variations on the theme of holography. The three main types of holography which are pertinent to the work presented in this thesis are reflection

holography (the imaging of three dimensional objects by reflection of a beam of light from an object onto a holographic plate), real-time holography and time average holography. The basic holographic method is used to record the image of a stationary object, in our case a membrane. Real-time holography is simply the observation in "real-time" (as it occurs) of the real membrane or object as it vibrates superimposed on the hologram of the stationary membrane. Time-average holography is what is used to record the image of the vibrating membrane onto the holographic plate. A hologram is made *while* the membrane is vibrating, and the out of plane displacement is recorded on the plate as a series of interference fringes which record the position of the membrane averaged over all time. It is these images from which the permanent images of the vibration patterns are made. The experimental details will be discussed below in section 2.4.3. The next section will discuss applications of holography from the beginning to some of the more recent work.

2.3.1 Background

As mentioned above, Powell and Stetson were the first to use holographic interferometry for the analysis of vibrations. They made note of the necessity of having the entire holographic system mounted very rigidly to some sort of isolation bench that damps all mechanical room vibrations. This is especially necessary for experiments that record motion in a system or use double exposure holograms. Any shift in position of more than half a wavelength of the illuminating light results in a complete inability to resolve motion of the object. In their work, Powell and Stetson demonstrated that the resonant modes of vibration of a metal film can bottom can be observed using real time holographic interferometry. Their main goal was to determine what the effect of sinusoidal motion is on making a hologram. They showed that the concentric rings or fringes observed on the vibration patterns are not nodes of vibration, but loci of equal

amplitudes of vibration. A node of vibration is evidenced by a bright diametric or circular line which indicates a line of zero displacement.

Several excellent papers have been written on the development and uses of holographic techniques. Holographic interferometry has been used to do modal analysis on vibrating objects for about twenty five years. Its applications include the determination of resonant frequencies of objects with complicated geometries [25, 26, 27, 28, 29], the observation of resonance patterns on circular disks (confirming the predicted mode shapes) [22, 30, 31], and the observation of debonding and determination of Poisson's ratio in composite materials [32, 33]. Heflinger, et al. used holographic interferometry to record the shock waves of bullets passing through gases [23]. Other uses have included the study of heat and mass transfer in materials and flow field imaging [34, 35, 36, 37, 38].

Still other researchers have been interested in holographic interferometry as a purely metrological device [39, 40, 41, 42, 43]. Both in-plane and out-of-plane displacements can be measured using variations of holographic techniques. Holographic interferometry has also been used in the past as a tool for stress measurement. Most of these techniques used holographic interferometry to measure the displacement in a body and then used Hooke's Law or finite element methods and material property data to determine the stress [44, 45, 46, 47].

2.3.2 Theory

For the sake of completeness, it is necessary to include some of the basic theory behind holography, specifically holographic interferometry. Before explaining the concept of vibrating objects, however, it is necessary to understand the basic premise behind holography. A schematic of the holographic recording process is given in Figure

2.3. A beam of coherent light is split into two parts with a beam splitter (not shown). One part of the beam is directed at the object and then reflected onto the holographic plate. The other part of the beam (the reference beam) is sent directly to the plate without phase or amplitude change. Every point on the object reflects light as a spherical wavefront. In the diagram shown in Figure 2.3 light is shown reflecting from three of the many points on the object, for simplicity of illustration. This complex reflected wavefront combines at the plate with the reference beam and forms a complicated interference pattern containing phase and amplitude information about the object. The actual hologram looks nothing like the object, as can be seen from the simulated pattern in the upper right hand corner of the figure. The virtual image of the object is only seen by looking through the plate when it is illuminated using the reference beam. The holographic image appears superimposed on the object in the object plane, and is observable even when the object is removed from this plane.

The out of plane vibrations of an object can be simply described for the case of one point source of light interfering with the coherent beam. First, consider two planes of reference, A and B (see Figure 2.4), where A is a plane just in front of the object and B is the holographic plate (upon which the reference and the object beam converge). The complex scalar field scattered from the object is denoted as $S(x,y,z)$ for points to the right of plane A. The source of S can be expressed as a complex amplitude distribution $S(x,y,0) = S_0(x_0,y_0)$ in the plane A. If there is some time dependent variation in S_0 at the object, there will be a corresponding disturbance of $S(x,y,z)$ in plane B. These disturbances are denoted as $S_0(x_0,y_0,t) = S_{0t}$, and $S(x,y,z,t) = S_t$. The coherent reference beam is denoted as $A(x,y,z)e^{i\phi(x,y,z)}$ and is added to the field S_t at B yielding, $E(x,y,z,t) = Ae^{i\phi} + S_t$. The intensity of the image is simply the product of E and its conjugate E^*, and the image obtained over time is the time average of this product over the length of the exposure time of this product. This above analysis is the case for changes to the reflected
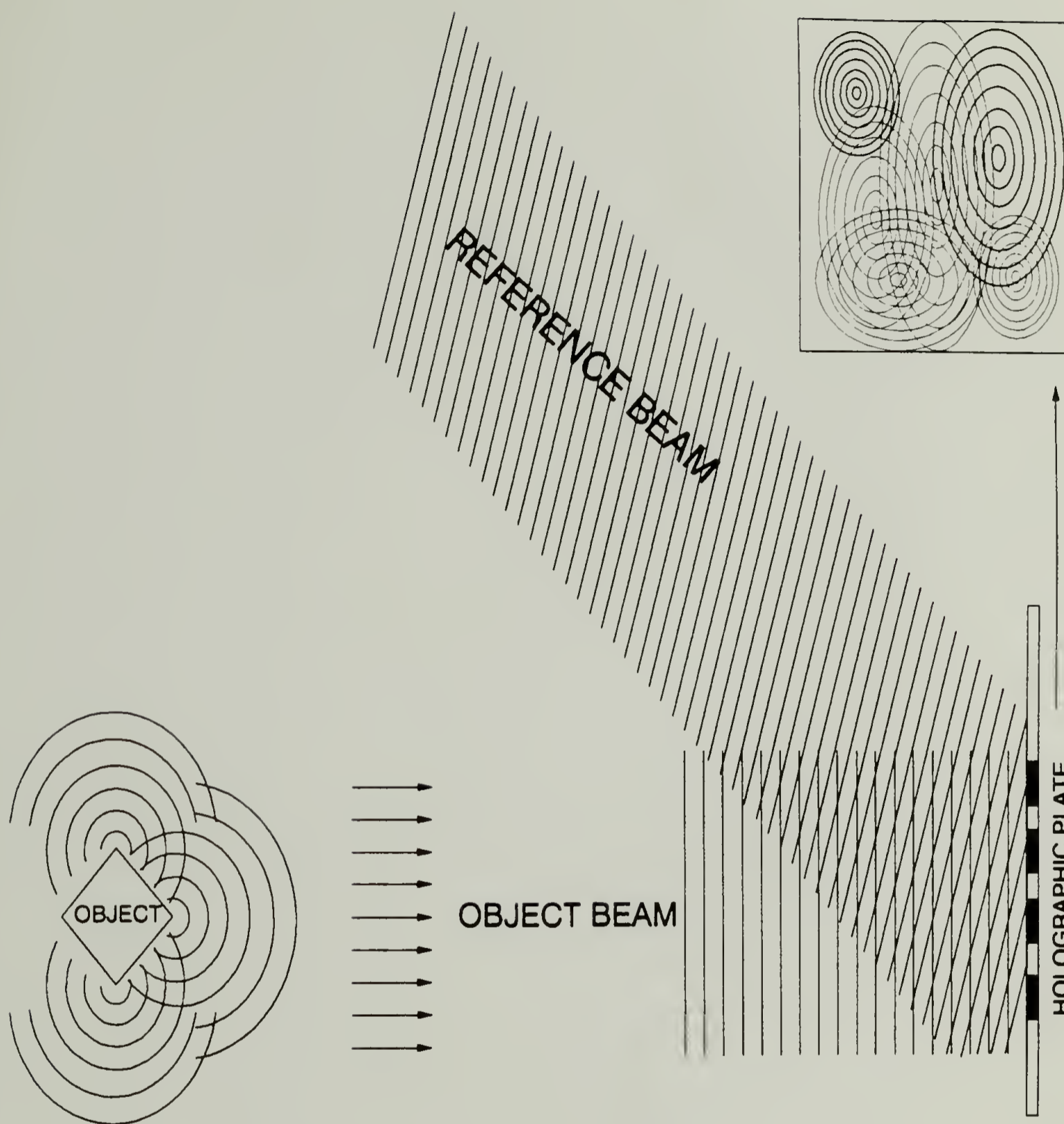
Figure 2.3   Schematic of the construction of a reflection hologram. The reference beam and the object beam are derived from the same coherent light source, passed through a beam splitter. The pattern in the upper right hand corner represents the actual hologram as recorded on the holographic plate.

light from a single point object as it interferes with the coherent beam. The more complex analysis can be found in [22] from which this was extracted.
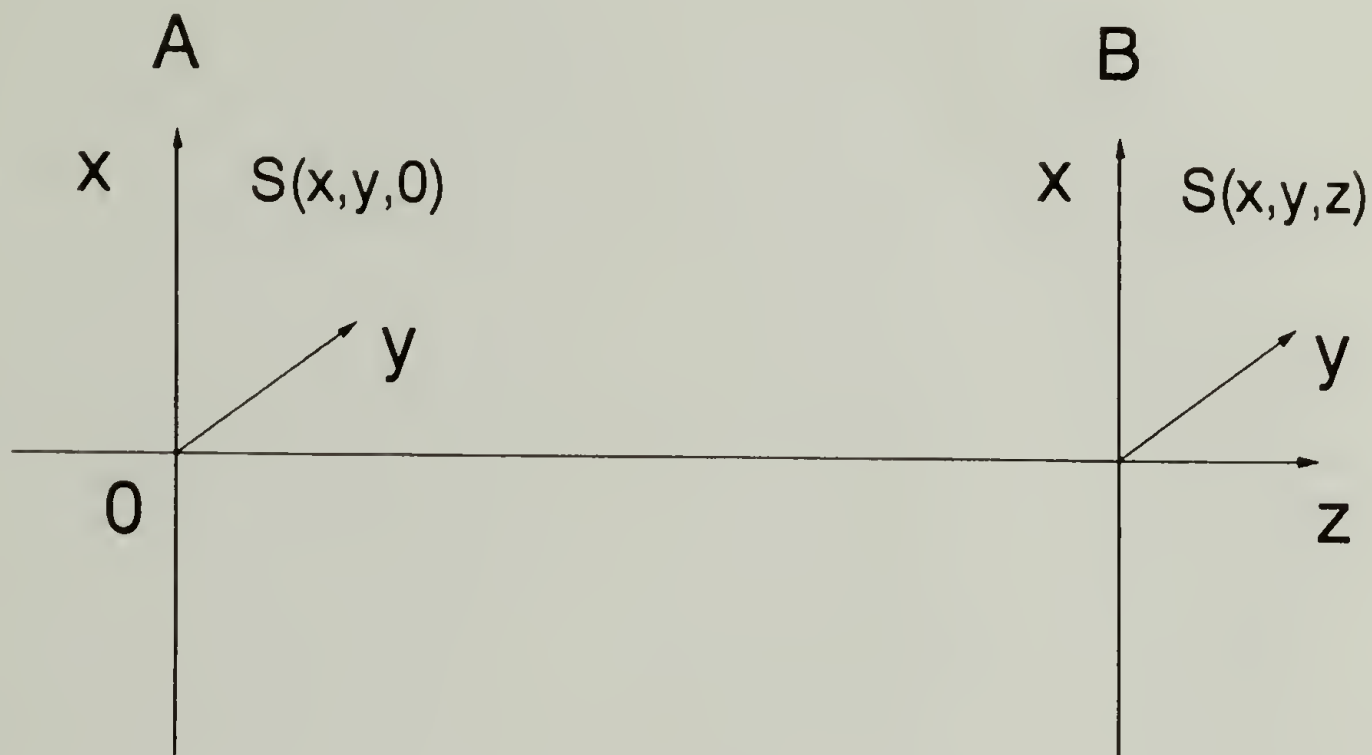
Figure 2.4   Diagram of the planes of reference for the description of time-average holography. Plane A is directly in front of the object, and plane B represents the holographic plate. S is a scalar field which represents the light reflected from an object.

2.3.3   Application to Stress Measurement

The materials studied in this dissertation are known to be under biaxial tensile stress subsequent to processing. In order to make membranes from these coating materials, either a portion of the substrate or the entire substrate (with the coating held in place by a rigid washer, or other frame, mounted on top) must be removed. It has been demonstrated by several authors that for bilayer or multilayer coating systems the state of stress in the entire system is one of self-equilibrating biaxial tension and compression

except in small boundary layers at the edges of the coating/substrate [17, 18, 48, 49, 50]. There are no normal or shear stresses between the coating and the substrate except in these boundary layers. Therefore, as discussed in chapter 1, the removal of a portion of the substrate does not affect the state of stress in the membrane. Once membranes are made in its manner, the in-plane tensile stress can be determined using a combination of vibrating membrane theory and holographic interferometry.

As discussed above in section 2.2.2, The stress in a membrane is directly proportional to the square of the product of the radius of the membrane and its resonant frequency and inversely proportional to the square of the zero of the Bessel function which describes its mode of vibration. Every ideal membrane has an infinite number of modes of vibration which occur at specific resonant frequencies at intervals corresponding to the increase in the zeroes of the Bessel functions. From each combination of resonant frequency and Bessel function zero which describes the vibration, a redundant value of stress should be obtained for a given membrane. The only way to unambiguously determine the modes of vibration for a large number of resonant frequencies is to use holographic interferometry. This gives a visual representation of each mode shape as the membrane vibrates, thus enabling the ascription of a zero of a particular order Bessel function to the resonant frequency at which the pattern appears. The correlation between vibration pattern and the order and zero of a Bessel function is described in Figure 2.5. Our technique has several benefits as compared to currently employed stress measurement techniques in that no linear elastic assumptions are necessary, and the only material parameter involved is the density, and several redundant measures of stress can be obtained. Another advantage of the vibrational imaging used in these experiments is that we are able to resolve the principal directions of stress in the plane of the film. Applications of the ability to resolve principal stress directions will be discussed in chapter 5.

m, n = 0, 1

m, n = 1, 1

m, n = 2, 1

m, n = 3, 1

m, n = 0, 2
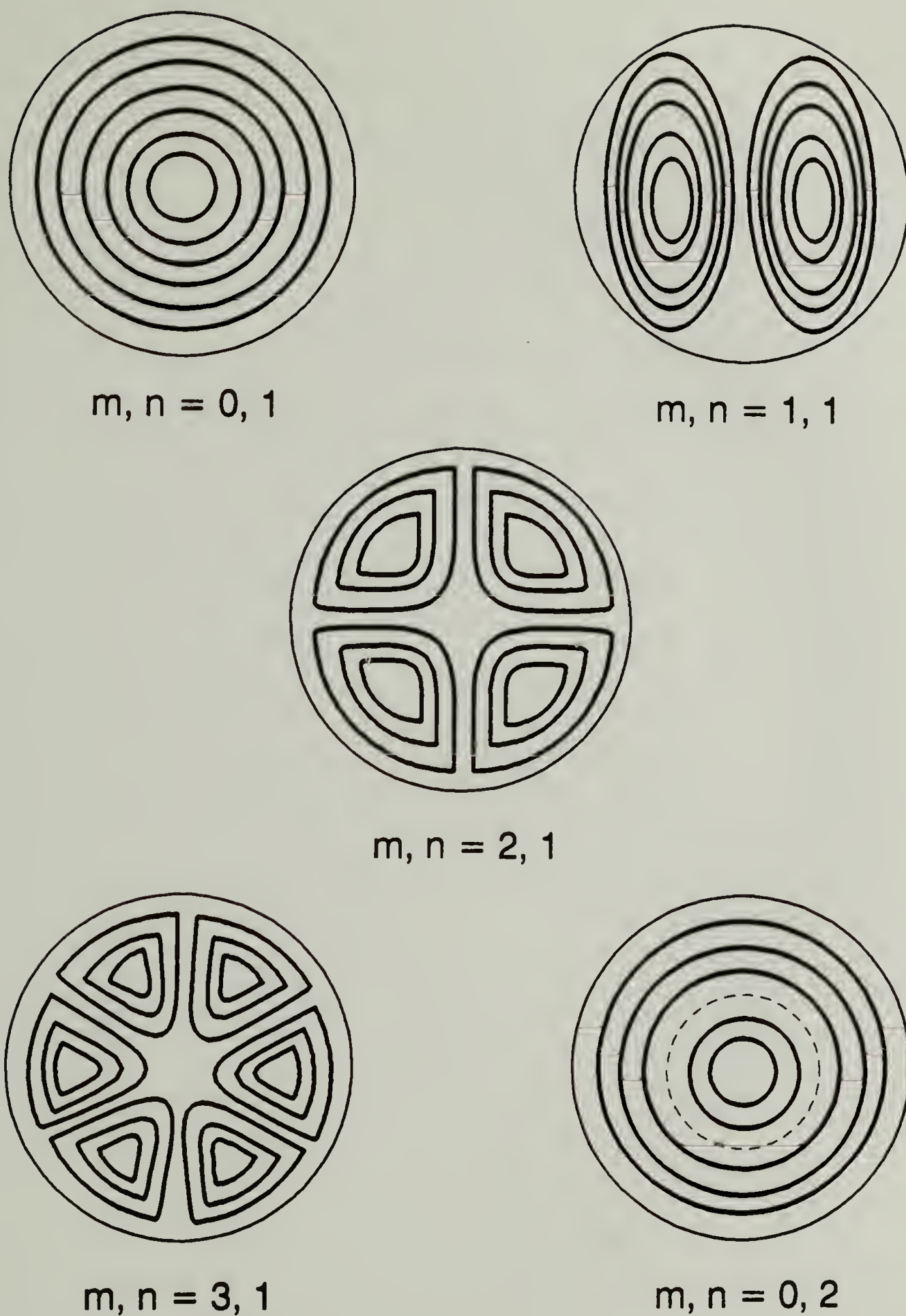
Figure 2.5   Schematic representations of the holographic patterns observed during the vibration of a membrane at its resonant frequencies and the corresponding nodal indices. The solid lines represent the radial nodes and the dotted lines represent the tangential nodes (points of zero displacement). The indices m and n represent the order of the Bessel function and the number of the zero of that Bessel function and are determined by counting the number of radial and tangential nodal lines respectively.

2.4   Experiments

The following sections describe the equipment which was built and used to perform the stress measurements on vibrating membranes, the techniques developed for making samples, and the method for determining the stress. The holographic equipment used in these experiments was assembled from components purchased from Newport Corporation. However, environmental chambers and fixtures were custom built to our specifications for use in controlled environment experiments. The use of holographic interferometry to determine the stress in coatings is unique to this work.

2.4.1   Equipment

The main requirements for a system which will physically shake a membrane at steadily increasing sinusoidal frequencies and record the vibration using the real-time holographic method described above are some kind of shaking device (speaker, transducer, etc..), a sine wave function generator, and amplifier, and a counter which accurately records the frequency of excitation, and the holographic equipment. The specifics of the set-up are described below. A membrane is placed in a fixture rigidly mounted to a Wilcoxon Research piezoelectric shaker, driven by a Wavetek Model 190 frequency generator connected to a Wilcoxon Research PA7 power amplifier. The frequency is monitored using a B & K Precision 80 Mhz frequency counter. An image of the stationary membrane is recorded on a thermoplastic holographic plate using a Newport Research Corporation HC301 holographic camera. The holographic image is seen through a security grade light sensitive video camera mounted so that it is looking through the holographic plate at the object and at the real image which is reconstructed by illuminating the holographic plate with the reference beam. The coherent light source used for this reflection hologram is a 5 mW helium-neon laser. A schematic and

photograph of the holographic setup are shown in Figures 2.7 and 2.8. The entire system is mounted on a small optical bench which is isolated from any mechanical room vibrations by several inflatable pillows underneath the bench. Isolation from vibration is critical in these experiments, as any displacement within the system of more than half a wavelength of the illuminating light source ($\lambda/2 \sim 3150$ Å) will cause a complete inability to resolve any subsequent motion of the membrane.

2.4.2   Sample Preparation

Two primary sample preparation techniques are used to prepare the membranes for testing. In the first, a thin copper sheet (~ 76 μm) is mounted on a 12.7 cm square glass plate (see Figure 2.8). Next, a polyamic acid solution is spin coated onto the copper substrate. The plates are cured to 230 °C under nitrogen. After curing, typical polyimide films are 10.0 ± 0.5 μm thick. The copper is removed from the glass and cut into four 6.3 cm square sections. The back of the copper sheet is then coated with positive photoresist using a Headway spin coating machine. Circular masks of 3.0, 4.0, and 5.0 cm in diameter are used to expose the photoresist. The resist is then developed and rinsed in a NaOH solution, removing the undeveloped areas. The exposed copper is then etched away using a 10M HCl/CuCl solution. After etching, the sample is rinsed with water and dried at 200 °C. The resulting specimen consists of a circular membrane of polyimide supported on a copper frame.

In the second fabrication technique, steel sheet coated with a thin layer of tin is used as a substrate (see Figure 2.9). A polyamic acid solution is spin coated onto a 12.7 cm square plate. The samples are then cured to 225 °C (a few degrees below the melting point of tin).
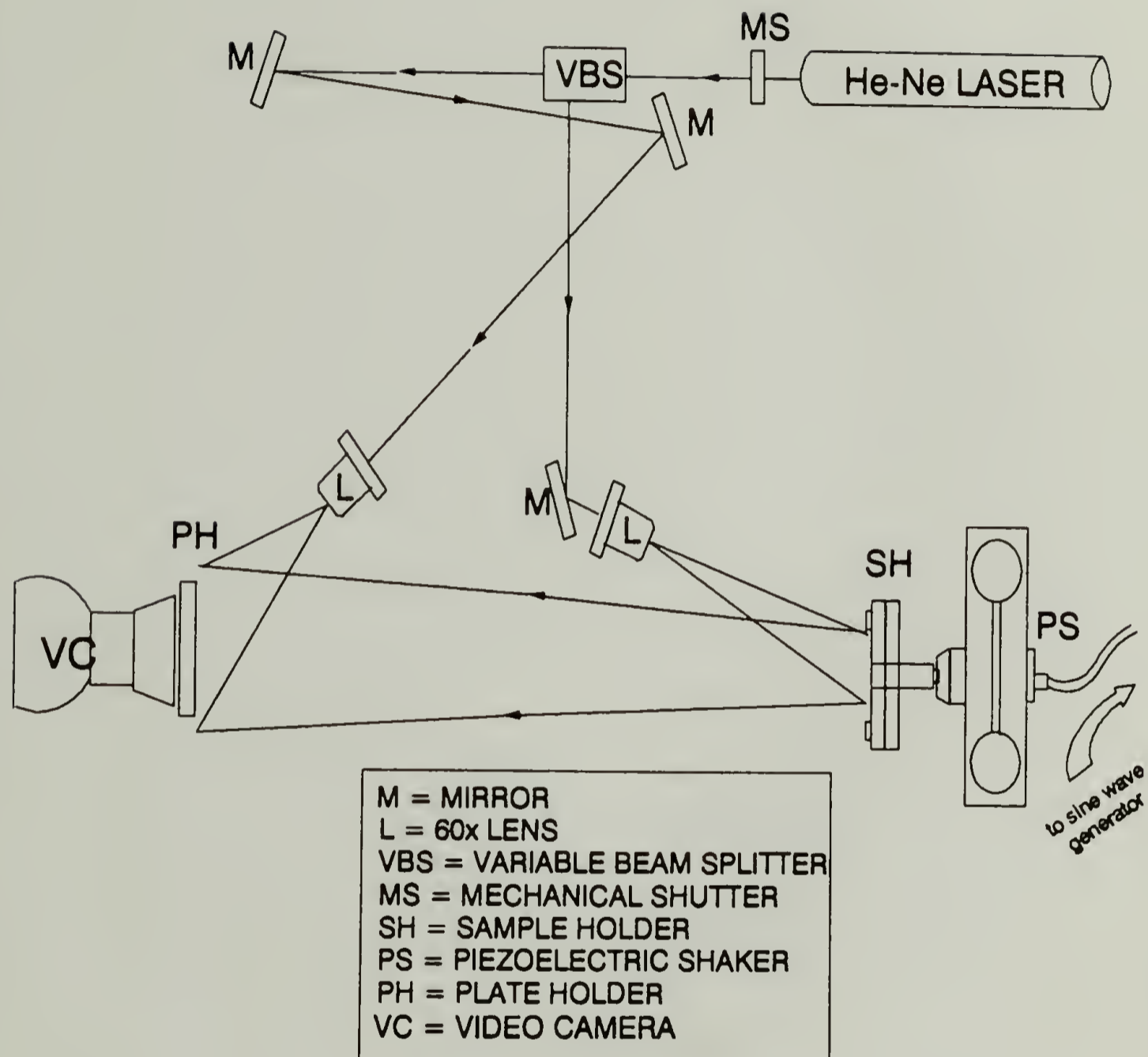
Figure 2.6   Holographic equipment - schematic of the holographic interferometry equipment set-up used in the real-time holographic interferometry experiments. The video camera is connected to a monitor on which the real time vibration patterns are observed, and to a video processor on which hard copies of the vibration patterns are obtained.

Figure 2.7   Holographic equipment - photograph of the holographic interferometry
set-up used in the real-time holographic interferometry experiments.
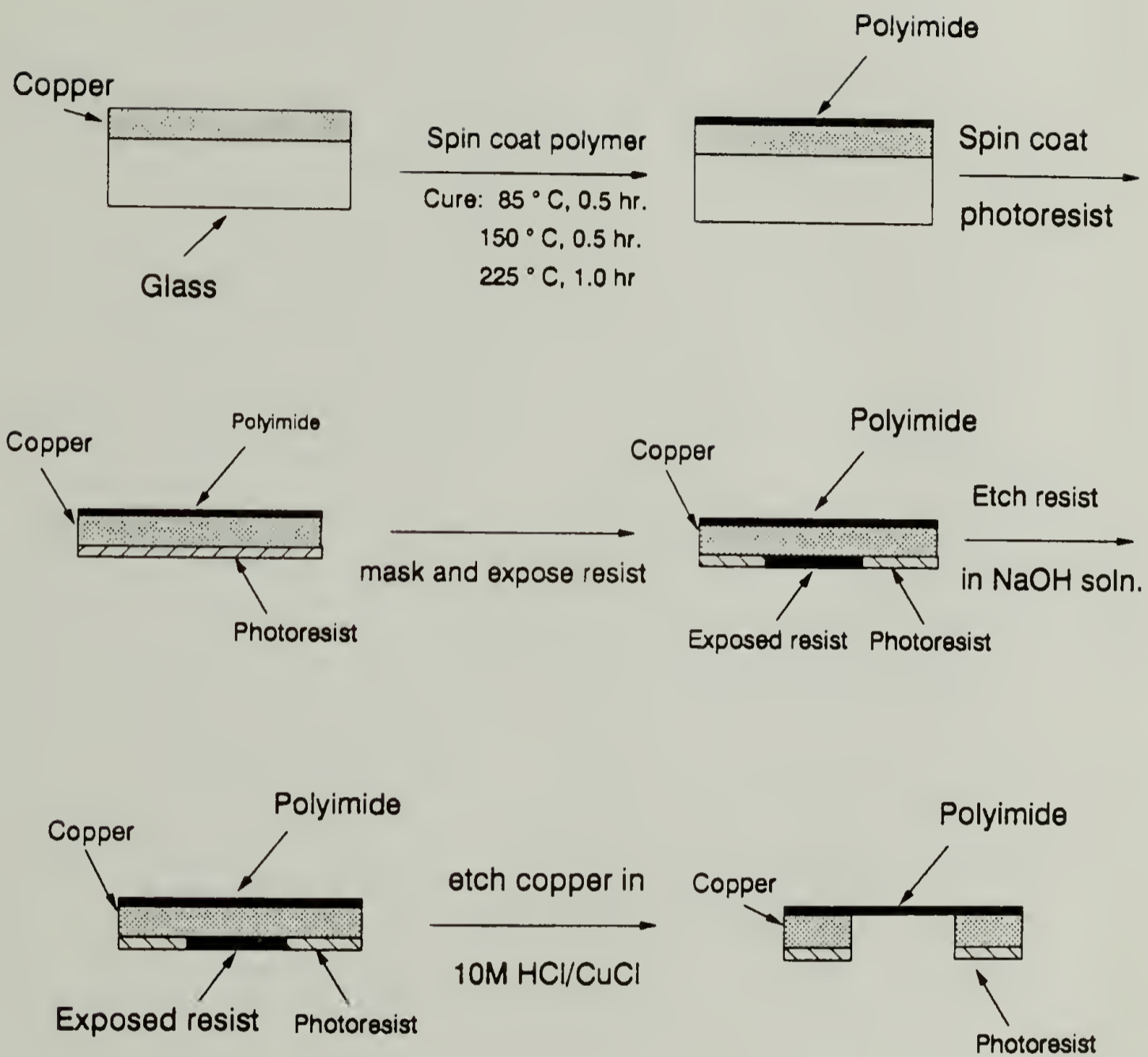
Figure 2.8   Schematic diagram of the process used to make polyimide membranes. These samples are supported on 80 μm thick copper substrates.
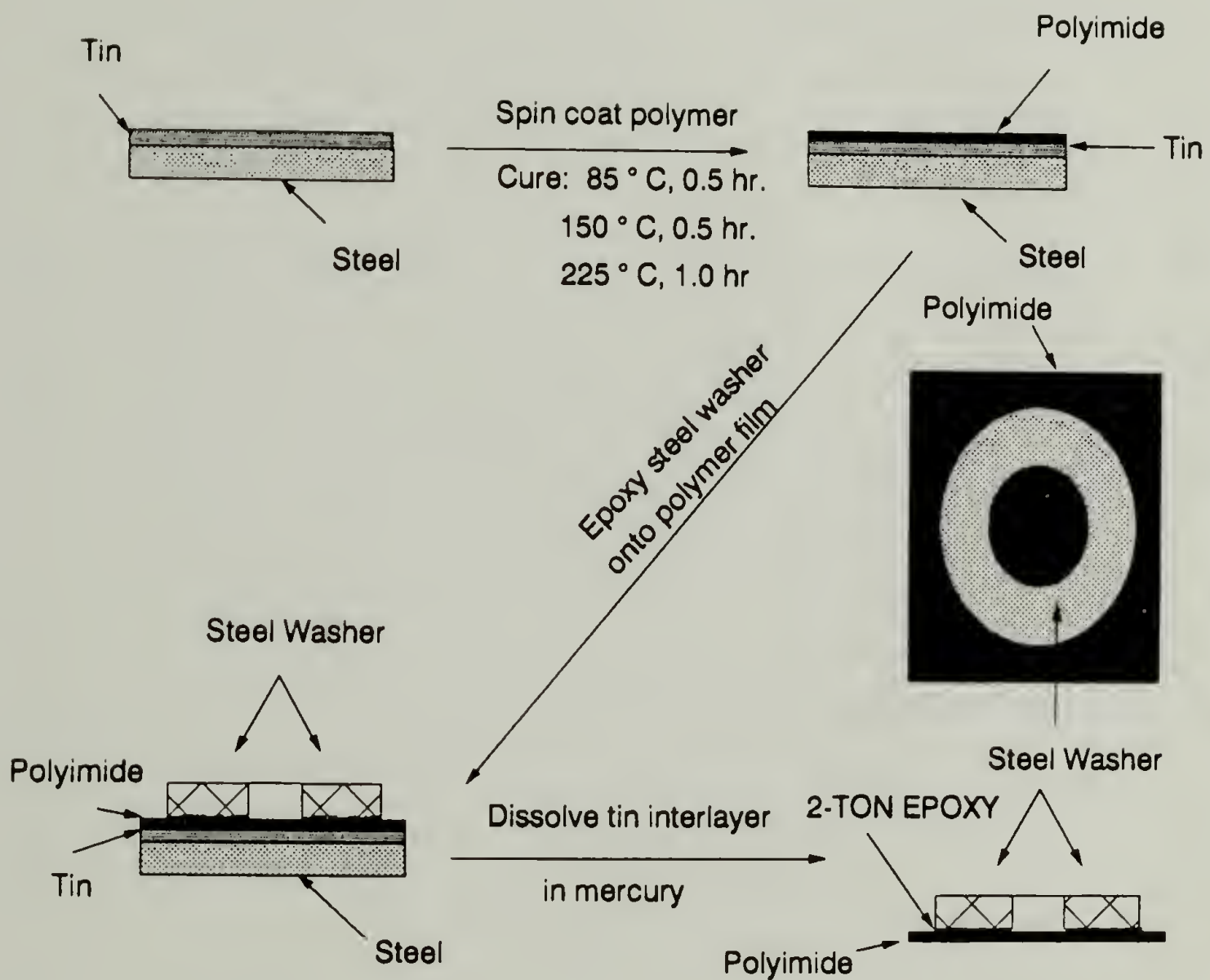
Figure 2.9   Schematic diagram of the process used to make polyimide membranes. These membranes are supported on 1 mm thick steel washers.

Steel washers (of radii from 0.95 - 2.54 cm) are mounted with epoxy on top of the polyimide. After scoring the polyimide film around the outside of the washers, the plate is placed in a mercury bath. The mercury forms an amalgam with the layer of tin between the polyimide and the steel, and the polyimide film attached to the washer can be easily lifted from the plate. This method was first used to make free standing films of phenolic varnishes [51]. Variations on this technique include steel sheets coated with silver which is also soluble in mercury, use of a water soluble material as a substrate, or the removal of a film from a silicon wafer with a SiO_2 layer on top which can be etched away with hydrofluoric acid solution.

2.4.3 Experimental Method

The membrane on its frame is mounted rigidly in a fixture which is connected to the piezoelectric transducer, all of which is situated on the isolation bench as part of the holographic set-up. First, a hologram is made of the membrane while it is stationary. Then, using the frequency generator, the frequency of vibration of the sample is increased steadily until a resonant frequency of the membrane is reached. This point is evident from the appearance of a vibration pattern superimposed on the object. The pattern is visible when looking through the holographic plate with a video camera and monitor at the static hologram superimposed on the vibrating membrane. Samples of vibration patterns are shown in Figure 2.10. The concentric light and dark fringes are lines of equal displacement and the sharp white tangential or radial lines are the nodes of vibration (where the out-of-plane displacement is at all times zero). The number of tangential and diametral nodes indicates which zero of which Bessel function corresponds to a particular resonant frequency. The resonant frequency, along with the mass per unit volume and the radius of the membrane and the Bessel function zeroes are used to calculate the biaxial stress in the coating.

m, n = 0,1

m, n = 1,1

m, n = 2,1

m, n = 3,1
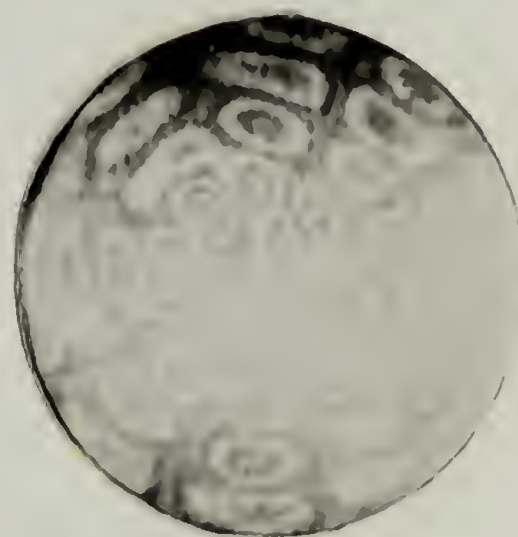
m, n = 4, 4

Figure 2.10   Vibration patterns (time-average holographic interferograms) of a PMDA-ODA polyimide membrane with a stress of ~ 10 MPa.

2.5   Results and Discussion

Early experiments performed on vibrating membranes make a very good case for the utility of the holographic/vibrational stress measurement technique. In one such experiment, a biaxially stretched rubber membrane was excited to its resonant frequencies by a speaker placed behind it driven at increasing sinusoidal frequencies. The response of the membrane was monitored using a small microphone mounted in foam rubber (to damp out room noises) and placed close to the front of the membrane. The amplitude of the response as a function of excitation frequency was monitored on an oscilloscope and is shown in Figure 2.11. The maxima in amplitude in this case do not occur at the theoretically predicted intervals of the zeros of Bessel functions, and therefore, would not yield correct values of stress in the membrane. This is most likely due to the fact that the measurements are conducted in air, and air damping effects cause resonant vibrations to occur at lower frequencies than normal. The air damping effect will be discussed in detail in chapter 3. Measuring the resonant frequencies using the speaker/microphone technique has two distinct drawbacks which preclude its use in stress measurement experiments. The measurements must be done in air in order for the speaker vibrations to be transmitted to the membrane. Additionally, it is impossible to positively distinguish the first from the second, or third, or fourth mode of vibration of the membrane because the pattern cannot be seen. The use of holographic interferometry to observe the vibration of a membrane eliminates the ambiguity present in other methods which use photonics or magneto-electric detectors which cannot positively identify a given mode of vibration.

In Figure 2.12, a plot of stress vs mode number (an integer assigned to the modes of vibration in the order that they appear) for a PMDA-ODA membrane cured to 400°C shows that when experiments are done under vacuum, the membrane vibration behavior conforms to theory and each resonant frequency yields a redundant measure of stress

48

with a standard deviation of about 1 %. For this sample, we were able to observe vibration patterns as high as the thirty-fifth mode of vibration.
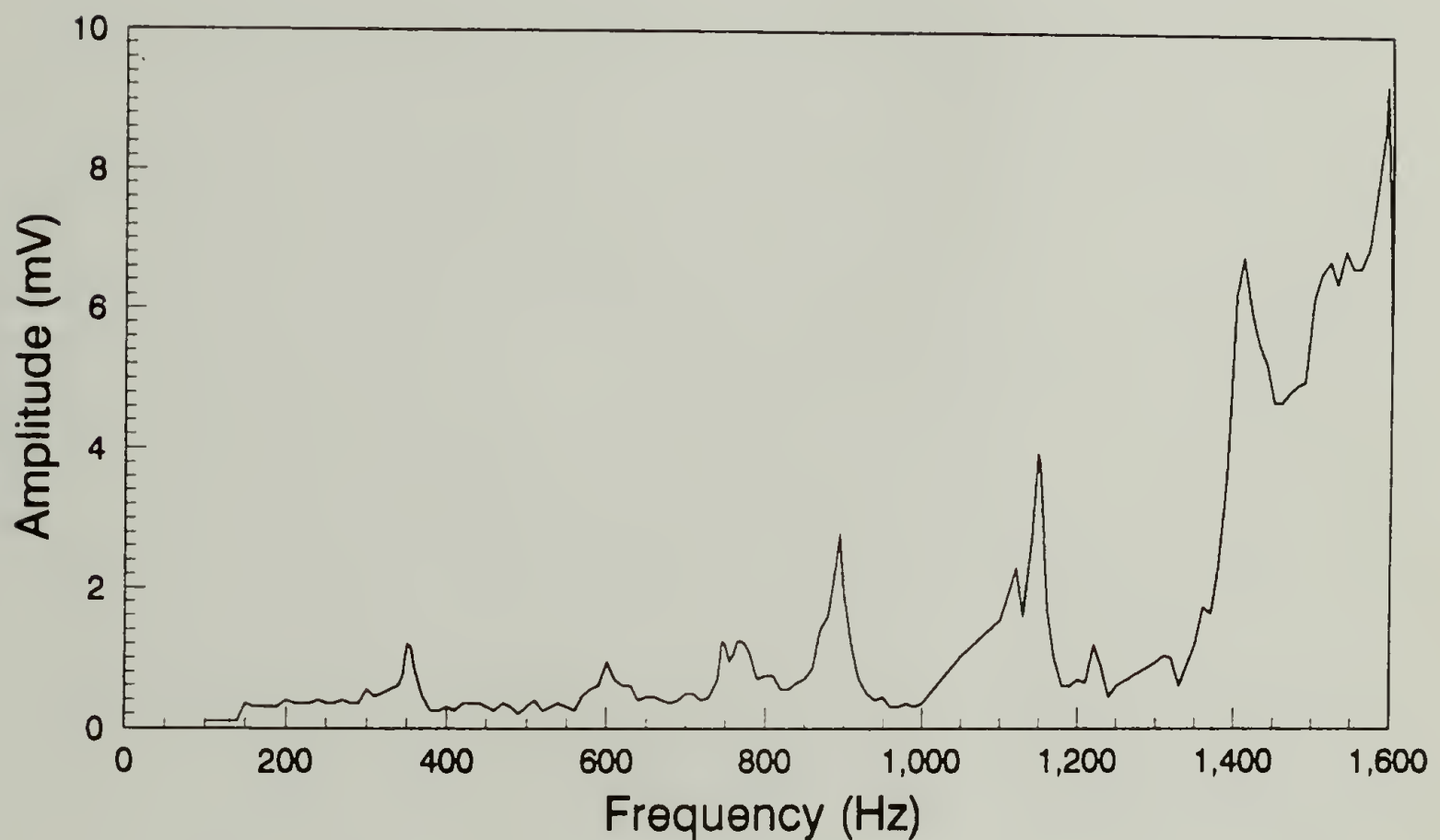
Figure 2.11   A plot of amplitude of vibration detected as a function of frequency (Hz) for a rubber membrane of radius 1.59 cm. The membrane was excited in air from behind by a speaker which was driven at a steadily increasing sinusoidal frequency. At resonant frequencies, an increase in the amplitude of vibration can be seen, however, the peaks cannot be matched with any degree of certainty to their mode of vibration (and thus to the correct Z_{mn} value).
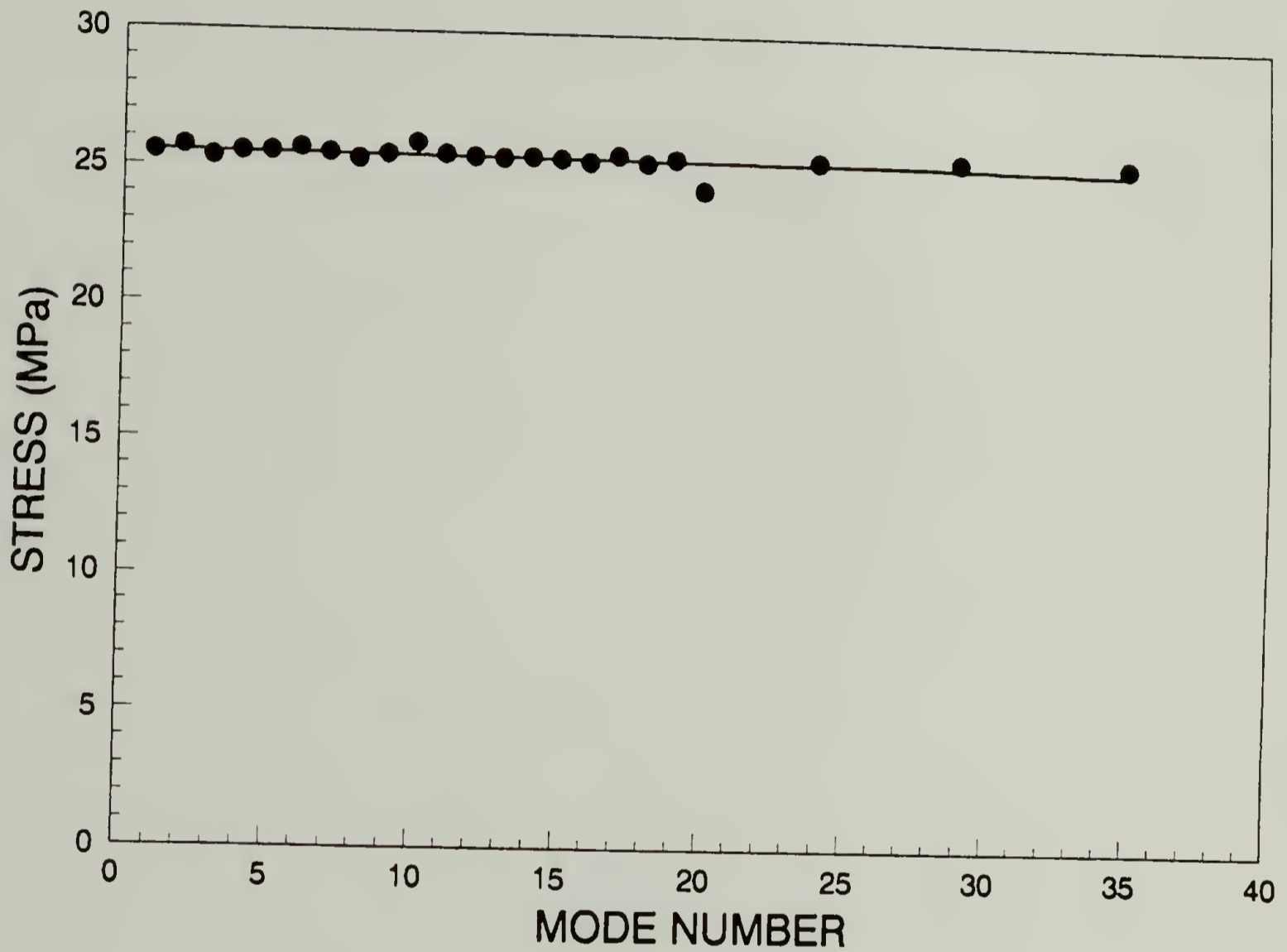
Figure 2.12   Stress as a function of mode number for a PMDA-ODA material cured to 400° C on a silicon substrate. Sample was tested in vacuum. Each resonant frequency yields a redundant stress value (to ~ 1.0% standard deviation).

A summary of the stress values and their corresponding mode number, m and n values, and frequency of vibration is given in Table 2.2. The mode number is simply an integer, 1, 2, 3,...which indicates the sequence of the modes of vibration of the membrane, and corresponds to an increase in resonant frequency.

Table 2.2   Value of stress, resonant frequencies, mode numbers and m and n values for PMDA-ODA membrane tested in vacuum. (See Figure 2.12).

Mode Number	m,n	ω_{mn} (radians/sec)	Stress (MPa)
1	0,1	25384	25.51
2	1,1	40583	25.71
3	2,1	54023	25.34
4	0,2	58295	25.54
5	3,1	67387	25.55
6	1,2	74305	25.69
7	4,1	80085	25.53
8	2,2	88505	25.32
9	0,3	91332	25.51
10	5,1	92639	25.92
11	3,2	103044	25.53
12	6,1	104936	25.46
13	1,3	107191	25.43
14	4,2	116679	25.47
15	7,1	117093	25.42
16	2,3	122189	25.32
17	0,4	124589	25.57
18	8,1	128981	25.31
19	5,2	130144	25.48
20	3,3	137394	24.36
24	4,3	151557	25.47
29	5,3	165870	25.56
30	5,4	200446	25.54

Average Stress: 25.45
Standard Deviation: 0.290

In Figure 2.13 a plot of the calculated stress (in MPa) vs the mode number of the resonant vibration of two polyimide membranes is shown. These experiments were performed in air. These samples were made from the same coating which was made on a tin-coated steel sheet. The radius of both membranes is 1.3 +/- 0.05 cm and the thickness is about 10 +/- 0.1 μm. There are two important aspects to note in this data. The experiments were done in air, and show that air damping noticeably lowers the resonant frequecies of vibration. The data represented by the solid circles is from a sample which contained a slight flaw in its surface which explains the lower stress values. Imperfections in samples cause a noticeable distortion of the vibration patterns, and if large enough, render the patterns incomprehensible. This also occurs if the sample is poorly bonded at its perimeter to the washer. Thus it is possible to characterize a sample as "bad" or "good" by observation of the vibration patterns. Data from "bad" samples are discarded.

The air damping effect is discussed at great length in the next chapter. Plots comparing measurements made in air and in vacuum for the same sample are presented along with theory and computer programs written to relate measurements made in air to those made in vacuum. It is important to understand the air damping effects, so that one may conduct experiments in air or some other atmosphere and determine the influence of the environment on the stress in the film.
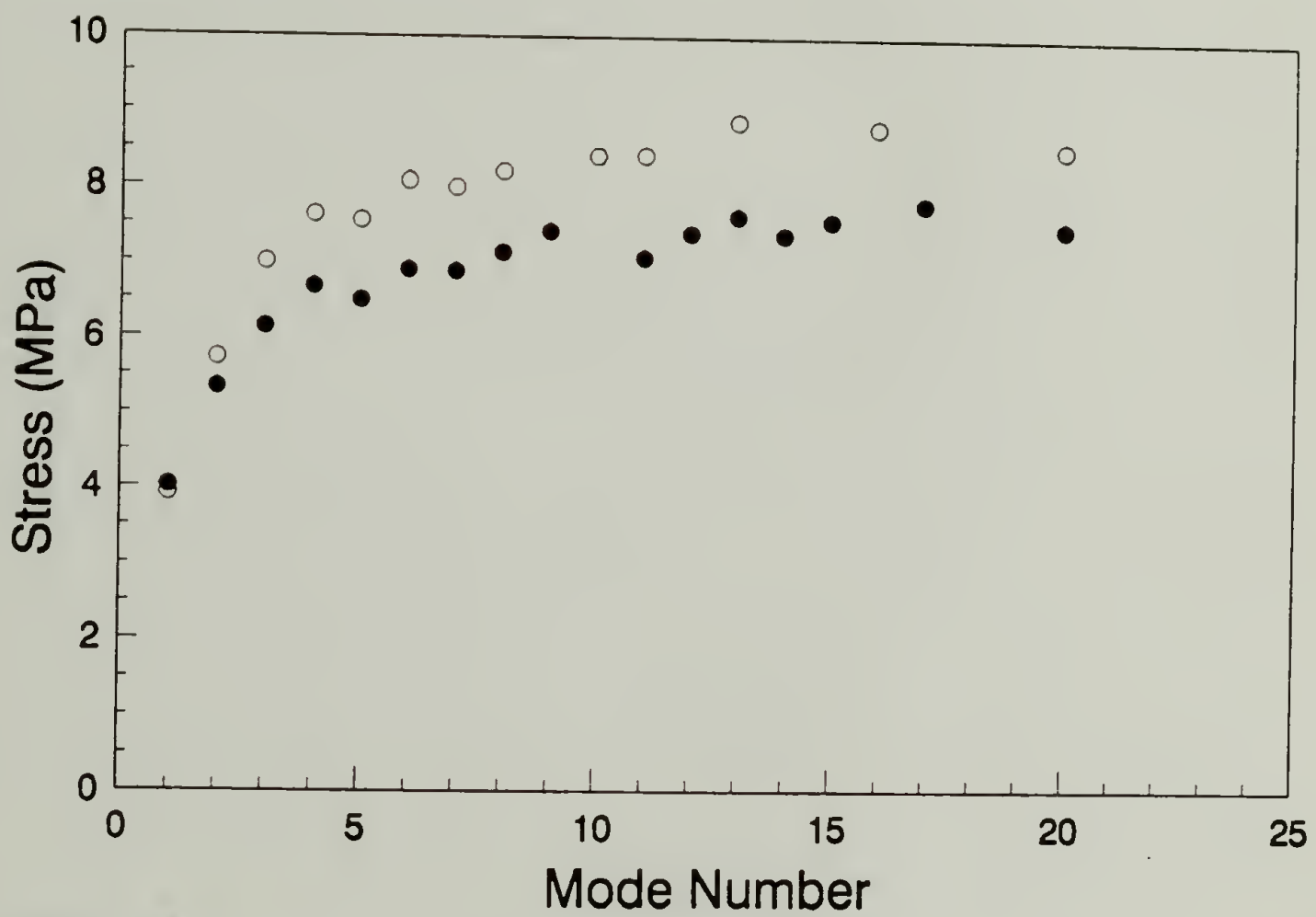
Two Samples
Mounted on Steel Washers
R = 1.27 cm

Figure 2.13   Plot of calculated stress vs mode number for two PMDA-ODA samples which were taken from the same tin plated steel sheet (see Figure 2.9). The radius of both membranes is 1.27 cm and the thickness is about 10 μm.

REFERENCES

1. R. B. Lindsay, preface, *The Theory of Sound,* by J. W. Strutt, 3rd Baron Rayleigh, (New York: Dover Publications, 1945).

2. R. B. Lindsay, *Acoustics: Historical and Philosophical Development,* (Stroudsburg, PA: Dowden, Hutchinson and Ross, Inc., 1966).

3. G. Galilei, *Dialogues Concerning Two New Sciences,* (1638), in *Acoustics: Historical and Philosophical Development,* ed. R. B. Lindsay, (Stroudsburg, PA: Dowden, Hutchinson and Ross, Inc., 1966).

4. B. Taylor, "De Motu Nervi Tensi," *Philosophical Transactions of the Royal Society,* **28**, 11 (1713), in *Acoustics: Historical and Philosophical Development,* ed. R. B. Lindsay, (Stroudsburg, PA: Dowden, Hutchinson and Ross, Inc., 1966).

5. E. F. F. Chladni, *Die Akustik,* (Leipzig: Breitkopf & Hartel, 1802).

6. S. D. Poisson, "Mémoire sur L'équilibre et le Mouvement des Corps Élastiques," *Mémoires de L'Academie de la Royale Institute des Sciences du France,* **8**, 357 (1829), from R. B. Lindsay, "The Story of Acoustics," *Journal of the Acoustical Society of America,* **39**(4), 629 (1966).

7. R. F. A. Clebsch, *Theorie der Elasticität Fester Körper,* (B. F. Teubner, Leipzig, 1862), from R. B. Lindsay, "The Story of Acoustics," *Journal of the Acoustical Society of America,* **39**(4), 629 (1966).

8. M. J. Bourget, "Memoire sur le Mouvement Vibratoire des Membranes Circulaires," *Annales Scientifiques d'Ecole Normale Superieure,* **III**, 55 (1866).

9. M. Kak, "Can One Hear the Shape of a Drum?," *American Mathematics Monthly,* **73**, 1 (1966).

10. K. Stewartson, and R. T. Waechter, "On Hearing the Shape of a Drum: Further Results," *Proceedings of the Cambridge Philosophical Society,* **69**(2), 353 (1971).

11. M. E. Taylor, "Estimate on the Fundamental Frequency of a Drum," *Duke Mathematical Journal,* **46**(2), 447 (1979).

12. H. P. W. Gottlieb, "Hearing the Shape of an Annular Drum," *Journal of the Australian Mathematical Society, B,* **24**(4), 435 (1983).

13. M. H. Protter, "Can One Hear the Shape of a Drum?: Revisited," *SIAM Review,* **29**(2), 185 (1987).

14. G. Arfken, "Bessel Functions," *Mathematical Methods for Physicists, 3rd ed.*, Chapter 11, p. 572, (New York: Academic Press, 1985).

15. A. W. Leissa, *Vibration of Thin Plates*, NASA Publication SP-160, (Washington, D. C.: NASA, 1969).

16. Q. K. Tong, and R. J. Farris, *"Measurement of Two-Dimensional Stresses in Thin Polymer Films Using Holographic Interferometry,"* submitted for publication, (1990).

17. B. J. Aleck, "Thermal Stresses in a Rectangular Plate Clamped Along an Edge," *Journal of Applied Mechanics*, **16**, 118 (1949).

18. M. S. Hess, "The End Problem for a Laminated Elastic Strip - II. Differential Expansion Stresses," *Journal of Composite Materials*, **3**(10), 630 (1969).

19. D. Gabor, "A New Microscopic Principle," *Nature*, **161**(4098), 777 (1948).

20. D. Gabor, "Holography, 1948-1971," *Science*, **177**(4046), 299 (1972).

21. E. N. Leith, and J. Upatnieks, "Photography by Laser," *Scientific American*, **212**(6), 24 (1965).

22. R. L. Powell, and K. A. Stetson, "Interferometric Vibration Ananlysis by Wavefront Reconstruction," *Journal of the Optical Society of America*, **55**(12), 1593 (1965).

23. L. O. Heflinger, R. F. Wuerker, and R. E. Brooks, "Holographic Interferometry," *Journal of Applied Physics*, **37**(2), 642 (1966).

24. K. S. Pennington, "Advances in Holography," *Scientific American*, **218**(2), 40 (1968).

25. R. J. Parker, D. G. Jones, "Holography in an Industrial Environment," *Optical Engineering*, **27**(1), 55 (1988).

26. B. Sharpe, "Fringe Benefits of Hologram Views," *Industrial Photography*, 36(8), A28 (1987).

27. R. Garza and B. Sharpe, "Holography for Non-Contact Structural Analysis," *Sensors*, September 1986.

28. C. F. Lewis, "What's Wrong in This Picture?," *Materials Engineering*, **106**(1), 49 (1989).

29. R. J. Pryputniewicz, "Time Average Holography in Vibration Analysis," *Optical Engineering*, **24**(5), 843 (1985).

30. A. D. Wilson, and D. H. Strope, "Time-Average Holographic Interferometry of a Circular Plate Vibrating Simultaneously in Two Rationally Related Modes," *Journal of the Optical Society of America*, **60**(9), 1162 (1970).

31. C. E. Taylor, "Holography," *Experimental Mechanics*, **19**(9), 339 (1979).

32. M. Kimoto, I. Nagata, A. Minowa, K. Moriwaki, T. Watanabe, "Evaluation of Disbondings and Measurement of Poisson's Ratio for Plastic Composites Using Holographic Interferometry," *Journal of Applied Polymer Science*, **40**(7), 1085 (1990).

33. I. Yamaguchi, and H. Saito, "Application of Holographic Interferometry to the Measurement of Poisson's Ratio," *Japanese Journal of Applied Physics*, **8**(6), 768 (1969).

34. G. H. Kaufman, and C. M. Vest, "Thermal Waves Visualized by Holographic Interferometry," *Applied Optics*, **26**(14), 2799 (1987).

35. A. Ito, and T. Kashiwagi, "Measurement Technique for Determining the Temperature Distribution in a Transparent Solid Using Holographic Interferometry," *Applied Optics*, **26**(5), 954 (1987).

36. D. Tentori, and M. Celaya, "Film Deposit Assessment with Hologram Interferometry," *Applied Optics*, **25**(16), 2707 (1986).

37. Y. H. Yu, J. K. Kittleson, "Measuring Flow by Holographic Interferometry," *NASA Technical Briefs*, July/August, 60 (1988).

38. J. D. Trolinger, "Outlook for Holography Strong as Applications Achieve Success," *Laser Focus/Electro-Optics*, **22**(7) 82 (1986).

39. C. A. Sciammarella, and J. A. Gilbert, "A Holographic-moiré Technique to Obtain Separate Patterns for Components of Displacement," *Experimental Mechanics*, **14**(6), 215 (1976).

40. J. A. Gilbert, and J. W. Herrick, "Dual-beam Holographic Deflection Measurement," *Experimental Mechanics*, **21**(9), 349 (1981).

41. J. A. Gilbert, and J. W. Herrick, "Holographic Displacement Analysis with Multimode-fiber Optics," *Experimental Mechanics*, **21**(8), 316 (1981).

42. J. A. Gilbert, and G. A. Exner, "Holographic Displacement Analysis Using Image-plane Techniques," *Experimental Mechanics*, **18**(10), 382 (1982).

43. L. Pirodda, "Conjugate Wave Holographic Interferometry for the Measurement of In-plane Deformations," *Applied Optics*, **28**(10), 1842 (1989).

44. M. J. Engelstad, D. A. Chambless, W. F. Swinson, and J. L. Turner, "Hybrid Stress Analysis of Vibrating Plates Using Holographic Interferometry and Finite Elements," *Experimental Mechanics*, **27**(1), 23 (1987).

45. R. J. Sanford, "Photoelastic Holography - A Modern Tool for Stress Analysis," *Experimental Mechanics*, **20**(12), 427 (1980)

46. R. O'Regan, and T. D. Dudderar, "A New Holographic Interferometer for Stress Analysis," *Experimental Mechanics*, **9**(6), 241 (1971).

47. R. J. Sanford, "Differential Stress-Holo-Interferometry," *Experimental Mechanics*, **11**(8), 330 (1973).

48. E. Suhir, "An Approximate Analysis of Stresses in Multilayered Elastic Thin Films," *Journal of Applied Mechanics*, **55**(1), 143 (1988).

49. A. Jagota, C. Y. Hui, "Mechanics of Sintering Thin Films - I. Formulation and Analytical Results," *Mechanics of Materials*, **9**, 107 (1990).

50. M. A. Maden, A. Jagota, S. Mazur, R. J. Farris, "Vibrational Technique for Stress Measurement in Films - I. Ideal Membrane Behavior," Submitted for publication in *Journal of Materials Research*, (1991).

51. M. Yaseen and H. E. Ashton, " Effect of Free Film Preparation Method on Physical Properties of Organic Coatings," *Journal of Coatings Technology*, **49**(629), 50 (1977).

CHAPTER 3

COMPLICATING FACTORS - AIR DAMPING AND STIFFNESS EFFECTS

3.1 Introduction

In this chapter, the focus is on the effects which cause a membrane to resonate non-ideally in response to an applied sinusoidal vibration. One of these effects was demonstrated at the end of chapter 2, where data from a membrane vibrating in air was presented. It is apparent from Figure 2.7 that somehow, the resonant frequencies deviate from their prescribed behavior (i.e., that each resonant frequency should yield a redundant stress value as calculated using equation (2.6)). Upon further investigation, it was found that this effect is a known phenomenon, sometimes referred to as air damping or mass loading. The mass loading of the medium on the membrane does not actually lower the stress in the film, but offers resistance to vibration thereby lowering the frequency at which the membrane resonates (causing erroneous stress calculations). Lax [1] however, derived an iterative formula based on the geometry of the sample which relates the resonant frequency measured in air to the frequency at which resonance would occur in a vacuum for circularly symmetric vibrations (m = 0). Using this correction for data taken in air, one can calculate the theoretical resonant frequency which would be measured in vacuum (thus obtain the true stress in the membrane). Another more simplistic model proposed by Karnezo [2] is also discussed and compared to results of the work done by Lax [1] and Gottlieb and Aebischer [3].

The second instance in which a membrane exhibits non-ideal vibration behavior is when it approaches plate conditions. This case has been treated in detail by Tong and others [4, 5, 6].For a membrane, the restoring force which acts on the vibrating membrane is completely due to the in-plane tensile stress. However, the restoring force

for the vibration of a plate is usually dominated by bending. A membrane begins to behave like a plate when a.) the radius to thickness ratio decreases "sufficiently" (to be defined in later sections) and/or .b.) the stiffness of the material is high. The stiffness effect will be discussed in detail in section 3.3 for silver samples of various geometries under uniform tensile stress.

3.2.1   Lax's Correction

The questions may be asked, "Why is it important to be able to correlate the resonant frequencies of membranes vibrating in air to their ideal resonant frequencies when measured under vacuum?," and "Why not simply perform all experiments under vacuum and directly calculate the stress values from this data?" The answer to these questions is that in the measurement of stresses in coatings, it is also desirable to be able to measure the stress as a function of humidity and temperature, as well as in other environments to which coatings may be exposed during processing. Because the density of the surrounding medium has an effect on the resonant frequencies of a membrane, it is important to be able to correct for this "air damping" to obtain more accurate stress values. Lax proposed a solution to this problem in 1944 [1], an outline of which is given below.

When the effect of air damping on the vibration of a membrane is taken into account, the initial equation of motion must be modified to include a pressure term on the right hand side.

$$\sigma \nabla^2 u \;=\; \rho \frac{\partial u^2}{\partial t^2} - \frac{P(r,\theta,t)}{h} \tag{3.1}$$

where $P(r,\theta,t)$ represents external loading, and is the pressure exerted by the surrounding medium on the membrane, u is the out-of-plane displacement of the vibrating membrane, ρ is the density, σ is the biaxial stress, and r and θ are the radial and tangential coordinates of position on the membrane. The analysis is restricted to the circularly symmetric modes for which the pressure can be written in terms of an integral of acceleration over the surface of the membrane (Rayleigh's integral [7]). The velocity of the vibrating membrane is written as a series expansion in terms of the eigenmodes of vibration in vacuum and is used along with Rayleigh's integral to obtain an expression for the pressure of the form,

$$p(r, t) = e^{i\omega t} \sum_{n=1}^{\infty} \sum_{m=1}^{\infty} b_n \rho_o c_o \alpha_{mn}(\omega) u_m(r) \tag{3.2}$$

where α_{mn} is the normalized acoustic impedance coupling the mth membrane mode to the nth pressure component, ρ_o is the density of air, ω is the resonant frequency of vibration, b_n is a coefficient of   and c_o is the speed of sound in air. The acoustic impedance consists of a radiation mass, m_{mn}, and radiation resistance, r_{mn}:

$$\alpha_{mn} = r_{mn} + i\,f\,m_{mn} \tag{3.3}$$

where $f = \omega R/c_o$, and $i = \sqrt{-1}$. Combining equations (3.2) and (3.3) with the equation of motion, (3.1) yields linear equations with coefficients b_n, which include the angular frequency, ω_{mn}, and can be written in terms of two dimensionless constants, f, and $f_n = \omega_{0n} R/c_o$,

$$[\,f^2 - f_n^2 - i\,\beta\,f\,\alpha_{mn}(f)\,]\,b_n = i\,\beta\,f \sum_{m \neq n} \alpha_{mn}(k)\,b_m \tag{3.4}$$

where β is a dimensionless parameter $\rho_0 R/\rho h$. This system of equations is solved for different modes, say $f = F_N$. The ratio of the frequency parameter in vacuum, f_n, to that experimentally measured in air, F_N, neglecting radiation resistance, is given by:

$$\left(\frac{f_n}{F_N}\right)^2 = 1 + \beta \, m_{NN}(F_N) + \beta \sum_{m \neq N} b_m^N \, M_{Nm}(F_N) \qquad (3.5)$$

where the coefficients, b_m^N for $m \neq N$ are

$$b_m^N = \beta \left(\frac{[m_{nN}(F_N) + \sum\limits_{m \neq N s \neq m} b_m^N \, m_{ms}(F_N)]}{\left[\left(\frac{f_m}{F_N}\right)^2 - (1 + \beta \, m_{nn}(F_N))\right]} \right) \qquad (3.6)$$

The above correction equations apply only to the solution of the zero[th] order Bessel function which describes the circularly symmetric modes of vibration, 0,1; 0,2; 0,3;.... The subscripts m, n, s, and N are equal to 1,2,3,4,5... and correspond to a given zero of the zero[th] order Bessel function. The values of m_{mN} as a function of F_N have been tabulated by Gottleib and Aebischer [3]. A value for f_N is obtained by substituting our experimental values for F_N into (3.5) and solving for the first two terms $(1 + \beta m_{NN}(F_N))$. The theoretical values of f_m are calculated using the fact that the ratio of f_m to F_N is directly proportional to the ratio of the zeros of the Bessel function describing its vibration as shown in (3.7) (Z_{0m}/Z_{0N} = constant for any given m and N).

$$\frac{f_m}{F_N} \sim \frac{Z_{0m}}{Z_{0N}} \qquad (3.7)$$

The $b_m{}^{(N)}$ values are then calculated using the first term of (3.6). The $b_m{}^{(N)}$ are

substituted into the third term (summation) of (3.5) and the second term (summation) of

(3.6) and the complete equations are solved by iteration. The measured values of F_N

may then be related to their theoretical *in vacuo* value. The quantity $(f_N/F_N)^2$ is directly

proportional to the ratio of the stress calculated in vacuum and the stress calculated from

measurements made in air. A Fortran program was written to perform these calculations,

given the sample geometry and air densities. The text of the program is included as an

Appendix.

The air damping effect is most important for light and thin membranes and the

first few modes of vibration. It is also affected by the geometry and density of the

membrane. The parameter, β which depends on the factors mentioned above is the key

to understanding when a membrane will vibrate ideally. The importance of this

parameter will be discussed in much greater detail in sections 3.5 and 3.6 with an

emphasis on how to minimize the air damping effect by varying sample geometry.

3.2.2   Karnezos' Correction

Another correction for air damping was used by Karnezos to study the stresses in

thin X-ray masks used in the microelectronics industry. He used a speaker to vibrate the

membrane and a photonics detector to sense its vibration. His experiments were

conducted in air. He used the equation

$$\upsilon_{vac} = \upsilon_{air} (1 + 1.34(R\rho_0/h\rho))^{1/2} \tag{3.8}$$

which when rearranged has the same form as Lax's correction (3.5),

$$\left[\frac{\upsilon_{vac}}{\upsilon_{air}}\right]^2 = 1 + 1.34(\beta) \tag{3.9}$$

where υ_{vac} and υ_{air} are the resonant frequencies measured in hertz. He then uses a form of the same stress equation used in this work to calculate the true stress (that which would be measured under vacuum).

3.2.3   Discussion

It is important to note that in Karnezos' treatment, only the fundamental mode of vibration is considered. His analysis is presented here to introduce the point that in order to interpret the air results rigorously, it is necessary in most cases to consider higher modes of resonant vibration. In equation (3.8) the constant used by Karnezos, 1.34, corresponds to the variable $m_{NN}(F_N)$ in equation (3.5) which depends upon the resonant frequency of the membrane in the argument F_N. It is unclear from his discussion or the references cited in his paper how he arrived at this value. Some error in his calculations are introduced by this factor. His analysis will be compared to that of Lax, and Gottleib and Aebischer as they apply to the data in this work in later sections.

3.3   Stiffness Effects

The effect of bending stiffness is important for thick and stiff films and becomes more significant for higher vibration modes. In this work, stiffness effects are studied using silver films of varying thickness and radius. The consideration of stiffness effects allows both the stress and the modulus of the film to be extracted simultaneously. The

use of holographic interferometry to study the behavior of thick films using the following

analysis has been pioneered by Tong and Farris [8].

3.3.1 Theory

As the thickness and modulus of the film increase, the bending stiffness begins to

play an important role in affecting the natural frequencies and linear elasticity must be

considered. The governing equation for vibration of a film with stiffness effects is:

$$D \nabla^4 u - \sigma \nabla^2 u + \rho \frac{\partial^2 u}{\partial t^2} = 0 \tag{3.10}$$

where,

$$D = \frac{Eh^2}{12(1 - v^2)} : \text{ flexural rigidity} \tag{3.11}$$

E: Young's modulus

h: thickness

u: out-of-plane displacement

σ: in-plane stress

t: time

v: Poisson's ratio

$\nabla^4 = \nabla^2 \nabla^2$ and ∇^2: the Laplacian operator

It can be seen that when D is small, equation (3.10) reduces to that of a vibrating

membrane, however, as D increases, bending effects play a dominant role in the

restoring force of the vibration. This effect has been studied extensively by Tong [8] for

thick polymeric photoresist films. For a membrane the only boundary condition is that at

r = R, the outer radius of the membrane, u = 0, however, for a plate there are two limiting boundary conditions, "simply supported" and "clamped" shown below:

$$u = 0, \quad \nabla^2 u = 0 \qquad \text{simply supported} \qquad (3.12)$$

$$u = 0, \quad \nabla u \cdot \mathbf{n} = 0 \qquad \text{clamped} \qquad (3.13)$$

where $\mathbf{n}$ is the normal to the boundary. It is believed that the silver samples behave as if they have boundary conditions intermediate between the two theoretical limiting cases depending on their dimensions.

Some general comments about the governing equation can be made before we examine particular solutions (as shown by Tong [5]). The stiffness effect can be neglected when

$$C \equiv \frac{D}{\sigma R^2} \ll 1 \qquad \text{(Circle)} \qquad (3.14)$$

$$C \equiv \frac{D\pi^2}{\sigma L^2} \ll 1 \qquad \text{(Square)} \qquad (3.15)$$

where R and L are length scale associated with the membrane, e.g., the radius of a circle, and the length of the side of a square specimen. In these limits, ideal membrane behavior is obtained. Therefore, C is an important parameter which indicates the significance of the stiffness effect on the vibration of the sample.

The simply supported case can be solved exactly for a square sample, and a good approximation to the exact result can be obtained for a circular sample. The following

derivation comes from work on thick polymer films done by Tong [5]. For square
samples, the ideal membrane mode shapes

$$u(x,y,t) = \sin(n\pi x/L)\sin(m\pi y/L)\sin\omega t \tag{3.16}$$

satisfy the governing equation (3.10) and boundary conditions (3.12). These, when
substituted into the governing equation (3.10), lead to the following result for the stress
σ:

$$\sigma = \frac{\rho\,\omega_{mn}^2}{(m^2 + n^2)}\left[\frac{L}{\pi}\right]^2 - D\left[\frac{\pi}{L}\right]^2(m^2 + n^2) \tag{3.17.a}$$

The first term on the right hand side of the expression is exactly the same as that for an
ideal membrane and the second term represents the bending stiffness effect. In other
words, if the stress is calculated using only the ideal membrane term and denoted as
apparent stress, σ_{ap}, it increases linearly as a function of $(m^2 + n^2)$. Therefore, in the
plot of σ_{ap} vs. $(m^2 + n^2)$, the y-intercept yields the real stress σ while the slope yields the
rigidity, D, and the modulus, E, of the film. This equation can also be written as

$$\frac{\sigma_{ap}}{\sigma} = 1 + C(m^2 + n^2) \tag{3.17.b}$$

The natural frequency for a circular membrane can be written in terms of the
roots α_{mn}, of a relation involving Bessel functions [5]:

$$\omega_{mn}^2 = \left(\frac{\alpha_{mn}}{R}\right)^2\frac{\sigma}{\rho}\left[1 + \frac{\alpha_{mn}^2 D}{R^2\sigma}\right] \tag{3.18}$$

When $C \equiv D/\sigma R^2 \ll 1$, equation (3.18) reduces to the expression for natural frequencies of a membrane and $\alpha_{mn} = Z_{mn}$. When $C < 0.1$, the roots α_{mn} are close to Z_{mn} and replacing α_{mn} by Z_{mn} in (3.18) as a good approximation yields

$$\omega_{mn}^2 = \left(\frac{Z_{mn}}{R}\right)^2 \frac{\sigma}{\rho} \left[1 + \frac{Z_{mn}^2 D}{R^2 \sigma}\right]$$

(3.19)

Therefore, the stress is given by

$$\sigma = \rho \left[\frac{\omega_{mn} R}{Z_{mn}}\right]^2 - \frac{Z_{mn}^2 D}{R^2}$$

(3.20.a)

which can also be written as

$$\frac{\sigma_{ap}}{\sigma} = 1 + C Z_{mn}^2$$

(3.20.b)

It is easy to see the similarity between (3.20.a) and (3.17.a) for a simply supported square membrane. The first term on the right hand side in both cases is the apparent stress, σ_{ap}, which is calculated if ideal membrane behavior is assumed. The second term is the correction due to the stiffness effect. The square of the roots of the Bessel functions, $(Z_{mn})^2$, in the case of a circular sample have an analogous role to $(m^2 + n^2)$ for the square samples. Again, if C is small, Z_{mn} can be used instead of α_{mn}, the real stress σ and the rigidity D of the film can be extrapolated by plotting the apparent stress σ_{ap} vs. the square of the roots $(Z_{mn})^2$. A schematic of such a plot is shown in Figure 3.1.
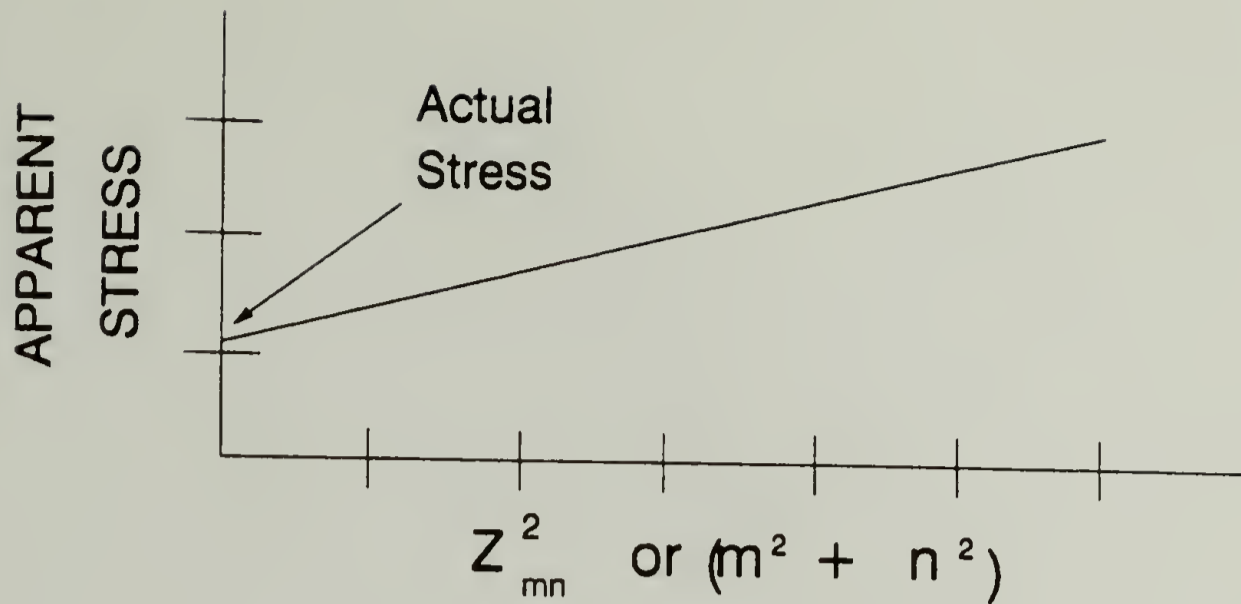
Figure 3.1   Schematic illustration of a plot of stress vs $(Z_{mn})^2$ for a film which exhibits some bending effects.

3.3.2   Parameters

The parameters β and C are central to the discussion of membrane and plate vibration. Their definitions were given previously, but for the sake of continuity, they will be defined again here as they are discussed. The parameter β is important in determining how large of a role air damping will have on the vibration of a membrane. It is defined as follows:

$$\beta = \rho_0 R/\rho h \qquad (3.21)$$

where,

$$\rho_0 \quad = \quad \text{density of medium (kg/m}^3)$$

$$\rho \quad = \quad \text{density of membrane (kg/m}^3)$$

$$R \quad = \quad \text{radius of membrane (m)}$$

$$h \quad = \quad \text{thickness of membrane (m)}$$

The two variables which can be controlled in this equation are the density of the medium and the geometry of the sample in the form of (R/h). The density of air at standard atmospheric pressure and 0 °C is 1.2929 kg/m^3. As the amount of pressure around the sample decreases, the density of the medium approaches zero. A simple relation between pressure and density of air is given by a version of the ideal gas law:

$$P = \rho_0 R'T \qquad (3.22)$$

where

P = Pressure

ρ_0 = Density of the medium

R' = Gas constant

T = Temperature

The radii of the samples used in these experiments vary from approximately 1 cm to approximately 3 cm and the thicknesses range from 10 μm to 250 μm for some of the metal films. Figure 3.2 shows a plot of how β changes with changes in relative density

The sole use of this analysis to design specimen geometry however, may cause problems. The first is that at sample sizes where R/h is on the order of 50, stiffness effects may become important. It is therefore necessary to calculate the value of the parameter C, to determine if stiffness would have an effect on the vibration of a particular sample. As given above, the expression for C for a circular membrane is:

$$C = \frac{D}{\sigma R^2} \tag{3.23}$$

where

$D = \dfrac{Eh^2}{12(1 - v^2)}$ = rigidity coefficient

R =   radius (m)

σ =   stress (N/m^2)
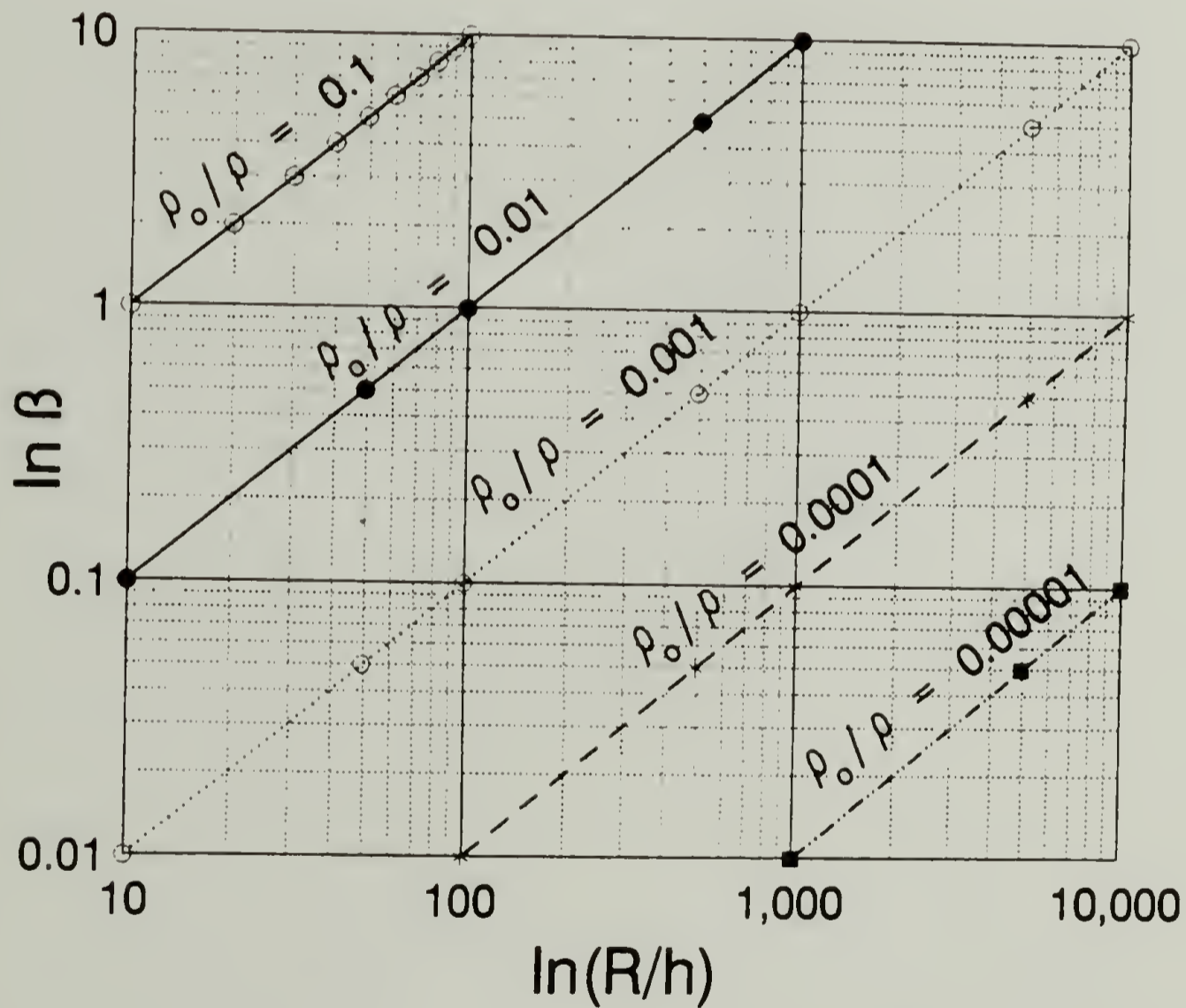
Figure 3.2   Plot of ln β vs sample geometry, ln(R/h) and relative density (ρ_o/ρ).

Values of β for a typical polymeric sample can vary from 0.42 to 2.5 and fall in the lower left hand quadrant of Figure 3.2. Using this sort of plot, one could ostensibly design samples with dimensions which yield very small values of β, and therefore, allow measurements to be made in air without need for corrections.

In Figures 3.3.a and 3.3.b the variation in C with changes in Young's modulus divided by one minus the square of Poisson's ratio and changes in the square of the thickness to radius ratio is plotted for values typical of polymeric materials (Figure 3.3.a) and for typical metal samples (Figure 3.3.b). In order for stiffness effects to have little influence on the vibration, C should be less than about 0.01 [5]. For the polymeric materials, the moduli were varied from about 3 GPa to 16 GPa in increments of 1 GPa, and Poisson's ratio was varied from 0.34 to 0.23 in increments of 0.01. The h/R values range from 0.01 to 0.001 in increments of 0.001. This corresponds to samples from 100 μm to 10 μm thick with a radius of 1 cm. It can be seen that for polymeric materials (except for those with the very highest moduli and smallest h/R value) C does not generally fall above 0.01 and in fact is generally much lower than that, indicating that stiffness effects should not be large.

In Figure 3.3.b the values of Young's modulus range from 50 to 200 GPa in increments of 10 GPa between 50 and 100 GPa and in increments of 20 GPa from 100 to 200 GPa. It is perhaps easiest to think of these values in terms of specific metals. A magnesium alloy (AZ31B) has a Young's modulus of about 45 GPa, that of aluminum is around 70 GPa, and the modulus of steel is around 200 GPa [9]. The Poisson's ratios are varied correspondingly from 0.38 to 0.31 in increments of 0.01. The dimensions are varied in the same way as for the polymer simulation above and the stress is taken to be 10 MPa.

It can be seen from these two simulations for polymer and for metal samples that the metal samples have C values greater than 0.01 for most typical h/R and $E/(1-v^2)$ values. It should therefore be much easier to design a polymeric sample with dimensions where the bending effect is reduced than a metal sample. A polymeric membrane with a stress of 10 MPa and a Young's modulus of 12 GPa and a Poisson's ratio of 0.25 has a C value of just greater than 0.01 for a thickness of 100 μm and radius of 1 cm. For a metal sample with a Young's modulus of 70 GPa (close to that of silver) a Poisson's ratio of
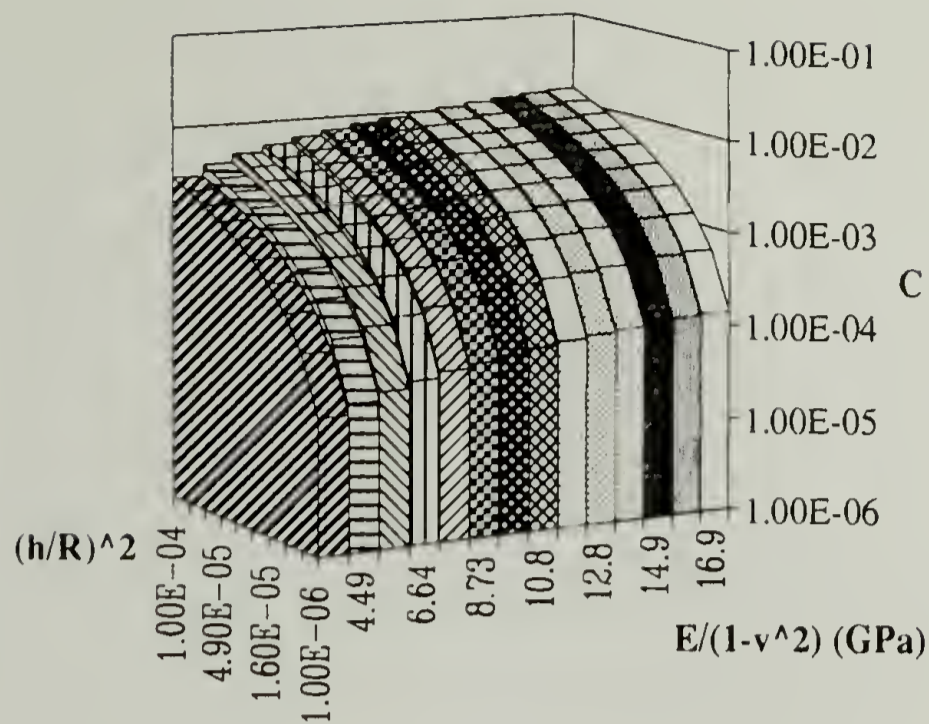
Figure 3.3   Change in C with respect to geometry and stiffness
a   for a typical polymeric material.
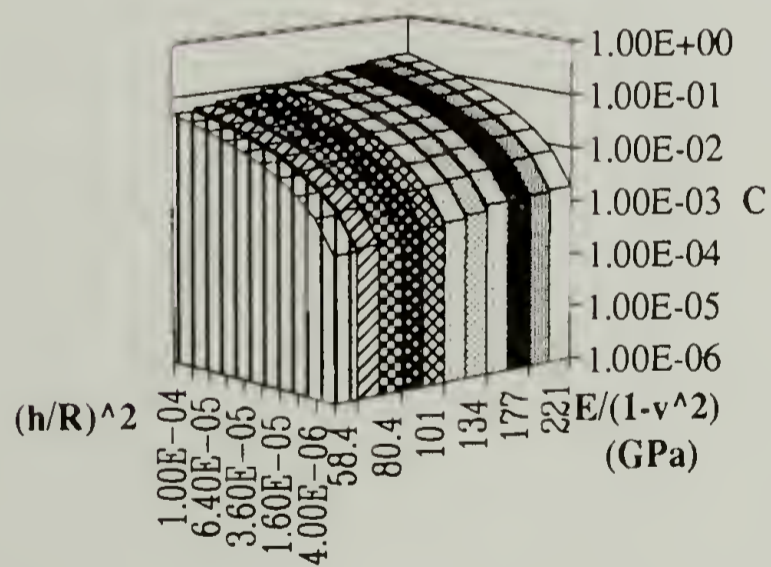
b   for metals.

0.36 and stress = 10 MPa, a C value of 0.01 is exceeded for a 1 cm radius sample when the thickness equals 40 μm. These observations will be discussed further with respect to some of the data presented below.

3.4   Experiments

The experiments described in this chapter are comprised of four different groups. For the first group, the objective was to understand the effect of air damping on stress measurements. The samples in this group were PMDA-ODA tested in various degrees of vacuum, including full vacuum and in air at ambient pressure. The data taken at each pressure was corrected using Lax's theory and compared to the measurements done in full vacuum.

The objective for the second group of samples was to understand the relationship between β and the ratio of stress values measured in air and in various degrees of vacuum to stress values measured in full vacuum. The samples in this group were epoxy paint base samples provided by Steve Mazur at E. I. DuPont & Nemours [10]. These samples have a good range of geometries and behave like membranes. In the third set of experiments, silver membranes, made by Anand Jagota at DuPont, that exhibit a range of behavior from membrane-like to plate-like were used. It is here that the discussion of the parameters β and C will be most useful. The last set of experiments were done to determine the effect of fillers on the stresses in membranes. The membranes were of one poly(tetrafluoroethylene) (PTFE) material and another filled PTFE material (2810 made by Rogers Corporation) which were laminated between two copper sheets at high temperature and pressure [11]. These samples were provided by Bob Wiley at IBM in Endicott, NY. The stress in the teflon layer was measured after removal of the outer copper layers.

3.4.1 Equipment

The membranes are placed in a fixture rigidly mounted inside of a vacuum chamber, where the degree of vacuum can be controlled. The entire chamber is connected to a Wilcoxon Research piezoelectric shaker driven by a Wavetek Model 190 frequency generator connected to a Wilcoxon Research PA7 power amplifier. The frequency is monitored using a B & K Precision 80 MHz frequency counter. An image of the static object is recorded on a thermoplastic holographic plate using a Newport Research Corporation HC301 holographic camera. The coherent light source used for this reflection hologram is a 5 mW helium-neon laser. The entire system is mounted on a small optical bench isolated from any mechanical room vibrations by several inflatable pillows.

3.4.2 Method

In this section, a description of sample preparation techniques for each of the types of materials will be given, followed by a discussion of the experimental procedure. The polyimide samples were made in the manner described in chapter 2, i.e. the polyamic acid solution was spin-coated onto a tin-coated steel plate and cured to 225 °C. Measurements were made on four samples taken from the same 12.7 cm x 12.7 cm square plate, to ensure that the state of stress in each membrane was as uniform as possible. After curing the polyimide film for 1/2 hour at 85 °C, 1/2 hour at 150 °C, followed by 1 hour at 225 °C, steel washers with inner diameters of 0.95, 1.27, 1.90, and 2.54 cm were mounted onto the film with epoxy. The samples were then removed from the steel substrate by scoring the top side of the polyimide film around the outside edges of the washers and dissolving the tin layer with mercury. The epoxy paint base samples were made in the same manner by Steve Mazur [12].

The silver samples were made by Anand Jagota [13] by placing silver foils between two presintered ceramic substrates [14] with holes punched in them before firing. The specimen is heated to 800 °C with no applied load to allow the film and the substrate to freely expand. At 800 °C the specimen is pneumatically clamped between two stainless steel plates with holes slightly bigger than those in the ceramic substrate [15].

The poly(tetrafluoroethylene) materials were supplied by Robert Wiley [11]. The filled and unfilled PTFE (50.8 μm thick) was laminated between two sheets of 0.5 ounce (~ 17 μm thick) or two sheets of 3.5 ounce (~ 120 μm thick) copper foils at 500 °F (370°C) and 700 psi (~ 4.8 MPa) for the unfilled or 1700 psi (~ 11.7 MPa) for the filled samples. The PTFE/copper system is a case of a flexible coating on a rigid substrate ($h_s E_s$ >> $h_c E_c$) where h is the thickness and s and c represent the substrate and the coating respectively. Therefore, the system will be in a state of self equilibrating stress where the coating is under tension and the substrate is under compression [13,16]. The material properties of PTFE and filled PTFE and copper are given in Table 3.1.

Table 3.1   Moduli, coefficients of thermal expansion (α), Poisson's ratio (ν) and density of PTFE, filled PTFE (Roger's 2810™), and copper.

Material	Young's Modulus (GPa)	α (mm/mm/°C)	Density (kg/m³)	Thickness (μm)
PTFE	0.40 [17]	10.0×10^{-5} [15]	2140	50.8
Filled PTFE	0.83 [18]	16.0×10^{-6} [19]	2110	50.8
Copper	120	17.6×10^{-6}	8968	17 or 120

The PTFE samples were made using epoxy to mount a washer to the outside of the copper/PTFE/copper laminate. The exposed copper was then removed by etching in 10 M nitric acid solution. This gives a PTFE membrane under tension supported on a metal washer.

Once the samples were completed, they were mounted rigidly in a fixture attached to the inside of the vacuum chamber mounted to the piezoelectric transducer on the holographic bench. A hologram was then made of the stationary membrane. While looking at the static hologram superimposed on the membrane, the membrane was shaken at steadily increasing sinusoidal frequencies and when a resonant frequency was reached, a vibration pattern was observed and the frequency and mode recorded. The samples were tested in this manner in varying degrees of vacuum, and in air and the apparent stress values calculated using equation (2.6). The samples were also tested in a separate sample holder outside of the vacuum chamber to determine if the walls of the chamber (about 1 in. away from the membrane on each side) affect the membrane vibration. The data from the air and vacuum measurements were then analyzed using the program "CORRECTION" and compared to the data measured under full vacuum.

The measurements made on the epoxy samples were conducted in virtually the same way as described above. Plots of stress vs mode number were made and, the effect of β (calculated in air) on the difference between air and vacuum stress values was plotted for a series of epoxy samples. The results are shown in section 3.5. The stress in the silver samples was measured in air and in full vacuum to determine if there was any effect of vacuum on the stress values and to observe the effect of sample geometry on the membrane- or plate-like behvior of the samples. The final set of stress measurements were done to determine the difference in stress (if any) between the filled and the unfilled PTFE materials.

3.5   Results

Data from the experiments on PMDA-ODA samples are presented in Figures
3.4.a - 3.4.d for the smallest to the largest membrane respectively. The stress is shown as
a function of different modes of vibration (in increasing order, i.e., m,n = 0,1; 1,1; 2,1;
0,2, ...). The effect of air loading on the lowering of the resonant frequency of a
membrane is seen to decrease for higher modes of vibration and as the radius of the
membrane decreases, both of which lead to lower β values. Although for the higher
modes of vibration (measured in air or partial vacuum) the computed stress values are not
as significantly affected by air damping, it can be seen that the computed stress value is
not accurate as compared to the measurements made in full vacuum which display a
highly consistent value of stress as calculated for different modes on the same sample and
between different samples.

The correction proposed by Lax [1], and Gottleib and Aebischer [3] has been
applied to these measurements and the results are shown in Figures 3.5.a - 3.5.d. The
standard density of air (at 0°C and atmospheirc pressure) and the speed of sound in air
were taken as 1.2929 kg/m^{3}and 346.29 m/sec [7]. The effects of relative humidity,
temperature and ambient pressure were accounted for using an expression for the density
of air taking these factors into consideration [7] and hourly barometric pressure readings
[20].

A comparison of Lax's and Karnezos' theories applied to stress measurement data
is shown in Table 3.1. The data is from the four samples for which data was shown in
Figures 3.4 and 3.5. The first two columns give the stress value measured in air and in
vacuum for the first resonant mode of vibration only. The second two columns are those
same values with Lax's and Karnezos' corrections applied. The next two columns are the
average measured values of the stress for the second through the fourth circularly
symmetric modes of vibration (measured in air and in vacuum). Finally, the last column
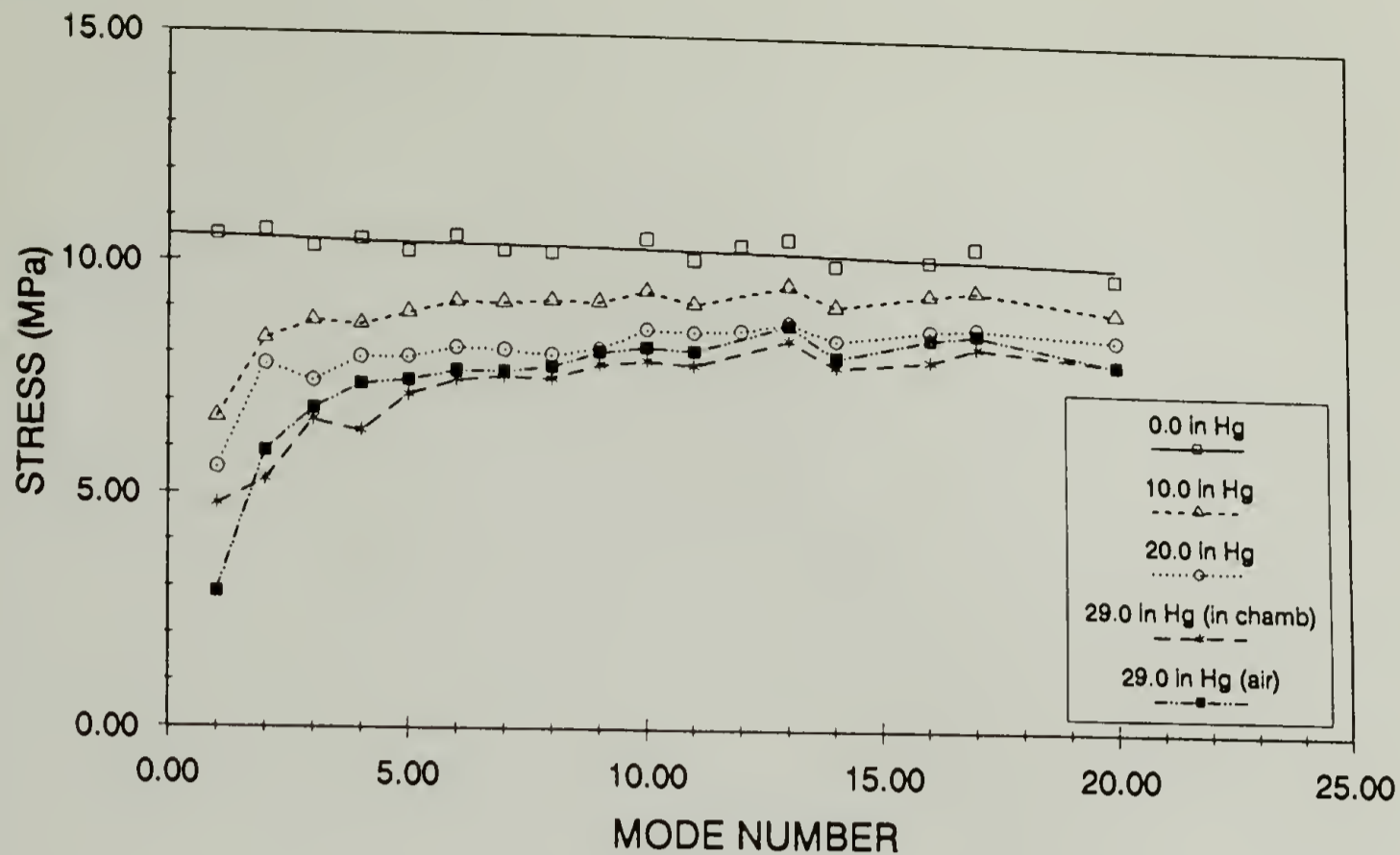
Figure 3.4.a   Stress vs. mode number for PMDA-ODA sample at different reduced pressures. The radius of this sample is 0.95 cm. Measurements were done at 26 °C and 25 % relative humidity.
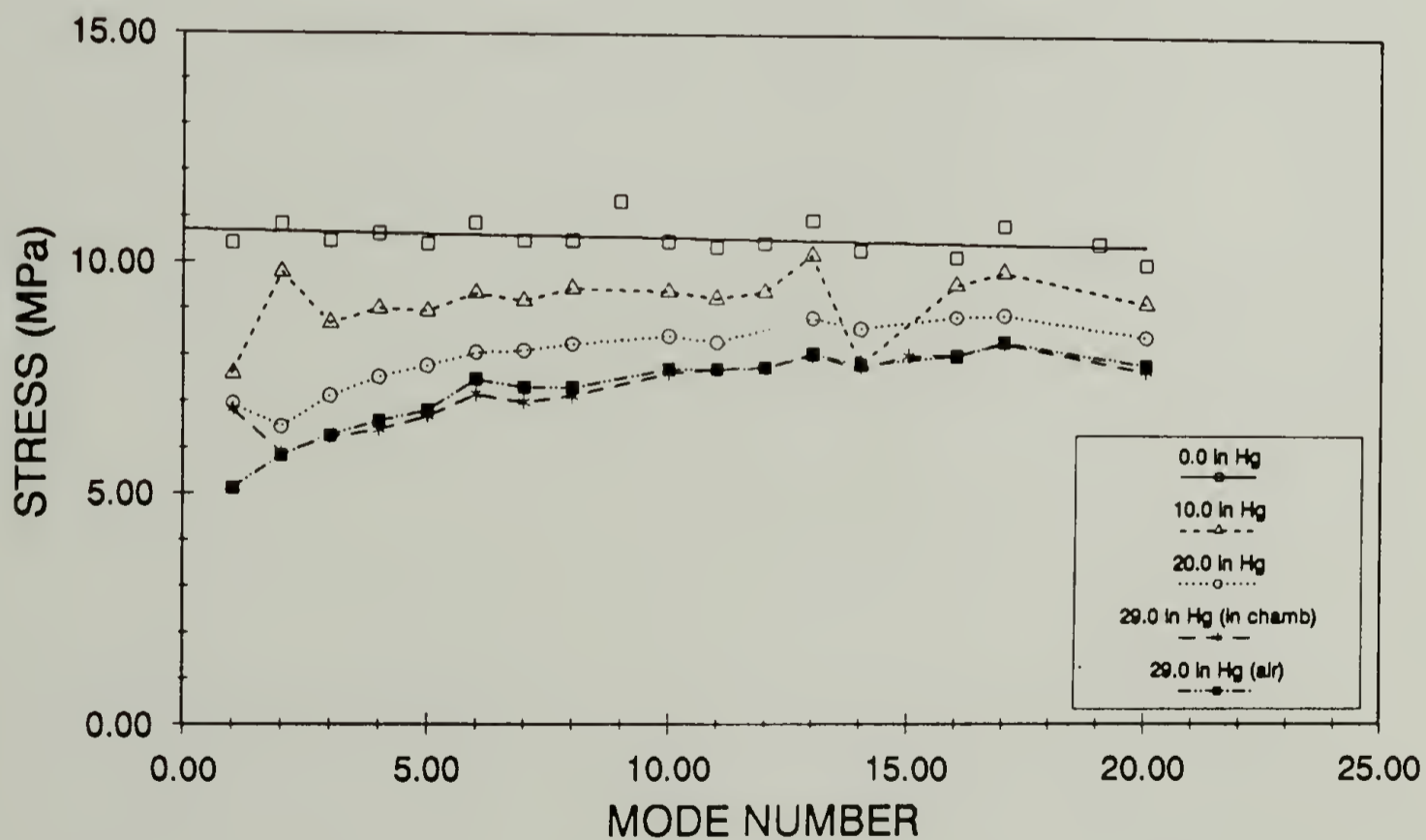
Figure 3.4.b   Stress vs. mode number for PMDA-ODA sample at different reduced pressures. The radius of this sample is 1.27 cm. Measurements were done at 26 °C and 25 % relative humidity.
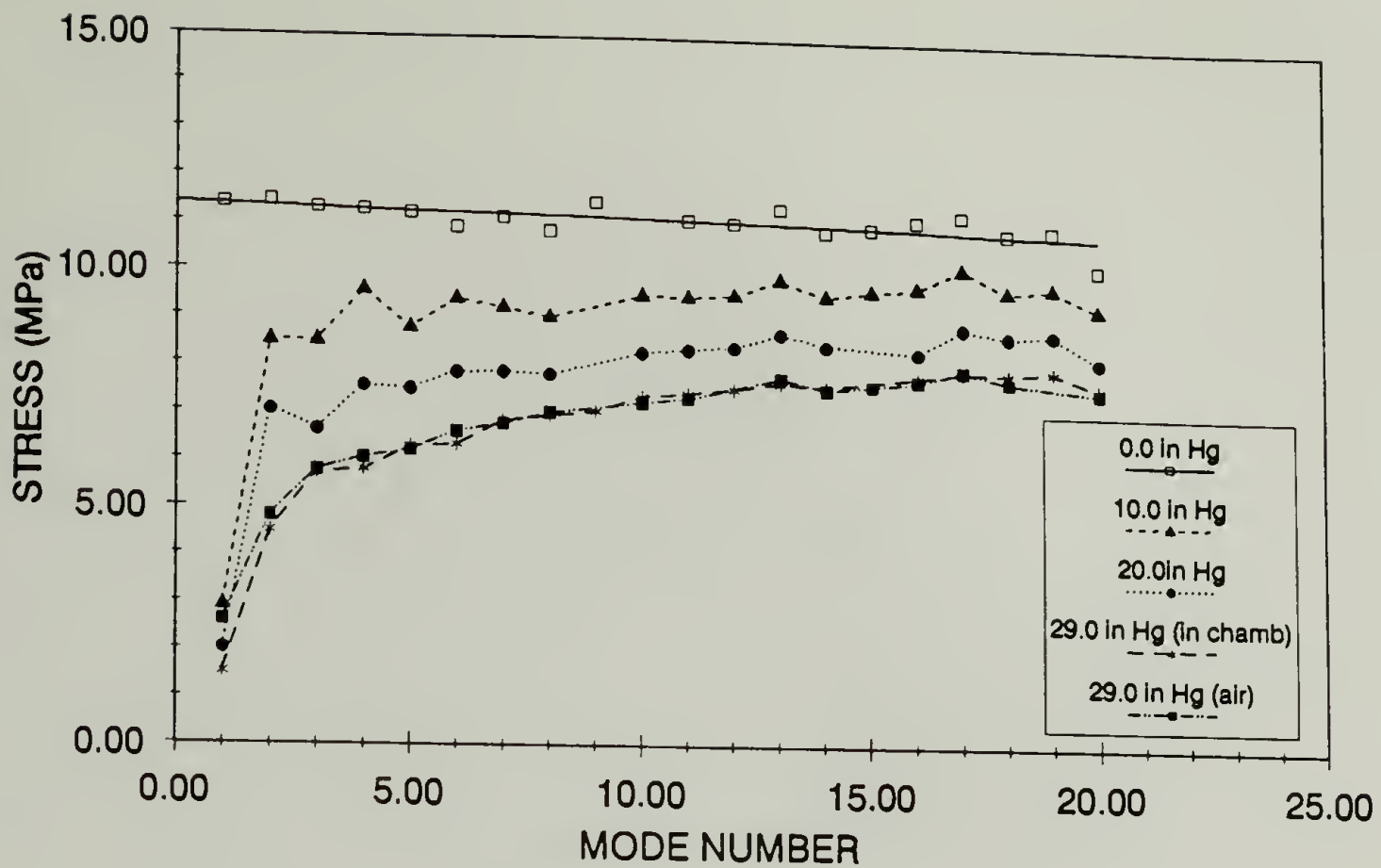
Figure 3.4.c (continued)   Stress vs. mode number for PMDA-ODA sample at different reduced pressures. The radius of this sample is 1.90 cm. Measurements were done at 26 °C and 25 % relative humidity.
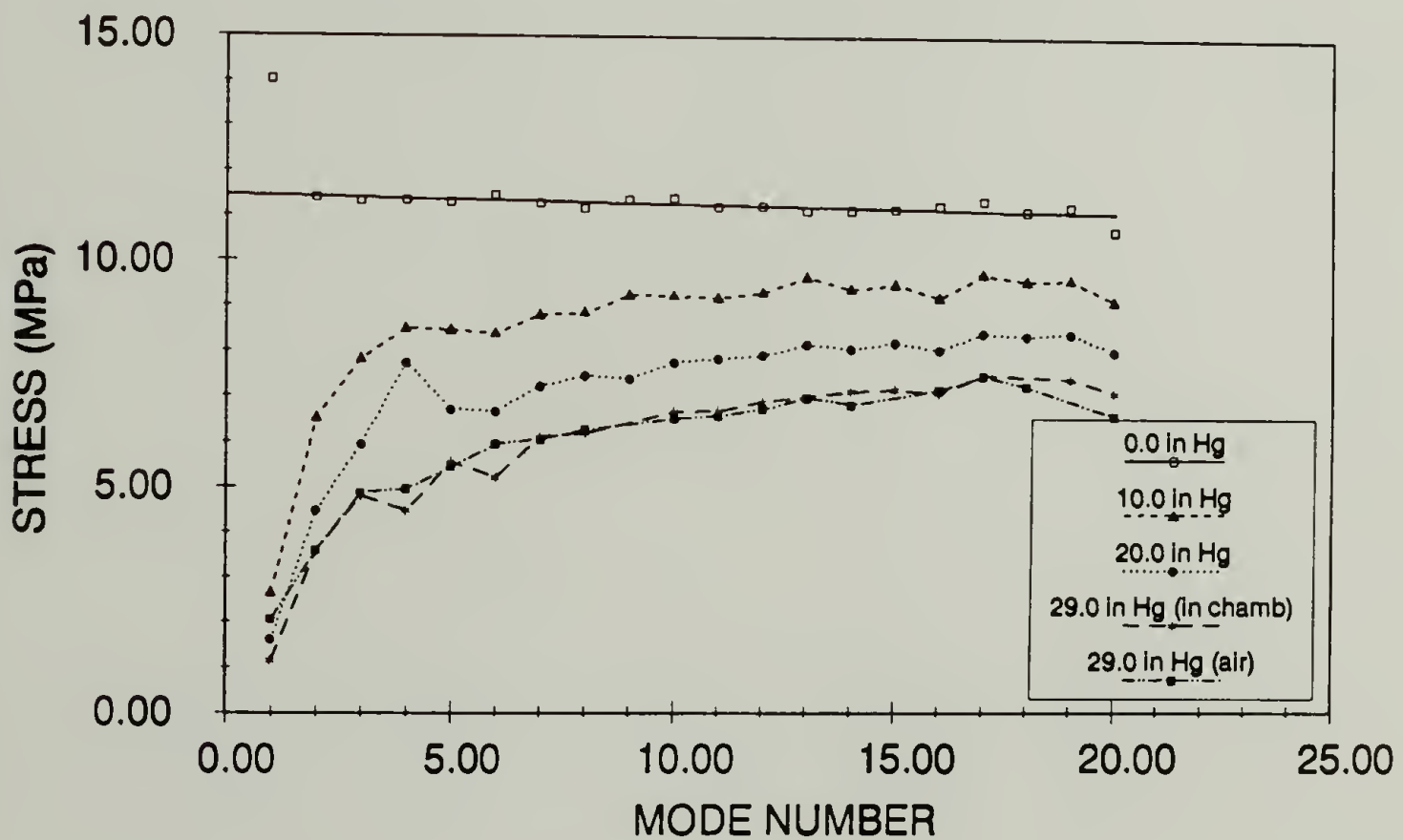
Figure 3.4.d   Stress vs. mode number for PMDA-ODA sample at different reduced pressures. The radius of this sample is 2.54 cm. Measurements were done at 26 °C and 25 % relative humidity.
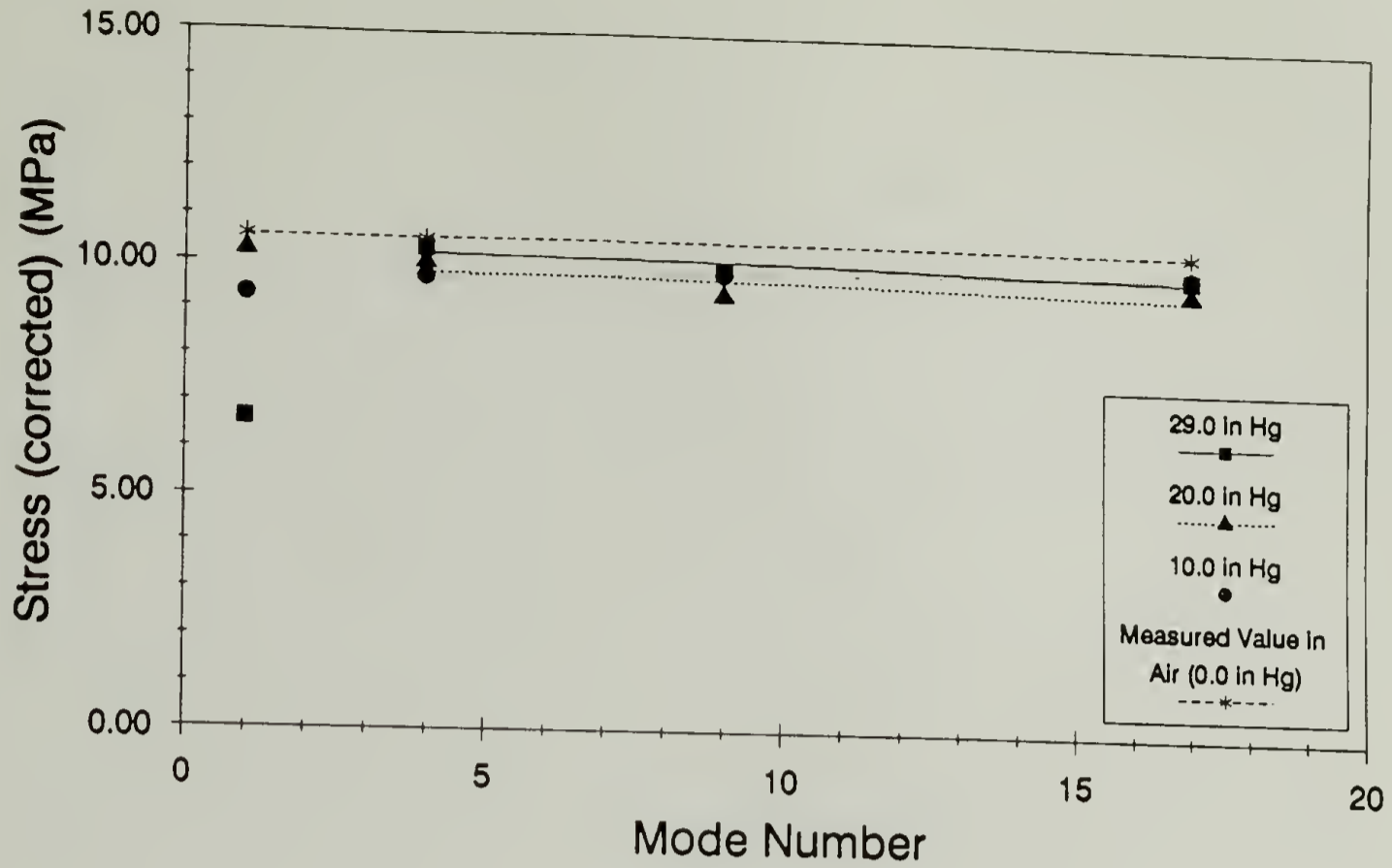
Figure 3.5.a   Plot of stress values from Figure 3.4.a at each reduced pressure corrected using Lax's theory vs mode number for the circularly symmetric modes of vibration. Radius = 0.95 cm.
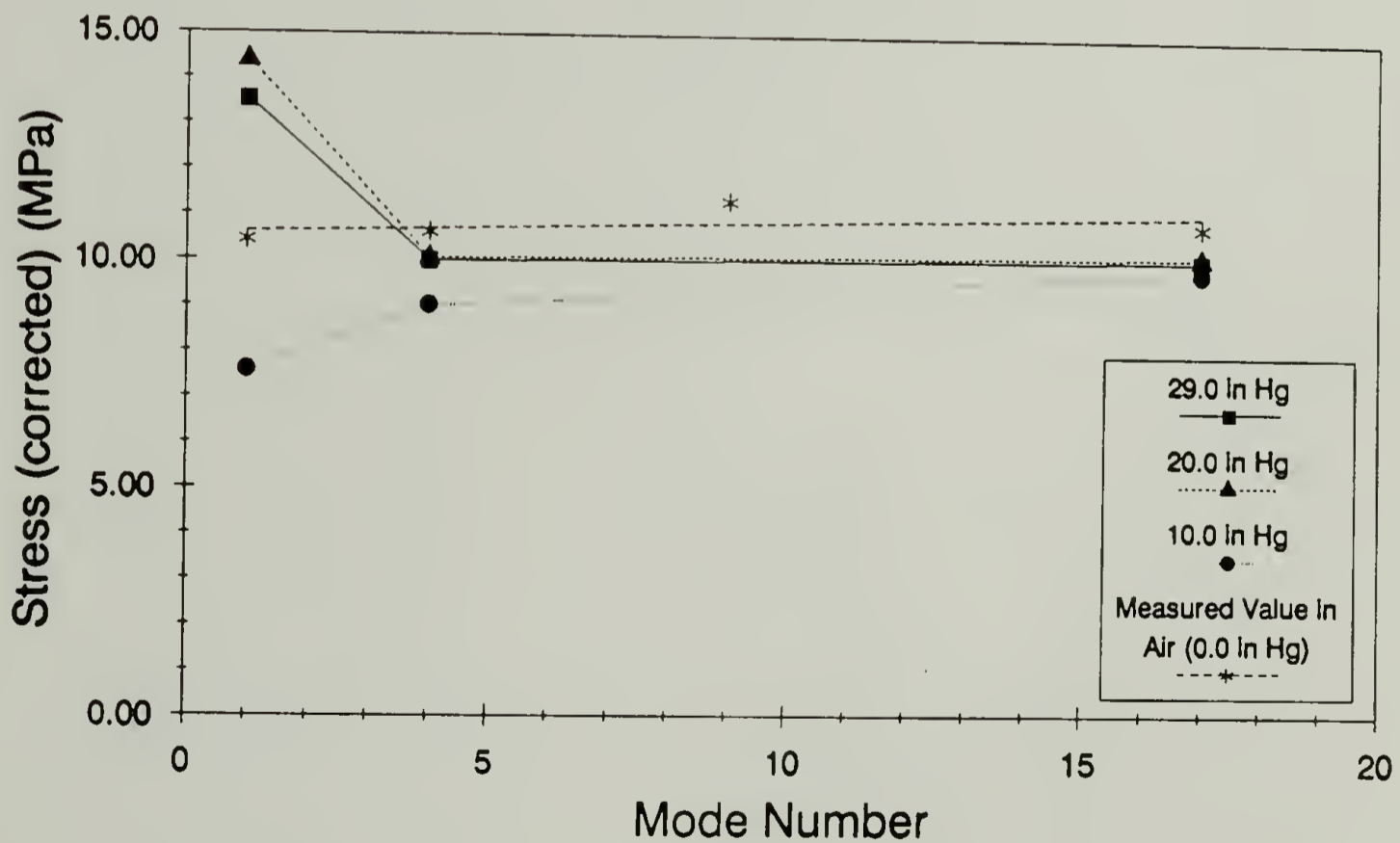
Figure 3.5.b   Plot of stress values from Figure 3.4.b at each reduced pressure corrected using Lax's theory vs mode number for the circularly symmetric modes of vibration. Radius = 1.27 cm.   (continued on next page)
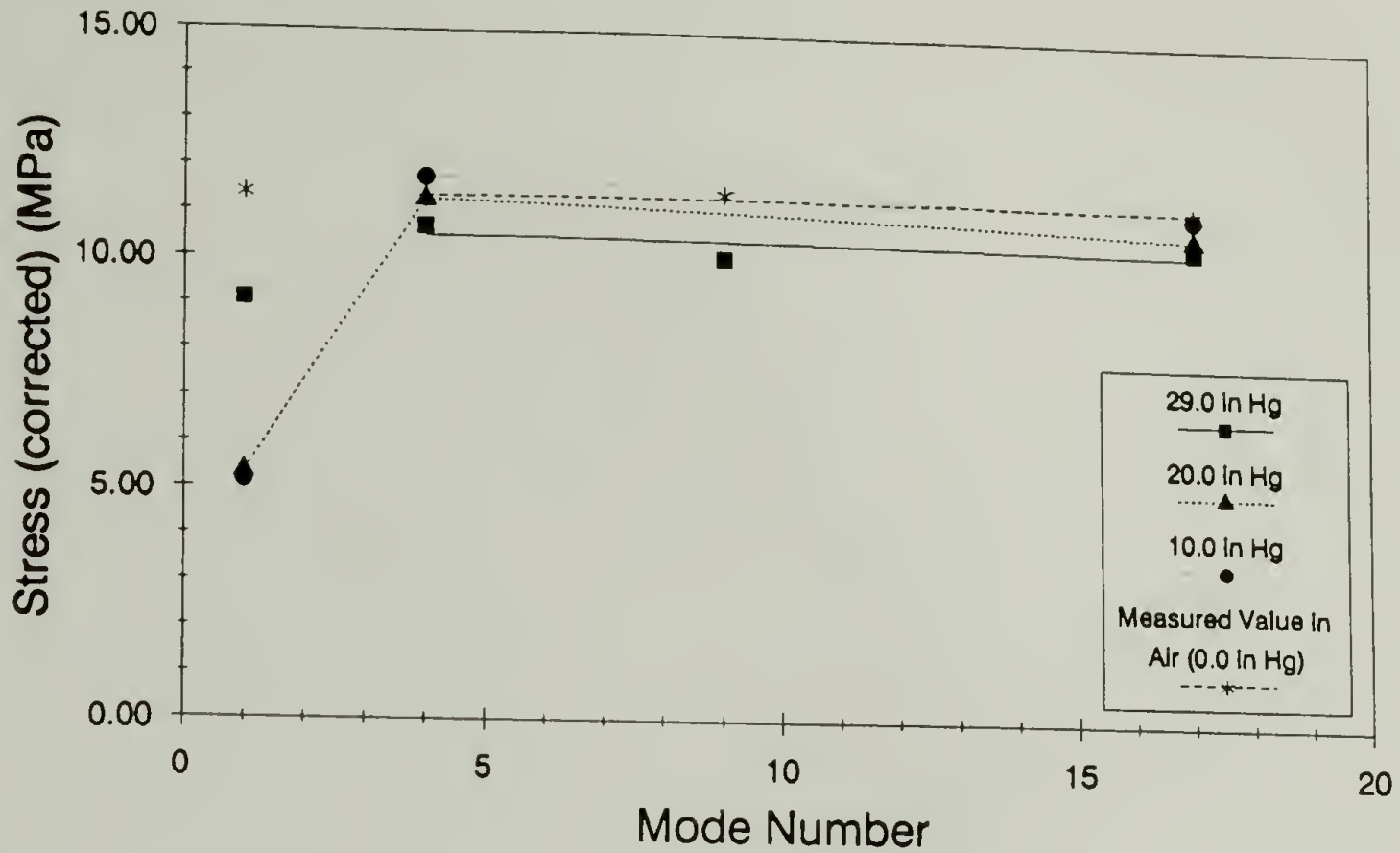
Figure 3.5.c (continued)   Plot of stress values from Figure 3.4.c at each reduced pressure corrected using Lax's theory vs mode number for the circularly symmetric modes of vibration. Radius = 1.90 cm.
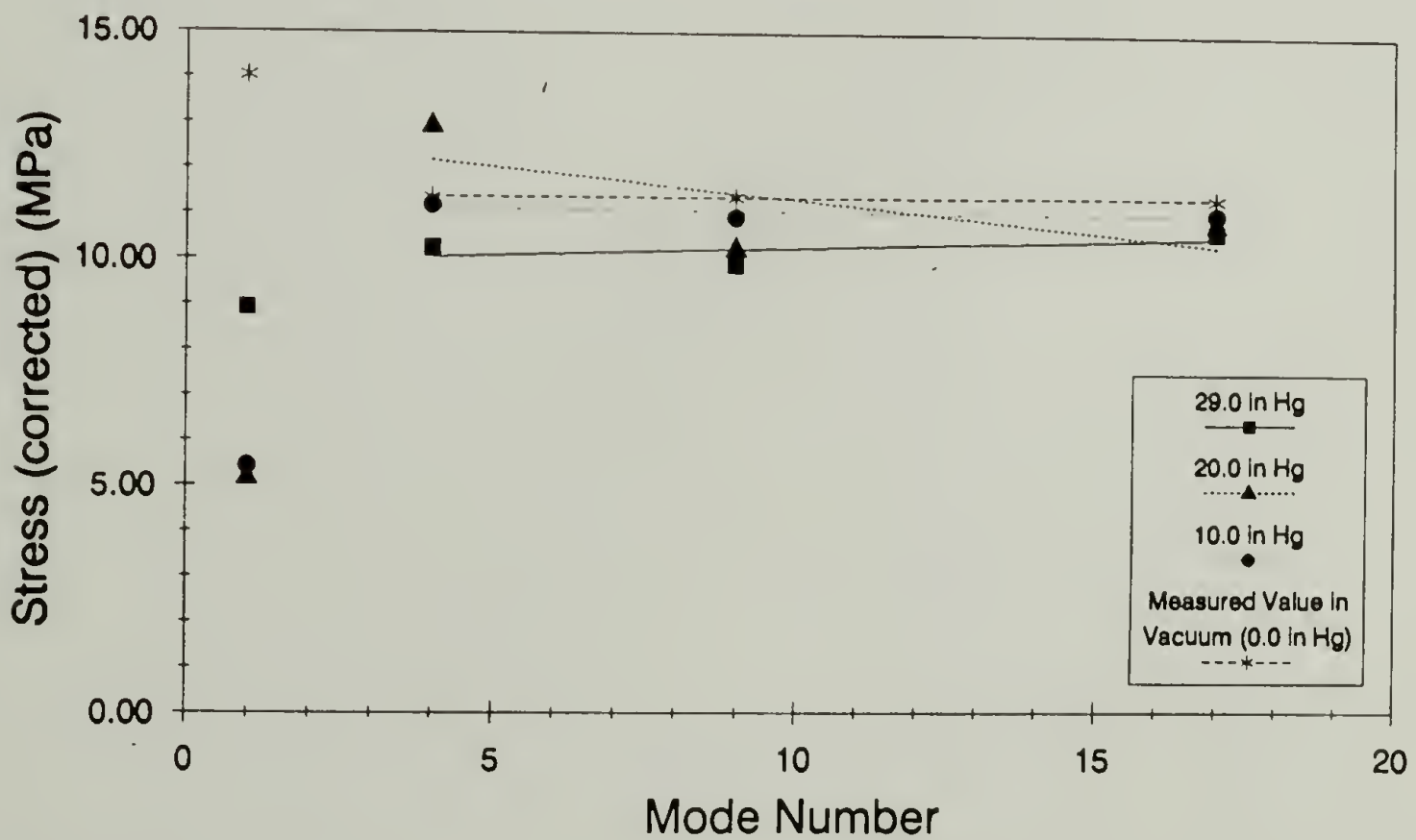
Figure 3.5.d   Plot of stress values from Figure 3.4.d at each reduced pressure corrected using Lax's theory vs mode number for the circularly symmetric modes of vibration. Radius = 2.54 cm.

Table 3.2   Data from PMDA-ODA samples cured to 225 °C (from the same tin-coated steel plate (G)). Comparison of Lax's and Karnezos' corrections for the first resonant modes only, then for the higher resonant modes of vibration. This table is to point out that it is insufficient to estimate the theoretical stress value based only on one mode of vibration. The higher order modes are required in order for correction equations to accurately predict the resonance of a membrane in vacuum based on the data measured in air.

		APPARENT STRESS (MPa)							
		First Resonant Mode Only		Corrected Values		Average of Modes 2 - 4		Corrected Values	
Sample	Radius	Air	Vacuum	Lax	Karnezos	Air	Vacuum	Lax	Karn.
G1	2.54 cm	2.06	14.03	9.69	8.30	6.39	11.39	10.70	-----
G2	1.90 cm	2.62	11.39	9.24	8.51	7.14	11.25	10.82	-----
G3	1.27 cm	5.12	10.42	14.43	12.87	7.50	10.55	10.32	-----
G4	0.95 cm	2.88	10.57	7.03	6.29	7.94	10.37	10.32	-----

shows the average value of the stress measured from the second through fourth modes of vibration in air with Lax's correction applied.

In Figure 3.6 a representative plot of stress vs mode number for an epoxy sample at several air pressures is shown. Table 3.2 is a list of the epoxy samples, their geometries, β and C values, and stress values. The variation in the values of β are due to differences in the sample thickness as well as variations in the density of air during each experiment. The ratio of the average plateau stress to the maximum stress value measured in vacuum for each value of reduced pressure is plotted for each epoxy sample and shown in Figure 3.7. The values of β (calculated using ρ_0 at atmospheric pressure) are noted in the legend on the graph. Note that as β increases, the ratio of the stress measured in air or under reduced pressure to the stress measured in vacuum decreases.

The next set of experiments are stress measurements on silver samples with a range of geometries and vibration behavior. A description of the samples including their rigidity parameter and C values is given in Table 3.3 below. The values of C range from 0.0003 to about 0.5, exhibiting behavior that ranges from membrane-like to plate-like. Plots of the stress vs zero of the Bessel function squared are given in Figures 3.8.a - 3.8.e for each sample.

A description of the PTFE samples used in our experiments is given below in Table 3.4. The differences in samples are primarily in the thickness of the outer copper layer (either 0.5 oz or 3.5 oz copper foil), in the material (i.e. either filled or unfilled), and in the pressures at which they were laminated. The stress measurement data is shown in Figures 3.9.a and 3.9.b for the filled and unfilled PTFE respectively. Once again, stress is plotted as a function of mode number. The average stress values and standard deviation are given in the legend. Three samples from each type of PTFE laminate were tested, and all are shown on each graph.
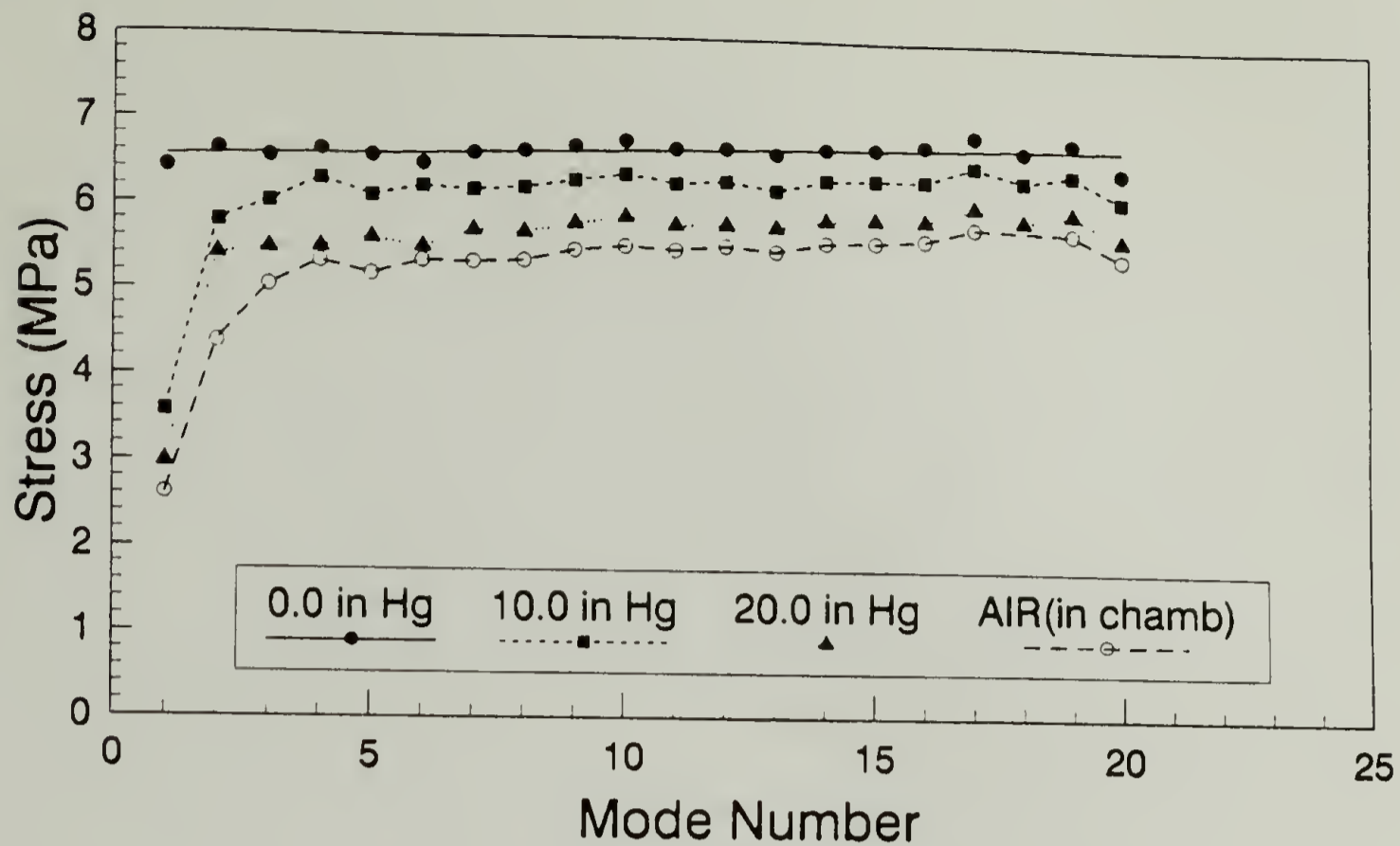
Figure 3.6   Plot of stress vs mode number for a typical epoxy sample measured at various reduced pressures. (Sample number 132-3).
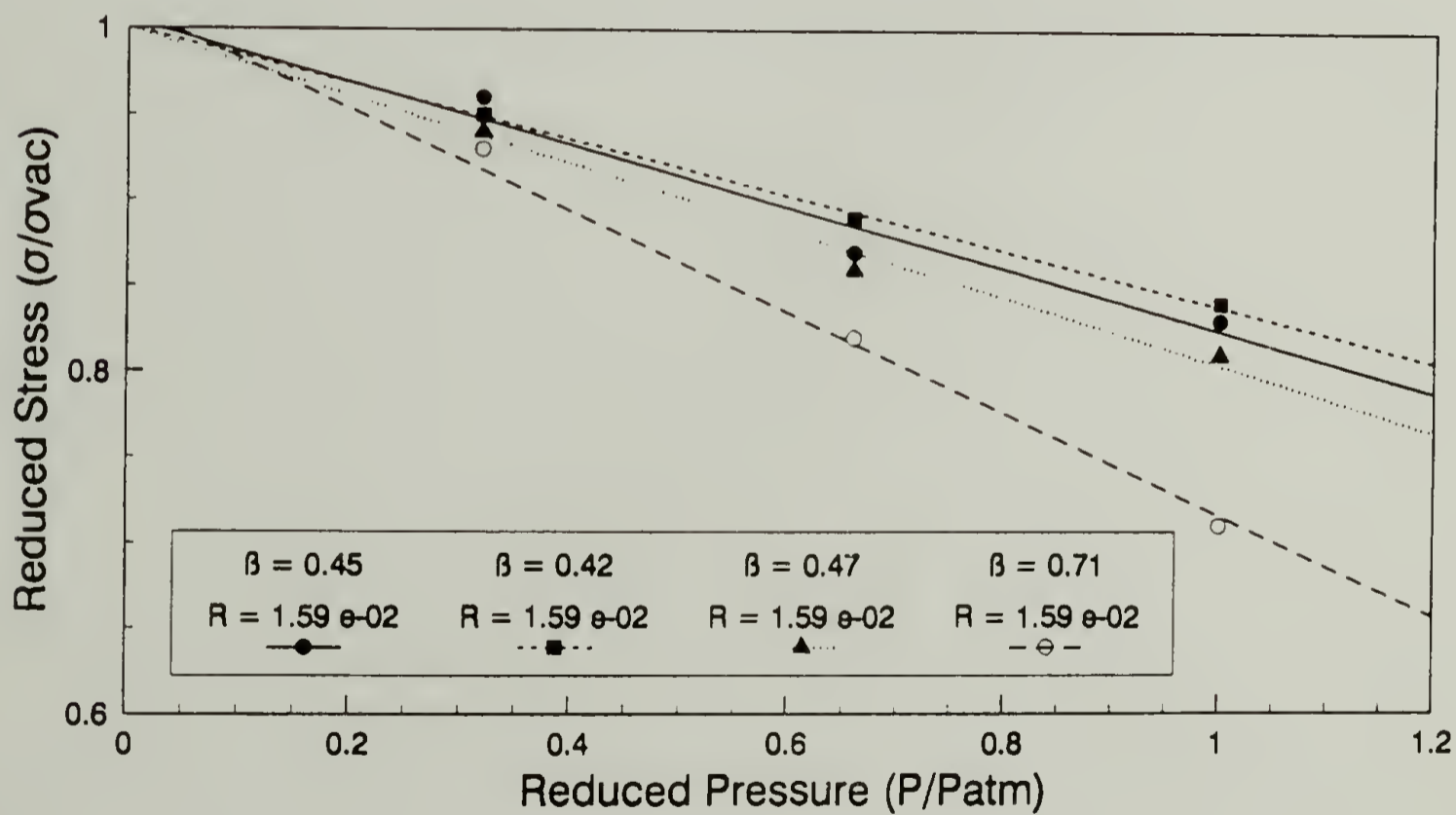
Figure 3.7   Plot of the ratio of the plateau stress at reduced pressure to the average stress measured in vacuum vs reduced pressure.

Table 3.3   Description of epoxy samples used in stress measurement experiments.

Sample	Radius (cm)	Thickness (μm)	Beta	C	Stress (MPa)
132-1	1.59	40.8	0.45	0.0012	2.68
132-2	1.59	41.0	0.42	0.0006	5.64
132-3	1.59	39.4	0.47	0.0004	6.66
132-4	1.59	29.5	0.71	0.0003	5.77
E = 5 GPa	ν = 0.34				

Table 3.4   Calculations of the rigidity and the parameter, C for silver films heated to 800 °C then cooled in an ice bath. The stress values were obtained from plots of stress vs Z_{mn}^2 where the stress in the film is taken as the value of the y-intercept.

Sample	Thickness (m)	Radius (m)	Stress (MPa)	Rigidity (D)	$C = D/\sigma R^2$
1	25.4 x 10^{-6}	6.35 x 10^{-3}	27.0	4.77	0.004
2	25.4 x 10^{-6}	1.90 x 10^{-2}	38.0	4.77	0.0003
3	101.6 x 10^{-6}	1.90 x 10^{-2}	4.5	76.4	0.053
4	254 x 10^{-6}	6.35 x 10^{-3}	25.0	477	0.47
5	254 x 10^{-6}	1.90 x 10^{-2}	29.0	477	0.05
E_{silver} = 75.8 GPa; ν_{silver} = 0.38				$D = \dfrac{Eh^2}{12(1-\nu^2)}$	
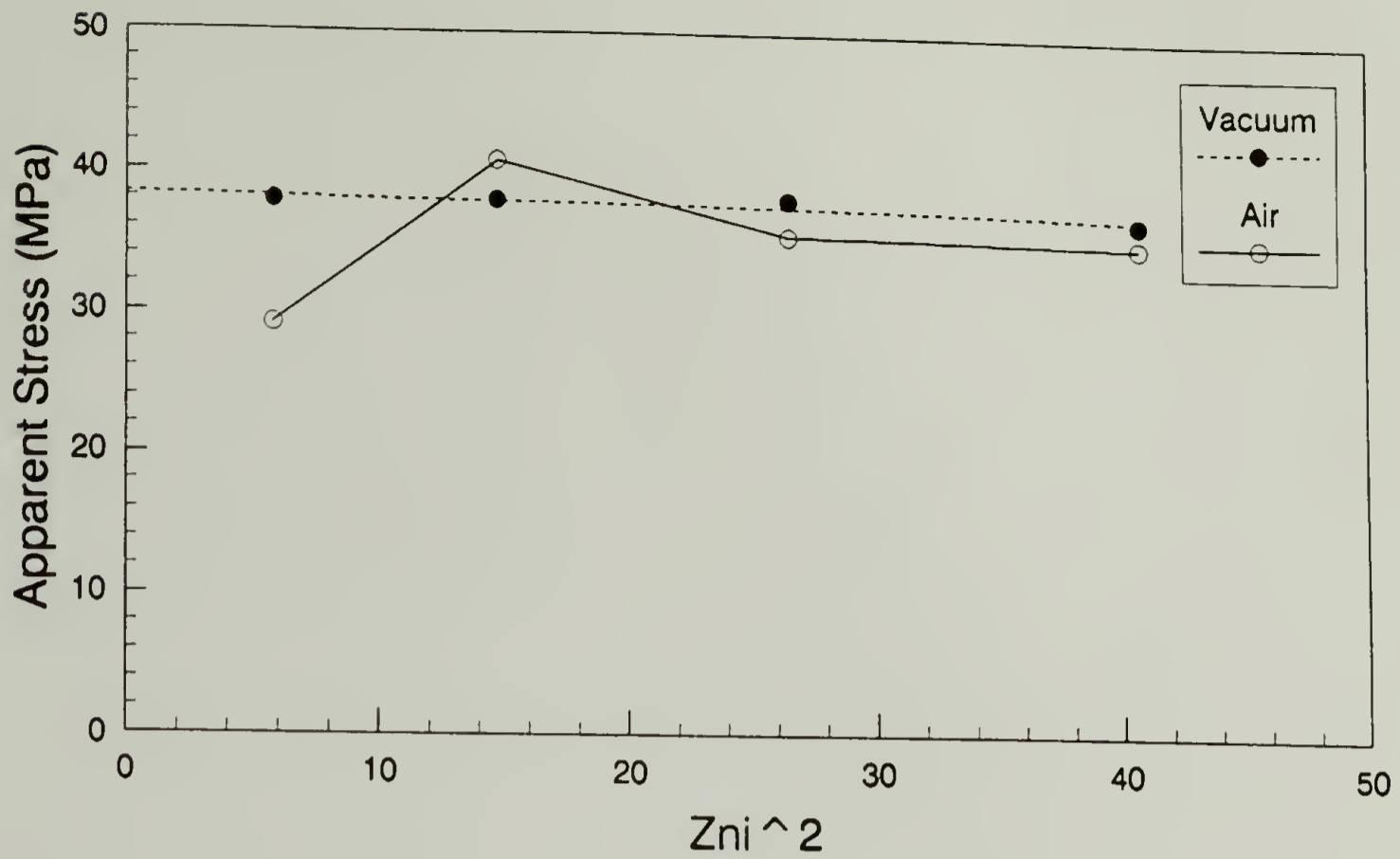
Figure 3.8.a   Stress vs zero of Bessel function squared for a silver film under tension.
R = 1.9 cm, t = 25.4 μm, C = 0.0003, and β = 0.092.
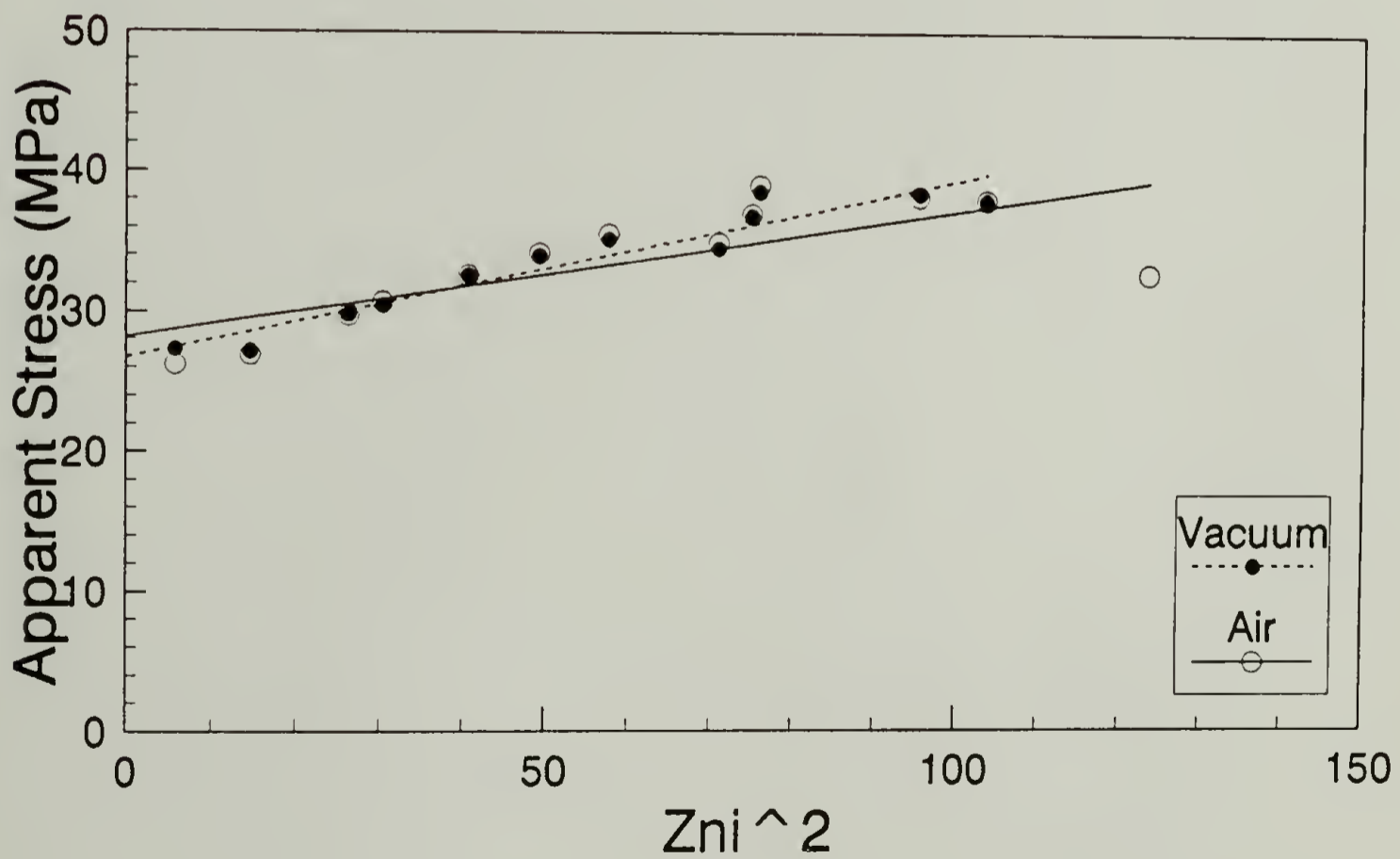
Figure 3.8.b   Stress vs zero of Bessel function squared for a silver film under tension.
R = 6.35 mm, t = 25.4 μm, C = 0.004, and β = 0.031.
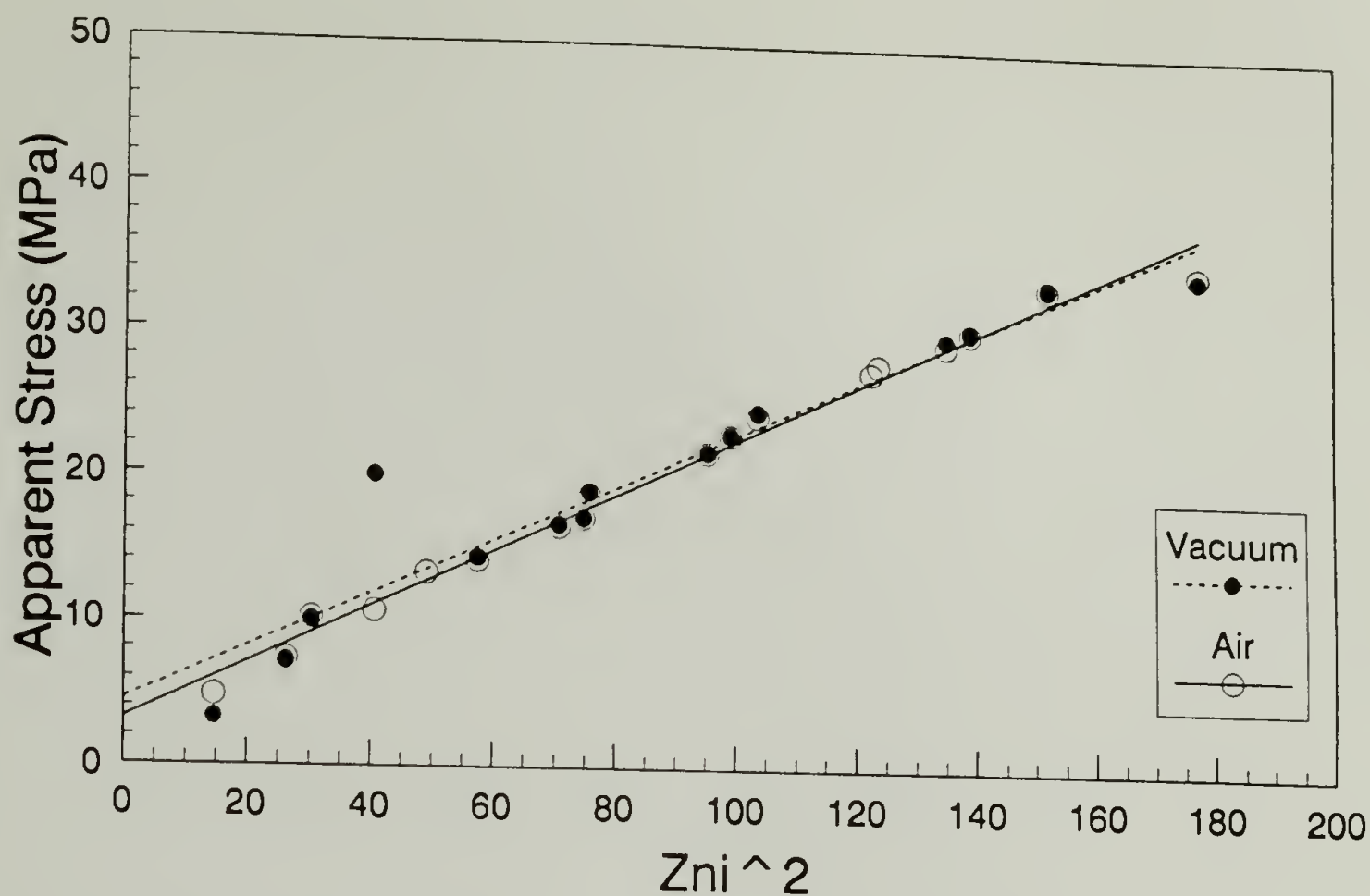
Figure 3.8.c (continued)   Stress vs zero of Bessel function squared for a silver film under tension. R = 1.9 cm, t = 101.6 μm, C = 0.053, and β = 0.023.
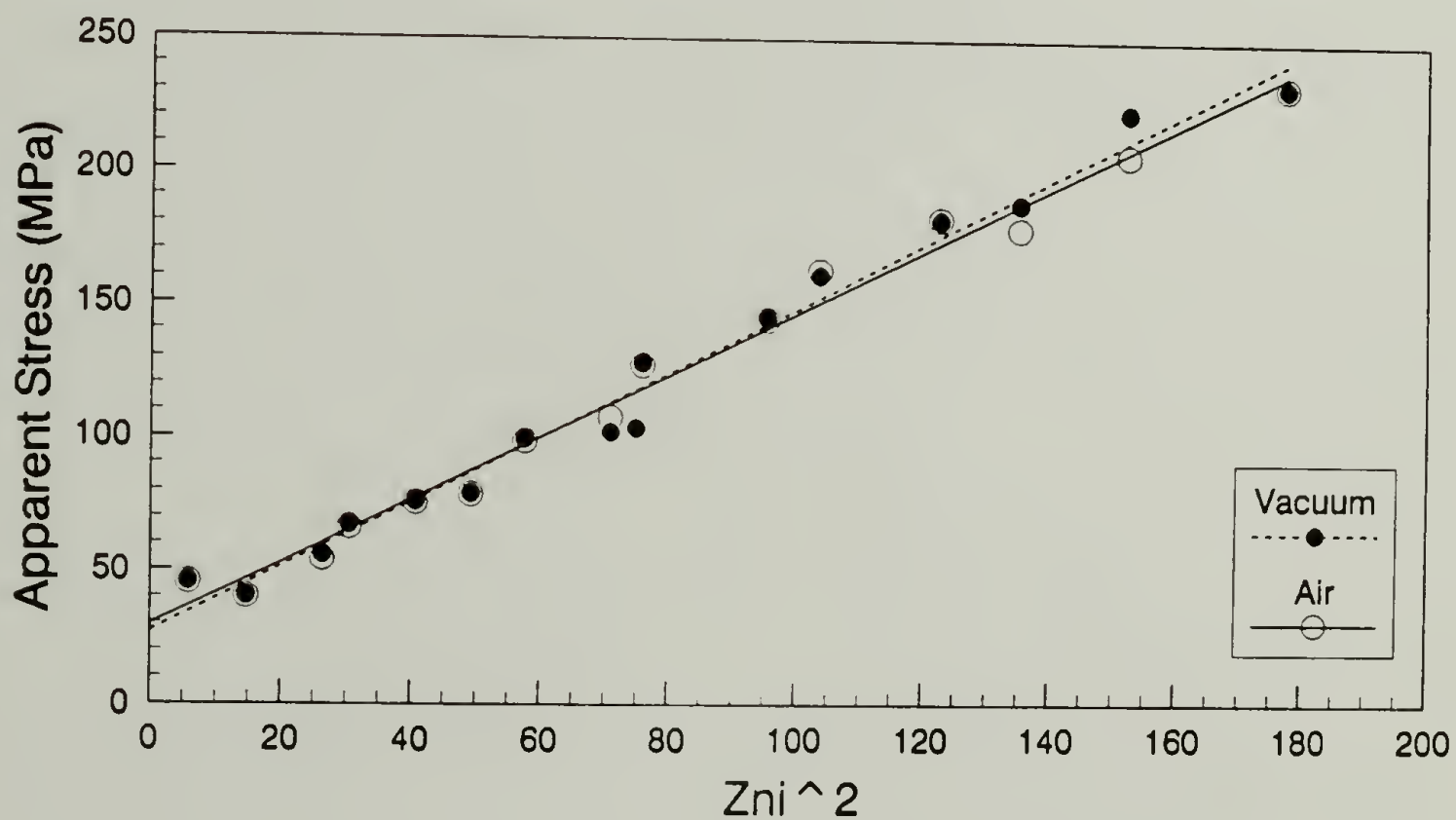
Figure 3.8.d   Stress vs zero of Bessel function squared for a silver film under tension. R = 1.9 cm, t = 254.0 μm, C = 0.05, and β = 0.009.   (continued on next page)
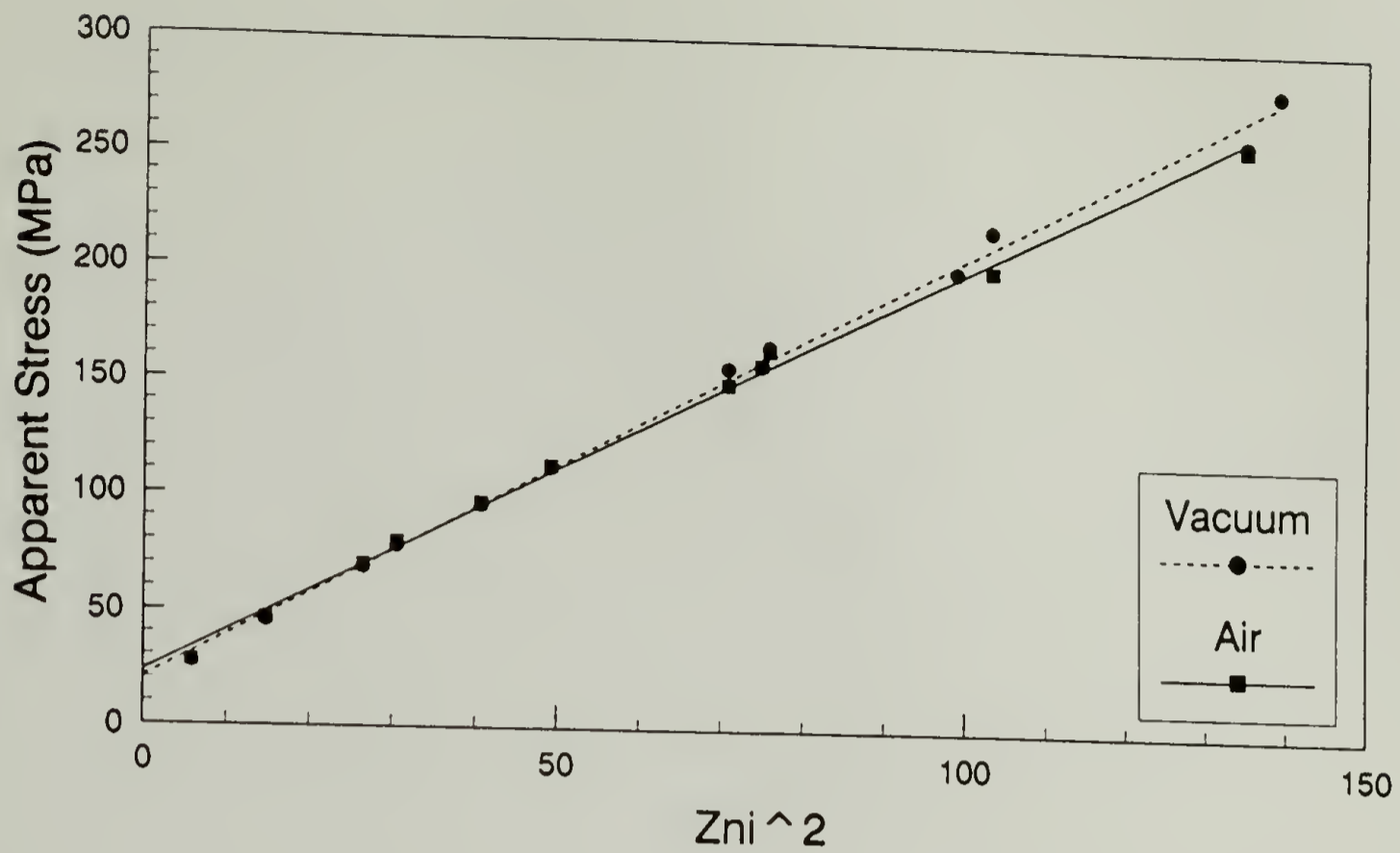
Figure 3.8.c (continued)   Stress vs zero of Bessel function squared for a silver film under tension. R = 6.35 mm, t = 254.0 μm, C = 0.47, and β = 0.003.

Table 3.5   Sample descriptions for filled and unfilled PTFE samples tested in this work, and shown in Figure 3.9 below.

Sample Number	Material	Copper Thickness (μm)	PTFE Thickness (μm)	Radius (cm)	Stress (MPa)	C
1D - F	PTFE	17	50.8	1.9	5.91	4.5 x 10⁻⁵
4 A - D	PTFE	120	50.8	2.54	5.28	
8 A - C	Filled PTFE	17	50.8	1.9	0.71	0.0007
11 A - C	Filled PTFE	120	50.8	2.54	0.79	
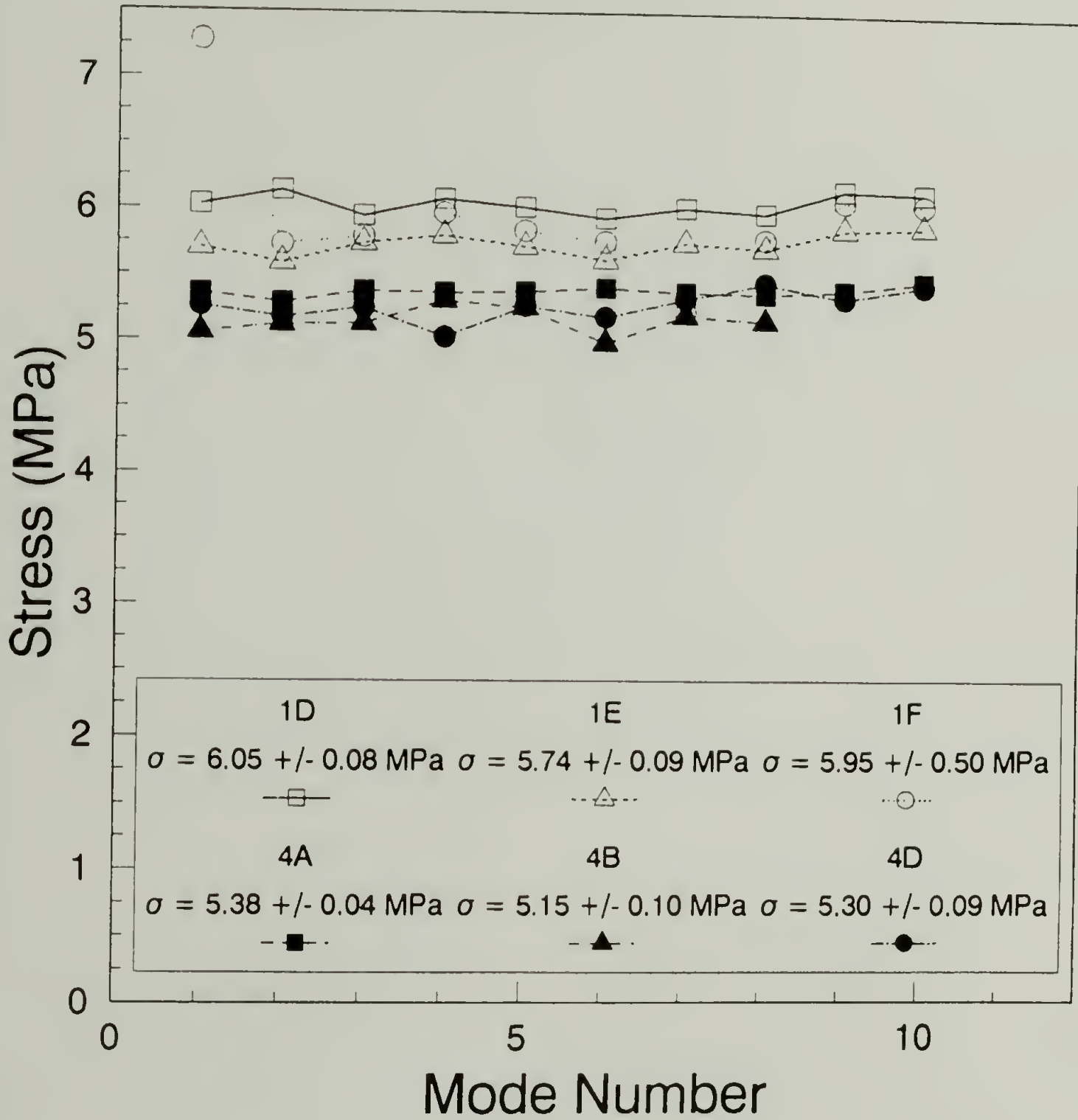
Figure 3.9.a Stress vs mode number for PTFE samples. These samples are unfilled PTFE. A typical C value for these samples is 4.5 x 10^{-5}. (continued on next page)
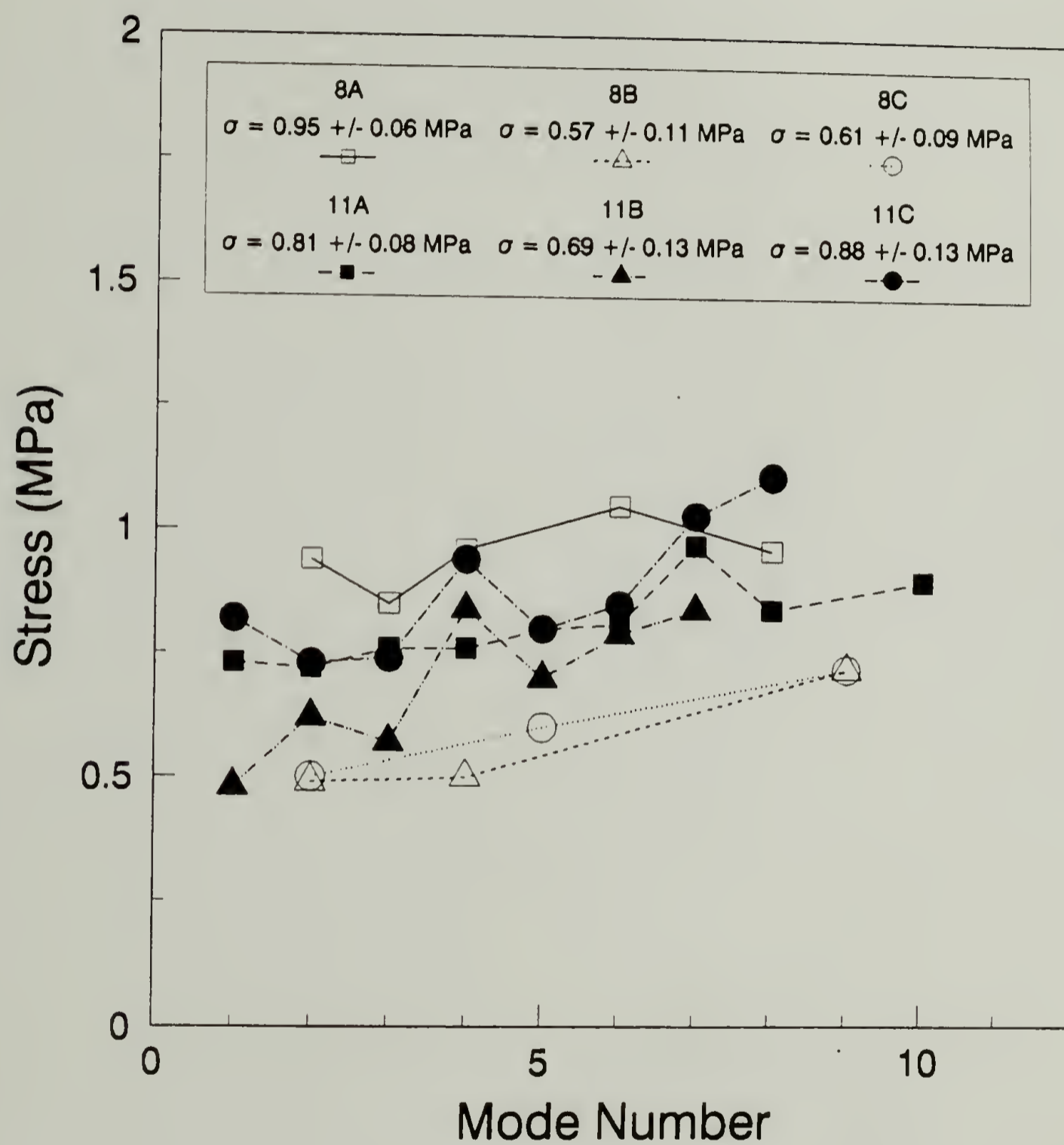
Figure 3.9.b (continued)   Stress vs mode number for PTFE samples. These samples are filled with aluminum oxide particles. A typical C value for these samples is about 0.0007.

3.6   Discussion

The following sections are discussions of the data presented above for the PMDA-ODA air damping studies, the epoxy studies where the effect of β on the air damping effect is investigated, the silver samples which exhibit plate-like behavior, and the filled and unfilled PTFE samples in which the effect of filler on stress is demonstrated.

3.6.1   PMDA-ODA Samples

The most notable effect, when looking at the data taken in various degrees of reduced pressure for the PMDA-ODA coatings is that as the radius of the membrane increases, the air damping effect also increases. This is evident from the lower ratio of the average plateau stress measured in air to the average stress value measured in vacuum for the large samples compared to the smaller samples. This can be attributed to an increase in β with an increase in radius of the sample (β ~ R/h) and is predicted by Lax's theory [1]. For these polyimide membranes, the values of β ranged from 0.95 to 2.51.

Another size effect should also be noted. The samples described above which were all taken from the same spin-coated plate, show a trend to lower stress values with decreasing radius. One possible explanation for this is that the shearing of the epoxy slightly affects the stress in the membrane. The epoxy used on these samples cures at room temperature, therefore its glass transition temperature is also close to room temperature. It is possible, therefore that some motion of the epoxy occurs. A change in the in-plane dimension of the epoxy, ΔL, would cause a corresponding change in the polyimide film. The strain in the polyimide will therefore change by some amount $\Delta L/L$ where L is the radius of the membrane. The strain in the membrane will decrease more

for the smaller samples (small $\Delta L/L$). This larger decrease in strain corresponds to a larger decrease in stress ($\sigma \sim \varepsilon$).

In Figures 3.5.a - 3.5.d Lax's correction has been applied to the data from each sample at each value of reduced pressure. The correction, as applied to the first 0,1 mode is inconsistent and does not match well with measurements in vacuum. However, as applied to higher circular symmetric modes, the average corrected stress values are within an average of five percent of the value measured in vacuum. The average stress values measured in vacuum and the average corrected values (based on Lax's theory) for each sample are given in Table 3.6 below. This leads us to conclude that in order to accurately determine the state of stress in a film when air effects are important, it is important to consider higher modes of vibration. One possible reason for the deviation in the correction for the first circularly symmetric mode of vibration is that in this mode, the entire surface of the membrane moves in and out at each vibration, displacing a finite amount of air each time. For the next mode of vibration, half of the membrane is moving in while the other half is moving out, therefore the net displacement of air is zero, so there is less of a damping effect.

Table 3.6   Average stress values calculated from in vacuo measurements of membranes taken from the same plate.

Sample	Radius (cm)	Average Stress (MPa) (in vacuum)	Average Corrected Stress (MPa)
G1	2.54	11.39	10.70
G2	1.90	11.25	10.81
G3	1.27	10.55	10.32
G4	0.95	10.37	10.32

The average stress calculated from *in vacuo* measurements on the four samples described here are consistent with each other within experimental error. This confirms that the state of stress of the spin-coated and cured polyimide film was uniform, which is an important assumption in the discussion of geometric effects on mass loading.

The magnitude of the stresses measured in vacuum is significantly lower than the reported stress value of 30 MPa for PMDA-ODA cured to 400 °C on a silicon substrate [21]. The films in our experiments however have only been cured to 225°C due to material constraints in both the polyimide on copper system (which oxidizes at high temperatures if even trace amounts of oxygen are present) and in the polyimide on tin coated steel which cannot be heated above 232 °C, the melting point of tin. One way of circumventing this problem is to coat substrates with silver which is also soluble in mercury, and can be heated safely to 400 °C (T_m^{silver} = 961.93 °C [22]). The dissolution of silver in mercury takes longer than the amalgamation of tin with mercury (about 5 days as opposed to 1) so the sample preparation time is longer. interlayer takes longer.

The stress values measured in our experiments are reasonable considering the mismatch in coefficients of thermal expansion of the substrate and the coating and the curing stresses which occur in this range of temperatures. The equation for thermal biaxial stresses in a coating on a rigid substrate is:

$$\sigma = \frac{-\Delta\alpha \, \Delta T \, E_c}{1 - \nu_c} \tag{3.24}$$

where

$\Delta\alpha$ = $\alpha_c - \alpha_s$ = mismatch in coefficients of thermal expansion between
substrate and coating (mm/mm/°C).

ΔT = change in temperature (°C).

E_c = Young's modulus of the coating (GPa).

ν_c = Poisson's ratio of the coating.

The Young's modulus and Poisson's ratio of PMDA-ODA film are 3.0 GPa and 0.34 respectively [23]. The coefficient of thermal expansion for steel is 12.0×10^{-6} mm/mm/°C [24], that of PMDA-ODA is about 18.0×10^{-6} mm/mm/°C [23], and that of silicon is 2.5×10^{-6} [25]. Using the above equation to calculate the thermally induced stresses gives, for PMDA-ODA cured to 225 °C or 400 °C on steel, 5.3 MPa or 10.2 MPa respectively. For PMDA-ODA cured to 400 °C on silicon, the thermally induced stress is 26.4 MPa. The difference in value between the calculated thermal stress of 5.3 MPa at 225 °C and the measured value of 10 -11 MPa can be accounted for by the stresses due to curing in the sample. Geldermanns et al. report that the imidization reaction is completed at 200 °C, but during the final cure to 400 °C molecular reorganization occurs and relieves the bulk of the curing stresses. The authors indicate that the residual stress in the polyimide is due solely to the thermal stresses caused by mismatch in coefficient of thermal expansion between the coating and the substrate [26]. Some further work on the nature of the two dimensional stresses in PMDA-ODA during curing will be discussed in chapter 4.

3.6.2 Epoxy Paint Base Samples

The results from the epoxy samples show that there is a definite increase in the air damping effect with an increase in the value of β as one would expect. This was also demonstrated with the measurements made on the PMDA-ODA samples discussed above. The question is whether there is ever a value of β at which the air damping effect can be practically neglected even for measurements made in air. This would be the value of β at which the slope of the reduced stress vs reduced pressure curve goes to zero with an intercept of one. Theoretically, the ratio of σ/σ_{vac} goes to one, and the slope of the reduced stress vs reduced pressure curve goes to zero at $\beta = 0$ ($\rho_0 = 0$). This is shown in Figure 3.10 where a plot of the slopes of Figure 3.7 vs β is shown. A linear regression analysis was done on this data, forcing the y-intercept to go through zero. The slope of this line gives the constant K for the equation

$$\frac{\sigma_{air}}{\sigma_{vac}} = 1 - K\beta \tag{3.25}$$

where $K = 0.49$ with a variance of $S^2 = 0.0025$. A plot of the ratio of the average plateau stress value measured in air to that of the average stress measured in vacuum vs β for both epoxy and PMDA-ODA materials is shown in Figure 3.11. This plot indicates that for $\beta < 1$ the linear solution ($K = 0.49$) does hold, however for $\beta > 1$, the more accurate correction proposed by Lax must be used [1]. This has important implications for sample design. If the β value is kept sufficiently low, (< 1) then a simple relationship between the stress measured in air and that measured in vacuum may be used. Since this is not the case for the PMDA-ODA samples, this may explain why Karnezos' [2] simple linear relation did not fit our data well.
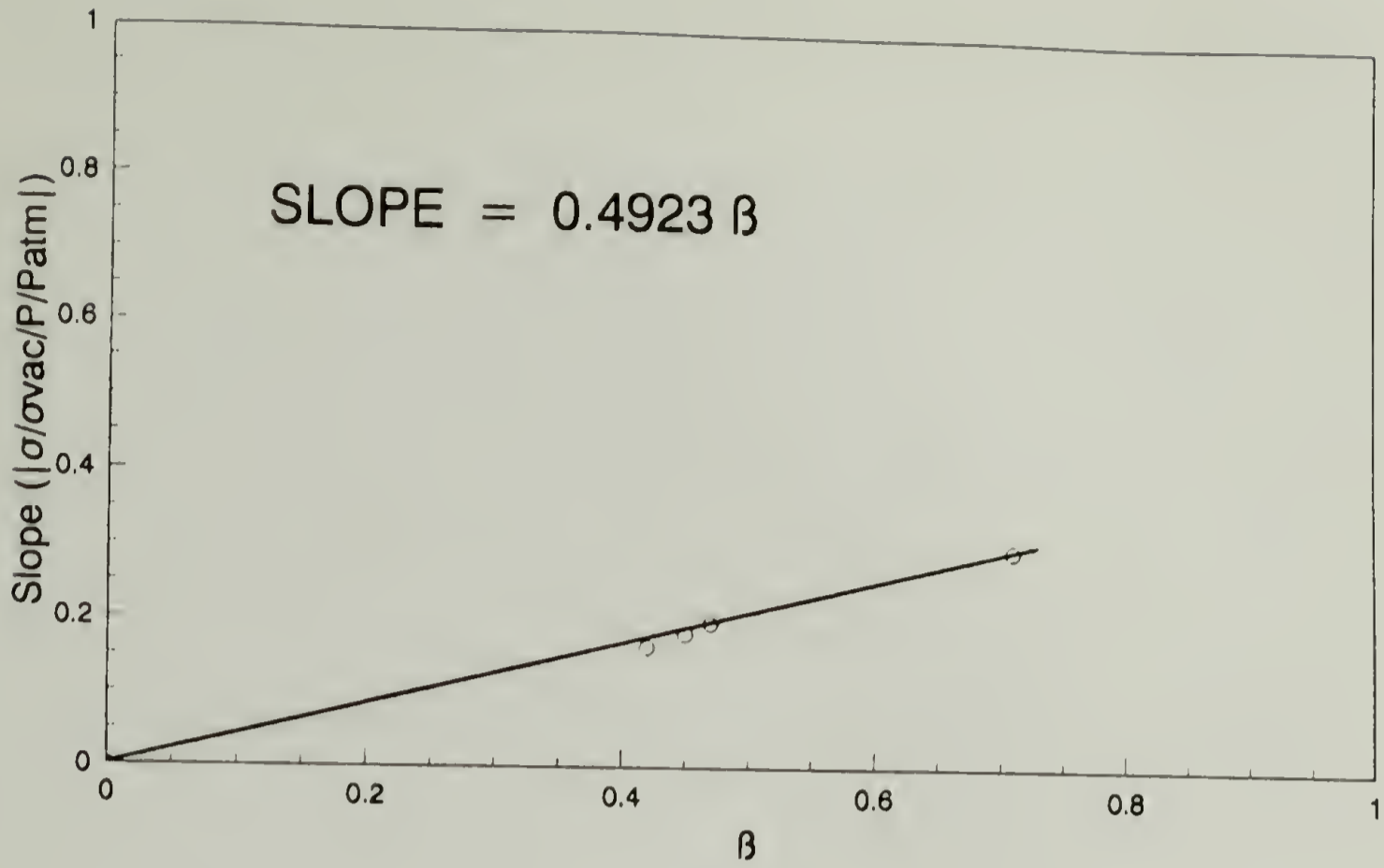
Figure 3.10   Plot of reduced stress divided by reduced pressure vs β.
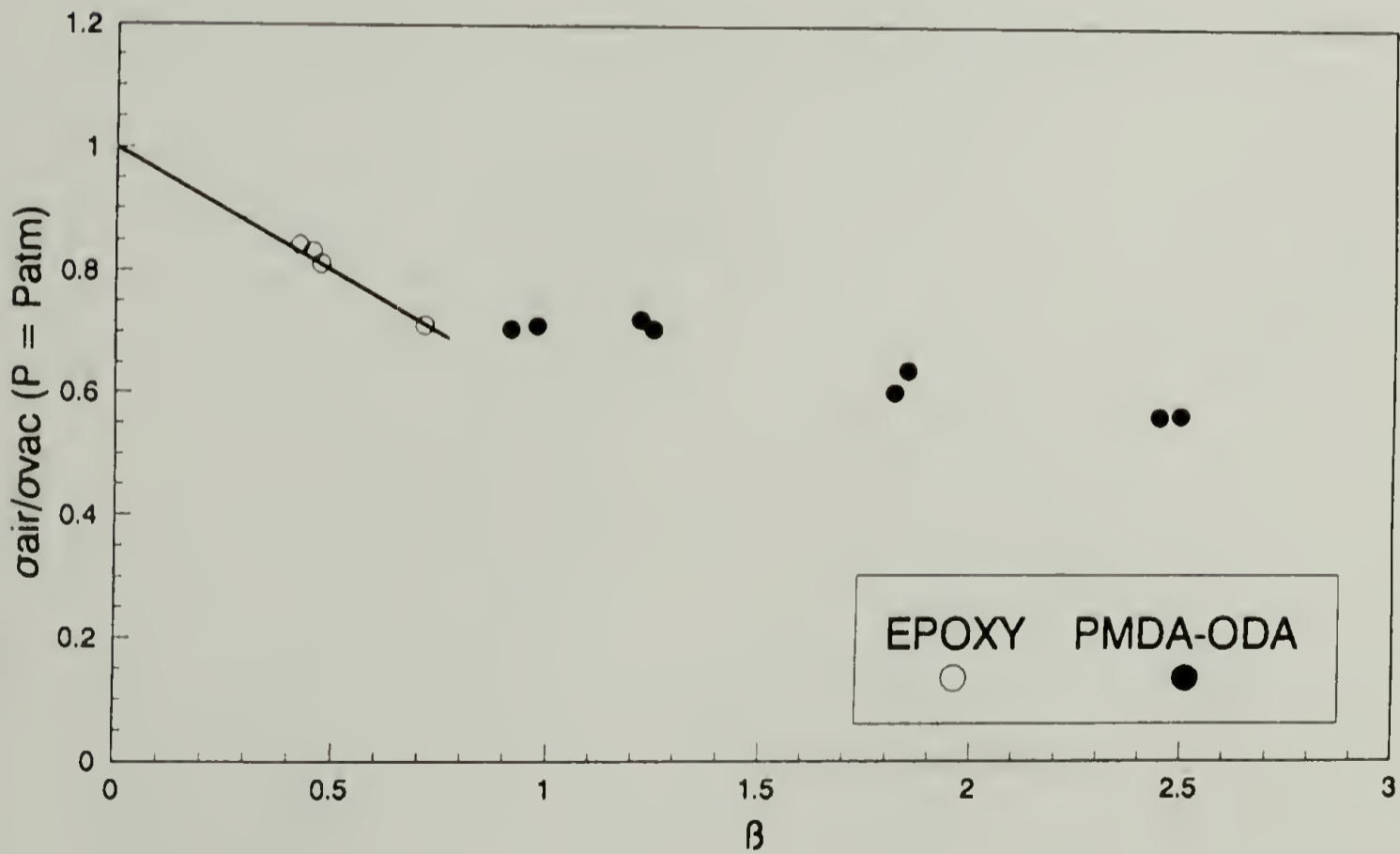
Figure 3.11   Plot of $\sigma_{air}/\sigma_{vac}$ vs β for epoxy and PMDA-ODA samples.

3.6.3 Silver Samples

The data for the silver samples is ordered from the sample with the lowest value of C to that with the highest value of C. The data from the first sample, shown in Figure 3.9.a indicates that there is some effect of air damping on the membrane, i.e. the stress measured in air differs from the constant stress measured in vacuum and exhibits the typical lower stress value for the first mode of vibration. This effect is slight in this sample, but it is present. For this film $C = 0.0003$ and $\beta = 0.092$. The next sample behaves noticeably differently, however. In Figure 3.9.b the data shows essentially no difference in the measurements made in air or in vacuum and there is also an increase in the calculated stress value with increasing mode of vibration (behavior indicative of some slight bending effect). The value of C at 0.004, however is still safely below the value where bending would have a dominant role. As the samples become increasingly thicker and/or smaller, bending plays an ever increasing role, which is evidenced in the steeper slopes of the apparent stress vs Z_{mn}^2 curves (Figures 3.9.c - 3.9.e).

There are several things to note about the measurements made on the silver samples. Firstly, this data indicates that the value of β where air damping would not be important is somewhere between $\beta = 0.092$ and 0.031. Also, from these plots one should be able to calculate the Young's modulus of the material from the slope of the line and determine the stress in the film which is simply equal to the intercept of the line [27]. One needs to be careful when analyzing this data however, for when C is too large, the slope of a straight line through the apparent stress vs zero of Bessel function squared does not give an accurate modulus value, and the intercept value of stress can be off by as much as thirty percent. This is the case when edge effects and bending play a dominant role in the vibration and numerical methods must be used to solve for the values of modulus and stress [6].

3.6.4 Filled and Unfilled Samples of Poly(tetrafluoroethylene)

The most notable observations to be made from the measurements conducted on the PTFE materials are that the stresses in the unfilled samples are about five times higher than those in the filled samples. This is a well known phenomena in general (i.e. that fillers can decrease the stress in a material especially if there is poor adhesion between the matrix and the filler material). It has also been shown that glass fillers decrease the stress in epoxy materials [28]. Also, the stress does not seem to be affected by the thickness of the outer laminate material. There is no systematic correlation between stress and copper thickness between the filled and the unfilled samples measured. There is considerable scatter in the data for the filled samples, this effect was not seen by other workers measuring low stress values in polymer films. The cause for this behavior is unknown.

3.6.5 Summary

This chapter presents experimental evidence for the influence of air damping and stiffness on the resonant vibrations of membranes. Membranes of several different types of materials have been tested, which lead to conclusions about limiting values of the air damping parameter, β and the stiffness parameter, C. The effects of air damping on the vibration behavior was evaluated in the experiments performed on the PMDA-ODA ployimide membranes. These experiments prove that Lax's correction equations can be applied to vibration measurements made in air to yield a stress value which is within experimental error of the value measured in vacuum. This analysis may be extended to study the effect of any environment of known density on the stress in a membrane.

The stress measurements conducted on the epoxy materials indicate that there is a value of β below which air damping can be approximated as a linear function of β. This

was demonstrated in Figure 3.11. The critical value of C is approximately 0.01 [5]. The epoxy samples and polymeric materials in general are quite useful for investigating the effects of air damping on membranes because for standard sample sizes the C values fall well below the critical value (C < 0.01) and therefore are not affected by bending effects.

The value of C for metal samples is much more sensitive to geometry than for polymeric samples as shown in Figure 3.3.b. Even at C values of as low as 0.004 silver samples begin to show an increase in calculated stress with increasing mode of vibration. At C = 0.05, the increase in calculated stress values with increasing mode of vibration is very large and bending effects dominate. In order to extract Young's modulus information from this data, more complicated analysis must be used [13].

It should also be noted that even in cases where C is small, bending can be inportant at high mode numbers. This can be seen from equations (3.17.b) and (3.20.b) where, an increase in the value of the mode numbers causes an increase in the ratio σ_{ap}/σ which is a measure of the role that bending plays in a system.

The stress in the unfilled PTFE samples is an order of magnitude higher than that measured in the filled PTFE material. This difference can be attributed to the filler content. When there is poor adhesion of the filler material to the matrix, as in this case, cavitation around the filler particles occurs that can lower the stress value in the material. The reason for the scatter in the data for the filled samples is unknown, one possible explanation may be an uneven distribution of filler in the samples, causing deviation in the occurrence of resonant frequencies.

In this chapter, the idea that measurements done in air can be corrected to yield the value of stress in a film was introduced. This enables work to be done on the stresses in membranes with variation in humidity or with exposure to other solvent atmospheres. The concept of designing samples with geometries such that air damping and stiffness do not complicate the measurements was also discussed. It is important to keep in mind

when doing this, however, that as one lowers β of a sample by changing its geometry, the value of C will increase. Keeping these concepts in mind, the holographic interferometry technique is a very versatile and widely applicable technique for tensile biaxial stress measurements in films and coatings.

REFERENCES

1. Lax, M. "The Effect of Radiation on the Vibrations of a Circular Diaphragm," *The Journal of the Acoustical Society of America*, **16**(1), 5 (1944).

2. M. Karnezos, "Effects of Stress on the Stability of X-ray Masks," *Journal of Vacuum Science and Technology*, **B4**(1), 226 (1986).

3. H. P. W. Gottlieb, and H. A. Aebischer, "Eigenfrequency Shifts of a Baffled Circular Membrane in a Fluid Medium," *Acustica*, **61**(4), 223 (1986).

4. Q. K. Tong, *Characterization of Processing Stress and Structure-Property Relationships on a Polyacrylate Photoresist Coating*, Ph.D. diss., University of Massachusetts, 1992.

5. Q. K. Tong, M. A. Maden, A. Jagota, and R. J. Farris, "Vibrational Techniques or Stress Measurement in Films - 2. Extensions and Complicating Effects," *Journal of Materials Research*, submitted for publication (1991).

6. A. W. Leissa, *Vibration of Thin Plates.* NASA Publication SP-160, (Washington, D. C.: NASA, 1969).

7. J. W. Strutt, 3rd Baron Rayleigh, *The Theory of Sound*, (New York: Dover Publications, 1945) (First published, 1877).

8. Q. K. Tong and R. J. Farris, "Measurement of Two-Dimensional Stresses in Thin Polymer Films Using Holographic Interferometry," submitted for publication, (1990).

9. *Handbook of Chemistry and Physics*, 64th Edition, ed. R. C. Weast, p. D-186, (Boca Raton: CRC Press, 1983).

10. S. Mazur, supplied these samples, 1989, CR&D, Experimental Station, The DuPont Company, Wilmington, DE, 19880-0356.

11. R. Wiley and G. Schmitt, IBM Corporation, Endicott, NY, (1990).

12. Prepared at CR&D, Experimental Station, The DuPont Company, Wilmington, DE, 19880-0356.

13. Prepared at CR&D, Experimental Station, The DuPont Company, Wilmington, DE, 19880-0356.

14. 851AT Green Tape™ substrate, The DuPont Company, Wilmington, DE 19880-0356.

15. M. A. Maden, A. Jagota, S. Mazur, R. J. Farris, "Vibrational Technique for Stress Measurement in Films - 1. Ideal Membrane Behavior," *Journal of Materials Research,* submitted for publication (1991).

16. C. L. Bauer, *The Determination of the Mechanical Behavior of Polyamic Acid/Polyimide Coatings,* Ph.D. diss., University of Massachusetts, Amherst, MA, (1988).

17. *Handbook of Plastics and Elastomers,* ed. C. H. Harper, p. 3-23 (New York: McGraw-Hill Book Co., 1975).

18. R. Wiley, IBM Endicott, Endicott, NY telephone conversation, (1990).

19. A, DeGreef-Sasst, private communication, Rogers Corporation, Rogers, CT, (1992).

20. Bradley Weather Station (updated hourly) Bradley Field, CT.

21. I. C. Noyan, and L. T. Nguyen, "Residual Stresses in Polymeric Passivation and Encapsulation Materials," *Polymer Engineering and Science,* **28**(16), 1026 (1988).

22. *Handbook of Chemistry and Physics,* 64th Edition, ed. R. C. Weast, p. B-32, (Boca Raton: CRC Press, 1983).

23. *Kapton Polyimide Film: Summary of Properties,* (Wilmington: DuPont Company, 1986).

24. D. Williams, and J. Spangler, *Physics for Science and Engineering,* p. 341, (New York: D. Van Nostrand Company, 1981).

25. S. K. Ghandhi, *VLSI Fabrication Principles: Silicon and Gallium Arsenide,* p. 45, (New York: John Wiley and Sons, 1983).CTE of silicon

26. C. Goldsmith, P. Geldermans, F. Bedetti, G. A. Walker, "Measurement of Stresses Generated in Cured Polyimide Films," *Journal of Vacuum Science Technology,* **A1**(2), 407 (1983).

27. Y. H. Hu and A. Jagota, "Stresses During Processing and Thermal Cycling of Metal Foils on Ceramic Substrates," *Mechanical Behavior of Materials and Structures in Microelectronics,* eds., E. Suhir, M. Jono, R. C. Cammarata, D. D. L. Chung, C. G. M. van Kessel, Materials Research Society Symposium, vol. 226, (1991).

CHAPTER 4

THE EFFECT OF TEMPERATURE ON STRESS

4.1   Introduction

One of the original goals of this work was to measure the effect of temperature and humidity (or solvent) on the stress in a coating using the holographic interferometry technique described in this thesis. This capability is necessary in order to predict stress behavior in coatings due to thermal cycling and exposure to solvents under typical operating conditions. The combined effect of temperature and humidity on the failure of coatings is also an area which is currently of great interest. The mechanisms for the blistering and delamination in such cases is still not fully understood. In BPDA-PDA films, compressive failure by blistering has been observed under conditions of increased humidity and temperature [1].

To study the effects of temperature and atmosphere on the stress in a membrane, an environmental chamber in which the sample temperature can be controlled, and into which gases or solvents may be introduced is required. The chamber must also be light and small enough to be mounted on and shaken by the existing piezoelectric transducer. There have been attempts in the past to build environmental chambers which will go to very high and very low temperatures in which holography experiments may be conducted. One of the main problems is the build-up of condensation on the front window at low temperatures and convection and thermal gradients may cause interference with making the hologram. Another prroblem is that in order to vibrate the membrane in a large chamber, such as the chamber design attempted by Newport Corporation, the elctronics and piezoelectric transducer must be able to operate at high and low temperatures. Because no such environmental chamber was commercially

available, it was necessary to design one. The problems mentioned above have been over come by design features which will be discussed later. A large part of the work done to obtain the results described in this chapter involved the design of this environmental chamber in which to conduct temperature and humidity experiments.

The change in biaxial stress in a membrane due to a change in temperature is given by the equation (frm linear elasticity theory),

$$\Delta\sigma = -\Delta\alpha\Delta TE/(1 - v) \qquad\qquad (4.1)$$

where,

$\Delta\sigma$ = The change in stress (Pa)

$\Delta\alpha$ = $(\alpha_f - \alpha_s)$, Difference in coefficient of thermal expansion

ΔT = Change in temperature (°C)

E = Young's modulus (Pa)

v = Poisson's ratio

The slope of a plot of stress vs temperature gives the quantity $\Delta\sigma/\Delta T$, and the coefficient of thermal expansion of the material can then be calculated using known values of Young's modulus and Poisson's ratio. However if a material is not fully cured, this may affect the calculations, and care must be taken in this analysis. Part of the usefulness of the environmental chamber is that it may be used to study the curing process of polymeric films.

4.2   Experiments

Initial temperature experiments described below were done in the small chamber originally used for the vacuum experiments. This chamber is shown in Figure 4.1. The purpose of these experiments was basically a feasibilty study, to determine whether a sufficiently constant temperature could be maintained so that thermal fluctuations in the chamber would not interfere with the holographic imaging. After determining that the temperature could be kept fairly stable in that crude system, during the course of a stress measurement (10 - 15 minutes) the second chamber design was started. The rest of the temperature experiments were done in the new chamber. The experiments were an attempt to study the stresses in two different types of polyimide films during their cure cycles. The stress in partially cured polyimide samples was observed during thermal cycling.

4.2.1   Environmental Chamber Design

Initially an attempt was made to find an environmental chamber that would go from -65 °C to 400 °C under vacuum and in which we could vibrate a membrane. The options were to get a large chamber into which a piezoelctric shaker would fit (which would also mean getting a bigger table) or to design our own which could be mounted to the existing piezoelectric shaker. As space limitations precluded the acquisition of a larger table, and there were few large chambers available which met our specifications, we have designed our own.

Our space limitations require special dimensional and weight restrictions. The specifications which we require are that it have an operating temperature range of -65 - 400 °C, be able to operate from 10^{-3} to 1000 torr, have extra electrical, thermocouple and gas feedthroughs, be well insulated, and weigh less than 20 pounds. The ports on

Figure 4.1   Photograph of the sample chamber originally used for biaxial stress vs temperature experiments.

the chamber have to include an an optical quality window on the front through which holography can be done, a sapphire window on the back for experiments that require heating a sample from behind, and for potential use in experiments utilizing an infrared temperature measurement system. We also need a chamber that can heat and cool the samples efficiently, and has a sample mount connected to the inside of the chamber which can accommodate different sample sizes, and has a port through which samples can be loaded easily.

The final chamber design is shown schematically in Figures 4.2.a - 4.2.c. Photographs of the chamber are shown in Figures 4.3.a - 4.3.c. This section will discuss some of the key elements of the design of the chamber. The first consideration was that the chamber be light enough to be suspended from the piezoelectric transducer. Therefore the body of the chamber is made from 1/16 " thick aluminum sheet. The body consists of two concentric tubes about 8" long with a gap of 1/4" between each wall. This is done so that air or cool gas from a liquid nitrogen container may be run through the walls to keep them cool during heating experiments. The front of the chamber is a window through which the holograms are made. It is important to ensure that condensation does not form on the windows during cooling experiments. Therefore, in addition to the single quarter inch thick pane of glass, there is a mount for three 1/16" thick windows separated by o-rings. The gaps between these windows can be evacuated so that the assembly acts as an insulating barrier to prevent moisture build-up on the outer window. The heating and cooling of the sample is done with a plate that fits directly behind the sample holder and is separated by about 1/64" from the sample holder. The plate is a 4" disc made of copper for good thermal conductivity, has cooling channels bored through the inside of the plate and has a resistance heated steel hot plate mounted to the back. The heating and cooling is controlled by a programmable temperature controller which is connected to a thermocouple attached to the plate, and controls the current to the hot plate, and a solenoid valve which allows the introduction
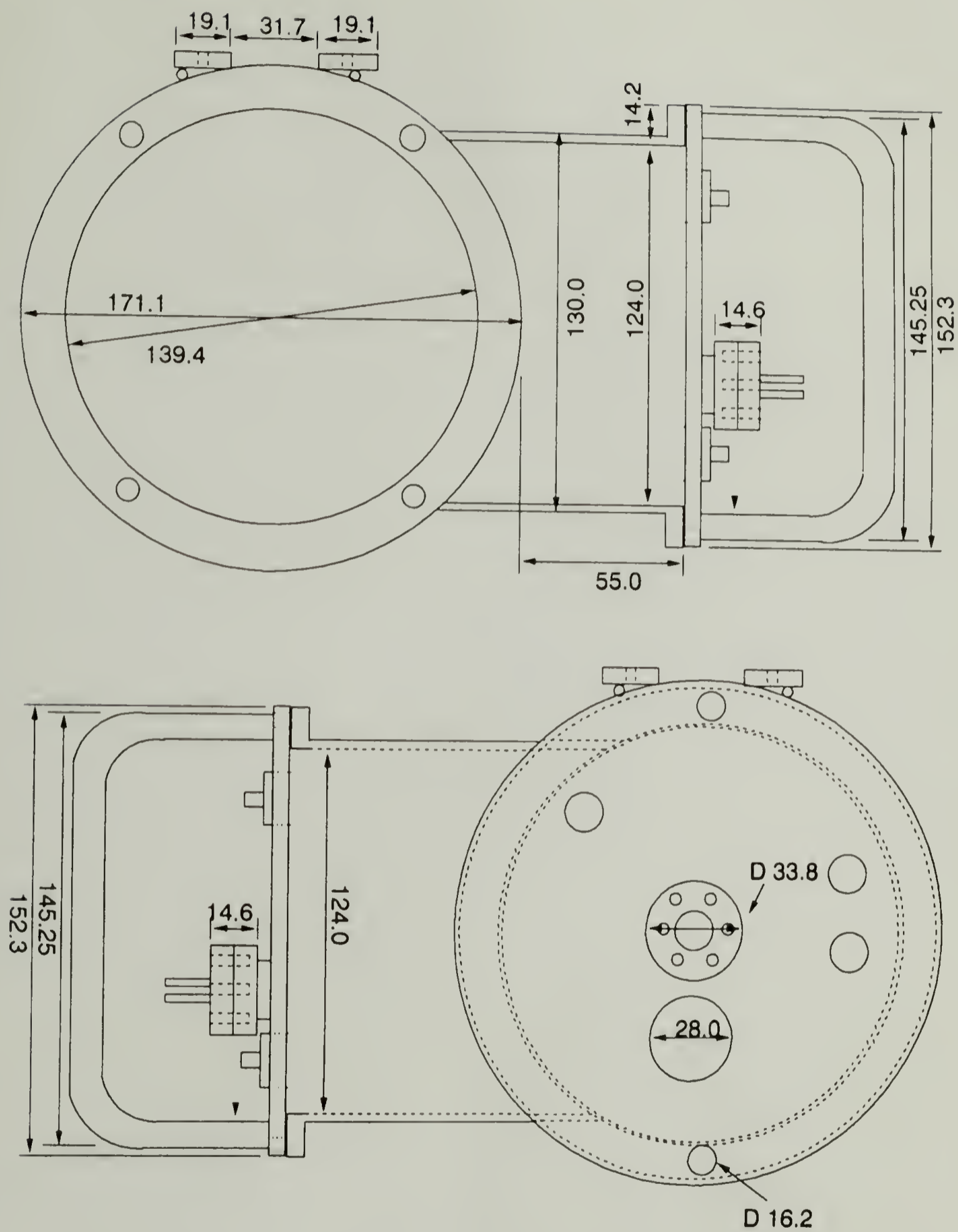
Figure 4.2.a   Schematic of the environmental chamber design. (continued on next page)

D 33.8

Liquid Nitrogen
Inlet and Outlet

Heat Shield

Heater

1.25

4.0

25.3

121.1

124.0

70.2

14.6

19.0

6.3

145.25

152.3

Thermocouple Feedthrough
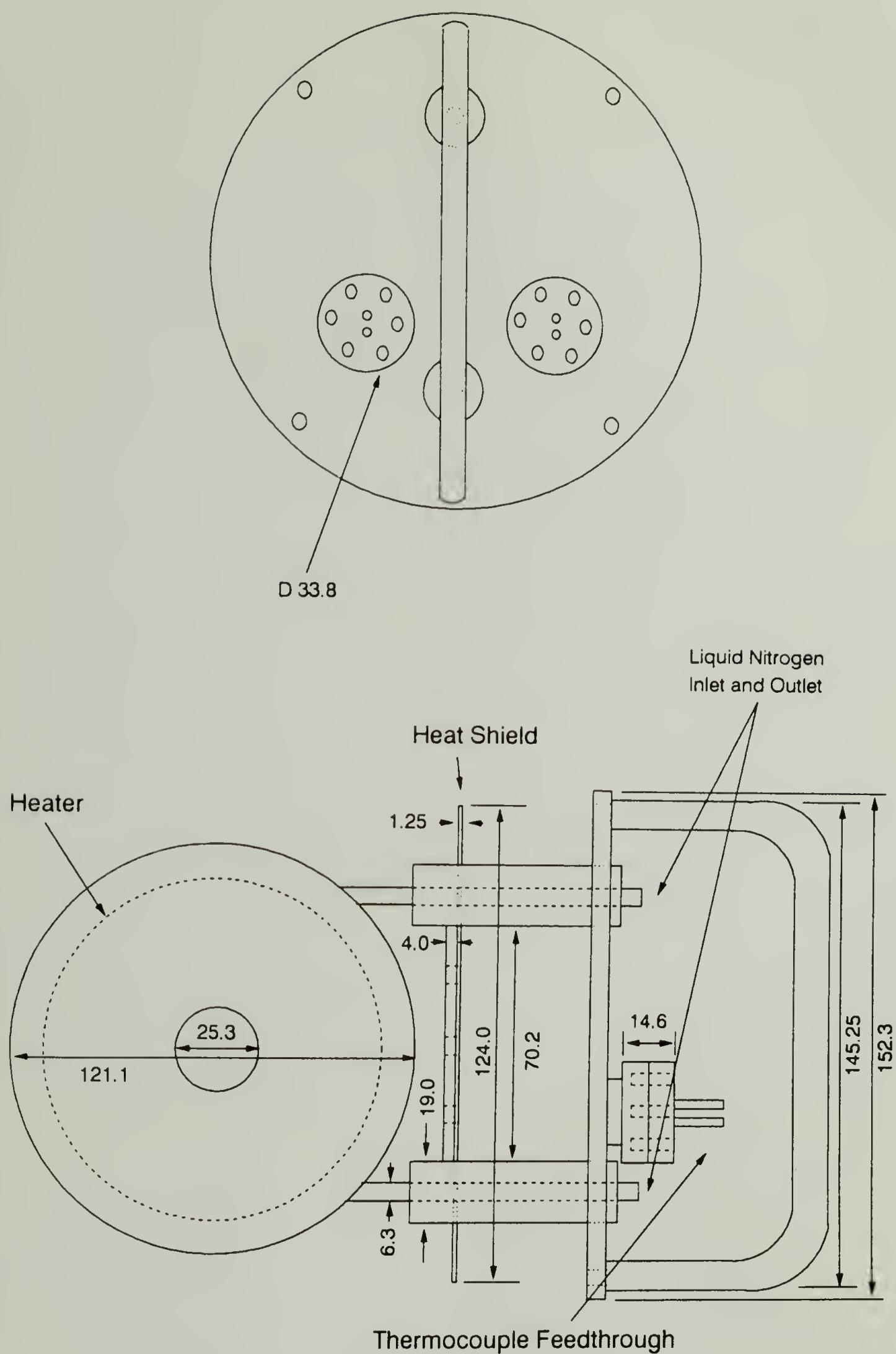
Figure 4.2.b (continued)   Schematic of the environmental chamber design.
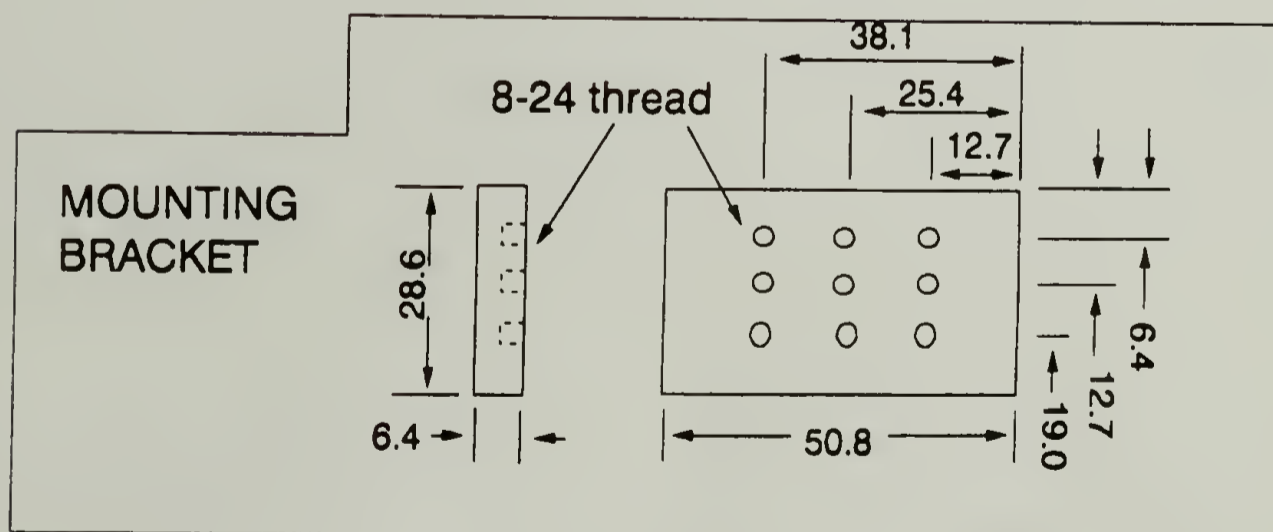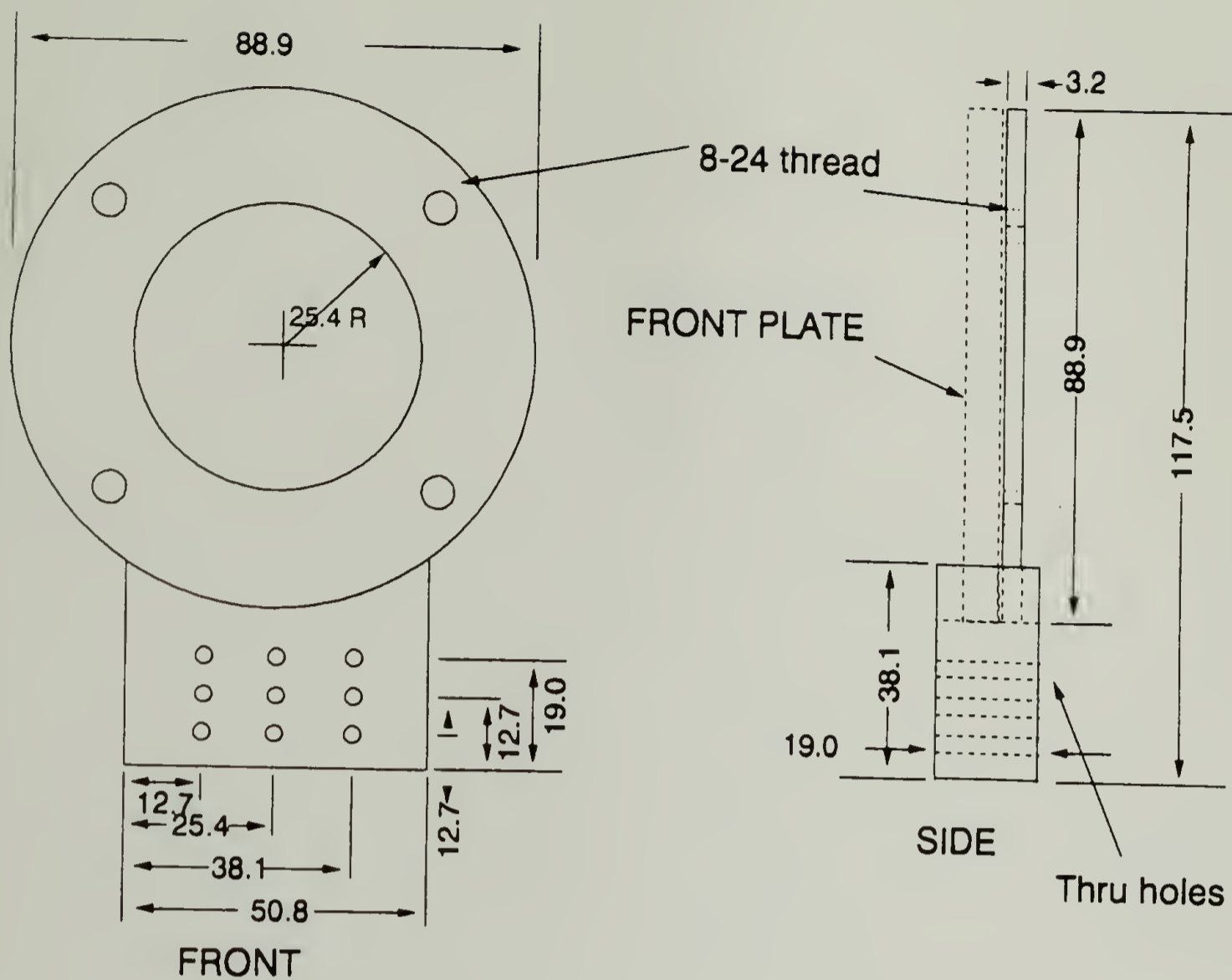
Figure 4.2.c (continued)   Schematic of the environmental chamber design.

Figure 4.3.a   Photograph of the environmental chamber. (continued on next page)
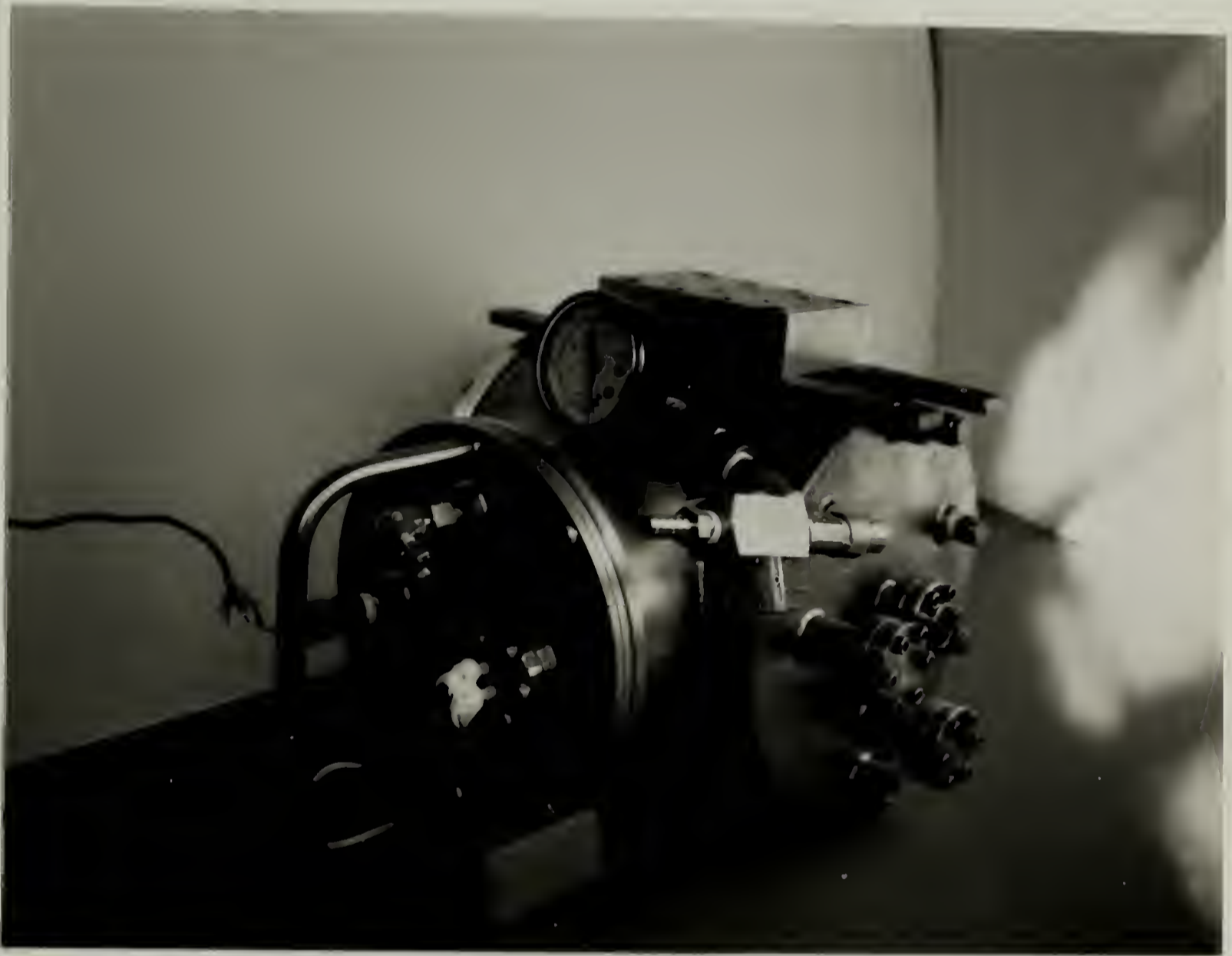
Figure 4.3.b (continued)   Photograph of the environmental chamber.

Figure 4.3.c (continued)   Photograph of the environmental chamber.

of gas or liquid nitrogen through the cooling coil. The plate is connected directly to the chamber door as is shown in Figure 4.2.b. This way, the heating wires, and thermocouple connection and the tubes for the cooling fluid are all run through the door of the chamber. The chamber, once designed was fabricated by Sharon Vacuum, Inc. of Brockton, Massachusetts.

4.2.2   Sample Preparation

The temperature experiments that are described in this chapter are conducted on three different types of samples. The first group consists of polyimide samples which are prepared in the same manner as those described in chapter 3. The second kind of polyimide sample is spin coated and cured to only 85 °C. A washer is mounted to the polyimide coating with an epoxy that is cured at 85 °C and the samples are then removed from the substrate by amalgamation of the tin interlayer in a mercury bath. The third group of samples is spin coated and cured to 85 °C on a hot plate overnight. The entire film is then removed from the substrate in a mercury bath. These free-standing films are mounted between two washers which are screwed together using bellville washers as spacers to accommodate thermal expansion and contraction. This keeps the sample firmly clamped during all experiments.

4.2.3   Methods

In the first experiments in the old chamber, a thin (~ 1/4" thick) hot plate is put in the chamber behind the sample and connected to a temperature controller with a thermocouple through the bottom of the chamber. This set-up is only good to about 70 °C before the glass in the back of the chamber cracks, breaking the vacuum. These tests are to establish whether or not we can conduct experiments under vacuum while heating.

Upon determining that good holograms can be taken at relatively high temperatures without distortions caused by thermal fluctuations, a more versatile chamber design was started. A sample of a hologram taken at 400 °C of the 0, 4 mode of vibration is shown in Figure 4.4.

The next experiments are done on samples that have only been cured to 85 °C. The stress is measured as the temperature is ramped to its final value. The temperature is controlled by a Yokogawa programmable controller which has the capability of ramping and soaking at a set temperature for a given amount of time. The program used in these experiments ramps at 5° per minute to fifty degrees and then maintains that temperature for about 1 hour before each stress measurement is made. This is to ensure that the temperature in the chamber and in the sample has stabilized. Experiments are done on the PMDA-ODA samples up to 400 °C and on the BPDA-PDA samples up to 250 °C. Problems with these experiments occur due to the fact that the epoxy holding the sample to the washer is not stable to sufficiently high temperatures (Only to about 350 °C). At temperatures above 350 °C the epoxy degrades and does not hold the polymer film to the washer. This is remedied by making spin-coated films (cured to 85 °C on a hot plate over night), removing them from the tin-coated steel plates and then mounting them between two rigidly clamped washers. These samples are heated to 85 °C, then to 150 °C, and then cooled in 50 °C increments. A stress measurement is taken at each step. Subsequently the samples are taken to 230 °C and cooled, then to 400 °C and cooled with stress measurements taken at each point. A schematic of the temperature cycles is shown in Figure 4.5.
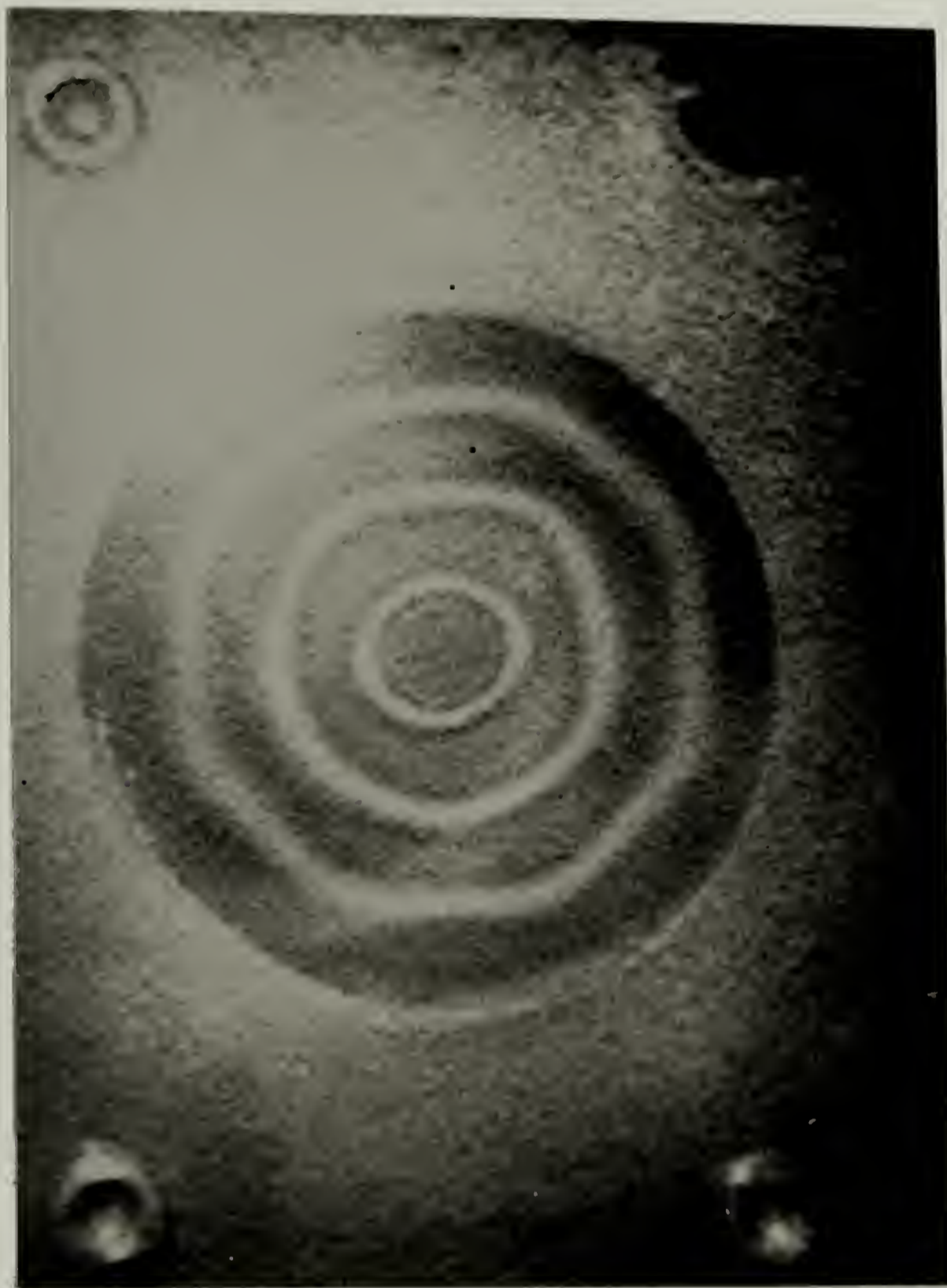
Figure 4.4   Photograph of real-time hologram taken at 400 °C in the new chamber.
This is the 0, 4 mode of vibration with a resonant frequency of 6281 hz.
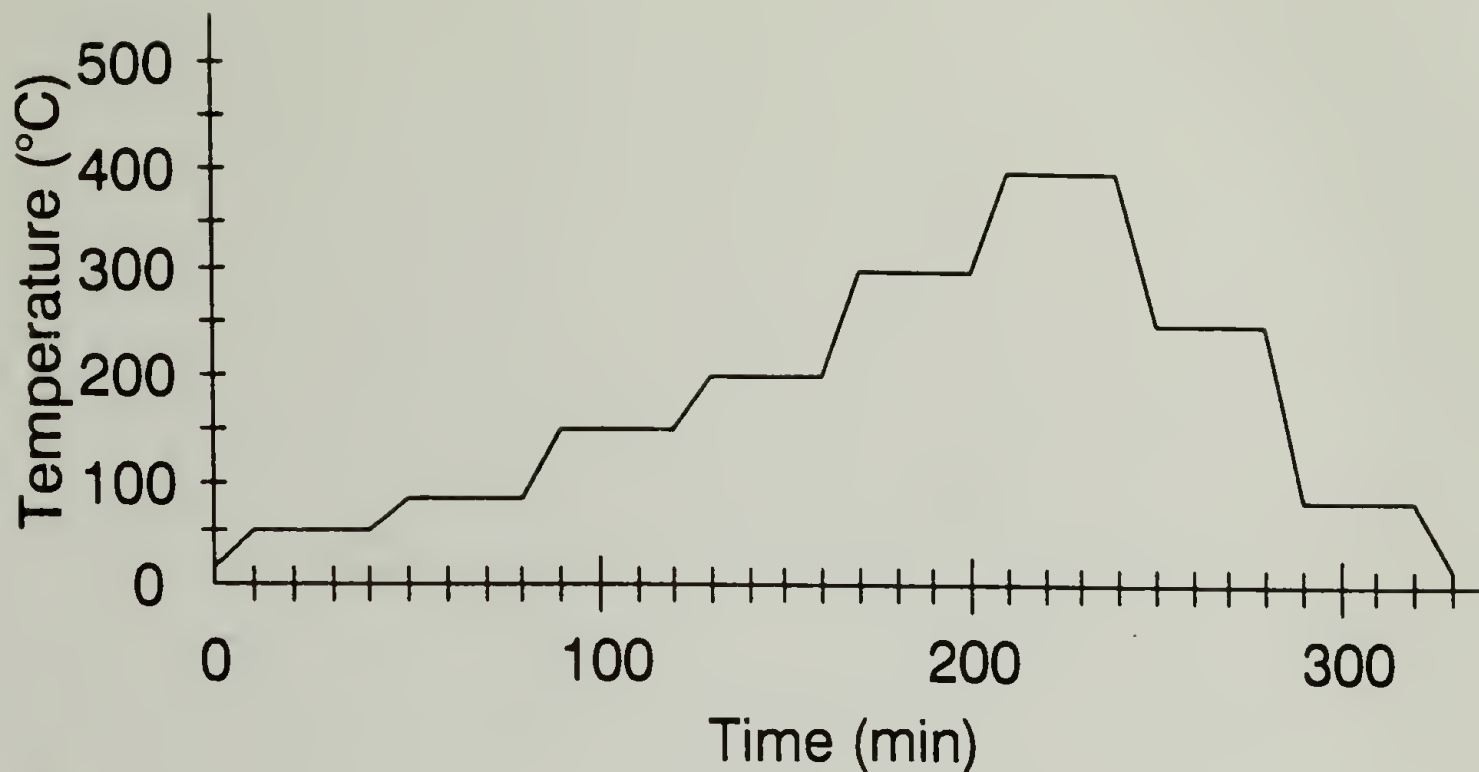
Figure 4.5   Temperature profiles for experiments conducted on clamped membrane samples and square BPDA-PDA samples.

4.3   Results

The plots of stress vs temperature for the initial temperature experiments done in the small vacuum chamber are shown in Figures 4.6.a and 4.6.b. Using value for E and v, measured by Bauer [2] for PMDA-ODA material, the biaxial coefficient of thermal expansion is calculated to be 16×10^{-6} and 15×10^{-6} ($°C^{-1}$) respectively. This compares well to a value of 18×10^{-6} ($°C^{-1}$) reported by Bauer for linear coefficient of thermal expansion measurements.

Experiments on the samples cured to only 85 °C yield highly inconsistent results for the change in stress with temperature. This was perhaps related to problems with the epoxy upon taking the samples to temperatures above the T_g of the epoxy which was cured at 85 °C. An attempt to remedy this error was made by using the clamped samples described above. Data from these experiments is shown in Figures 4.7.a and 4.7.b.
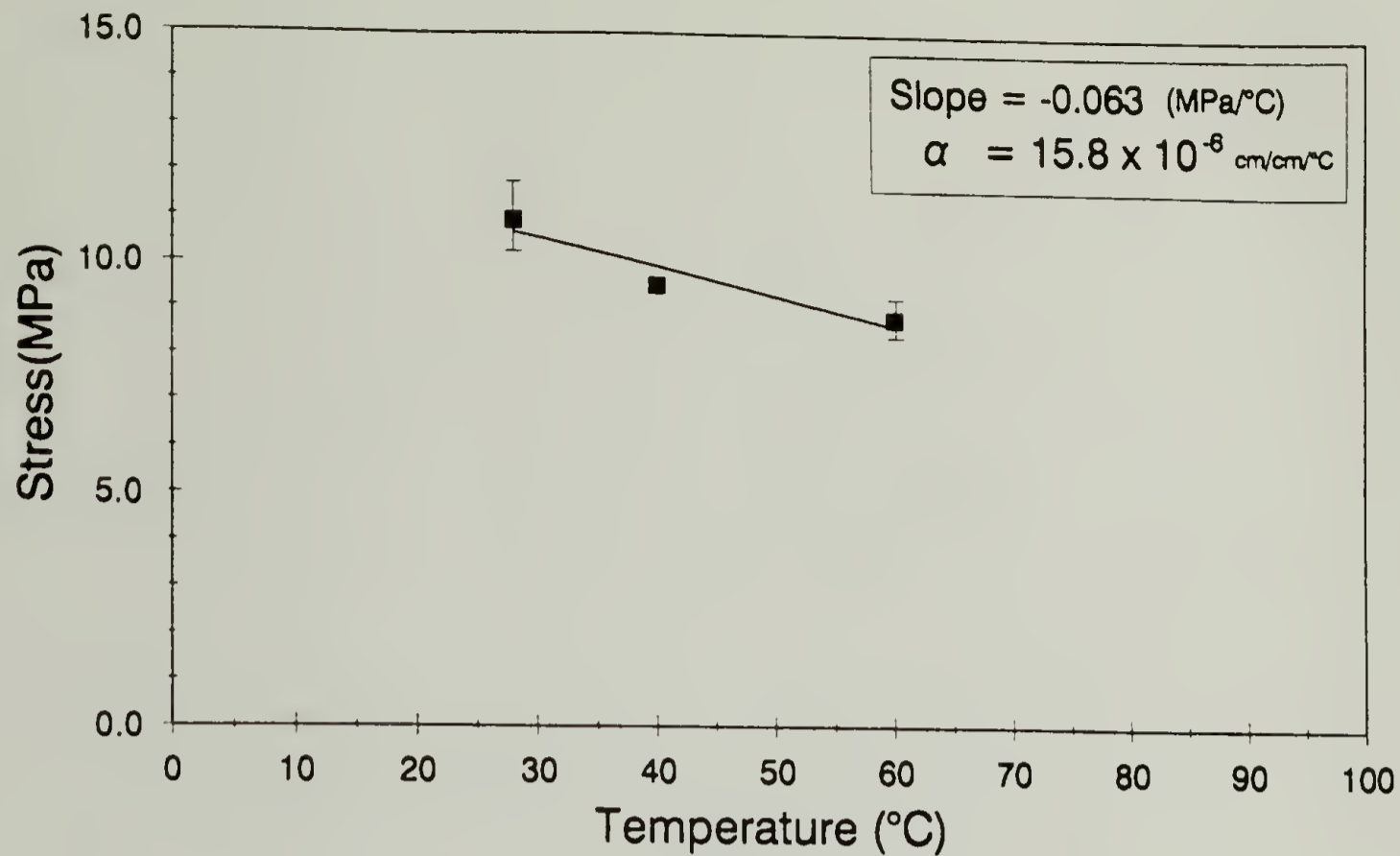
Figure 4.6.a   Plot of stress vs temperature for a PMDA-ODA membrane, heated in small vacuum chamber.
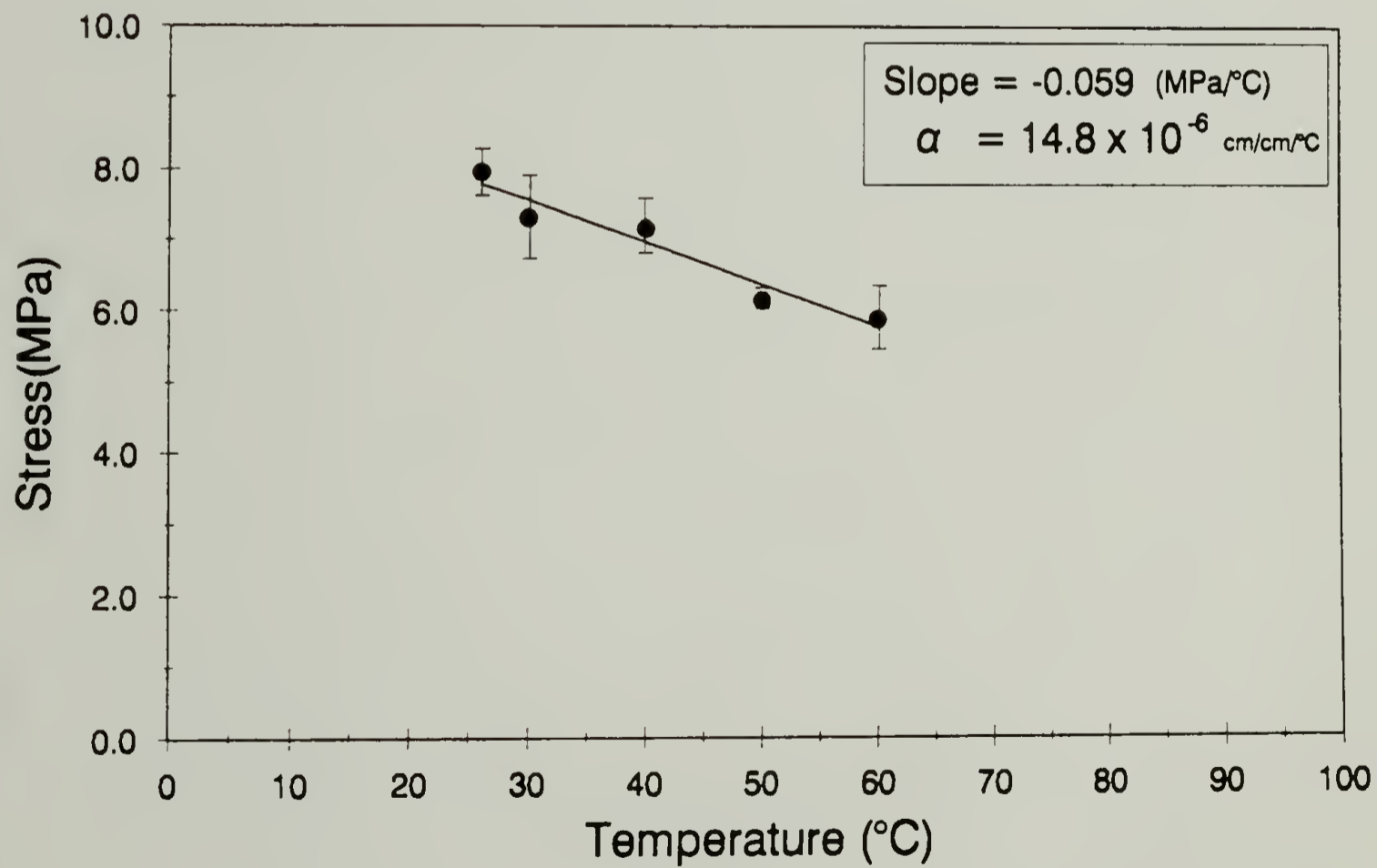
Figure 4.6.b   Plot of stress vs temperature for a PMDA-ODA membrane, heated in small vacuum chamber.
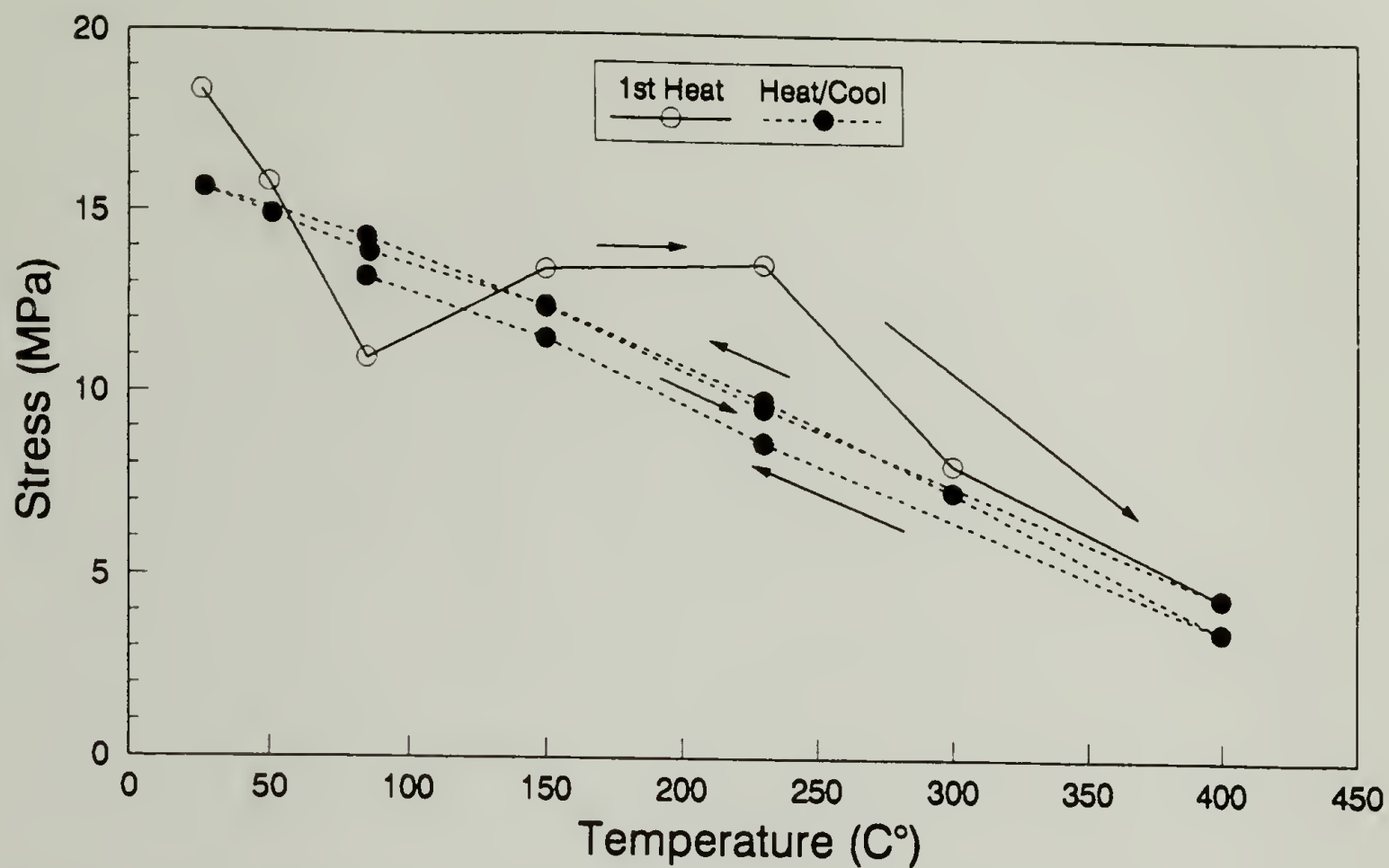
Figure 4.7.a   Plot of stress vs temperature for a clamped PMDA-ODA membrane, in large chamber.
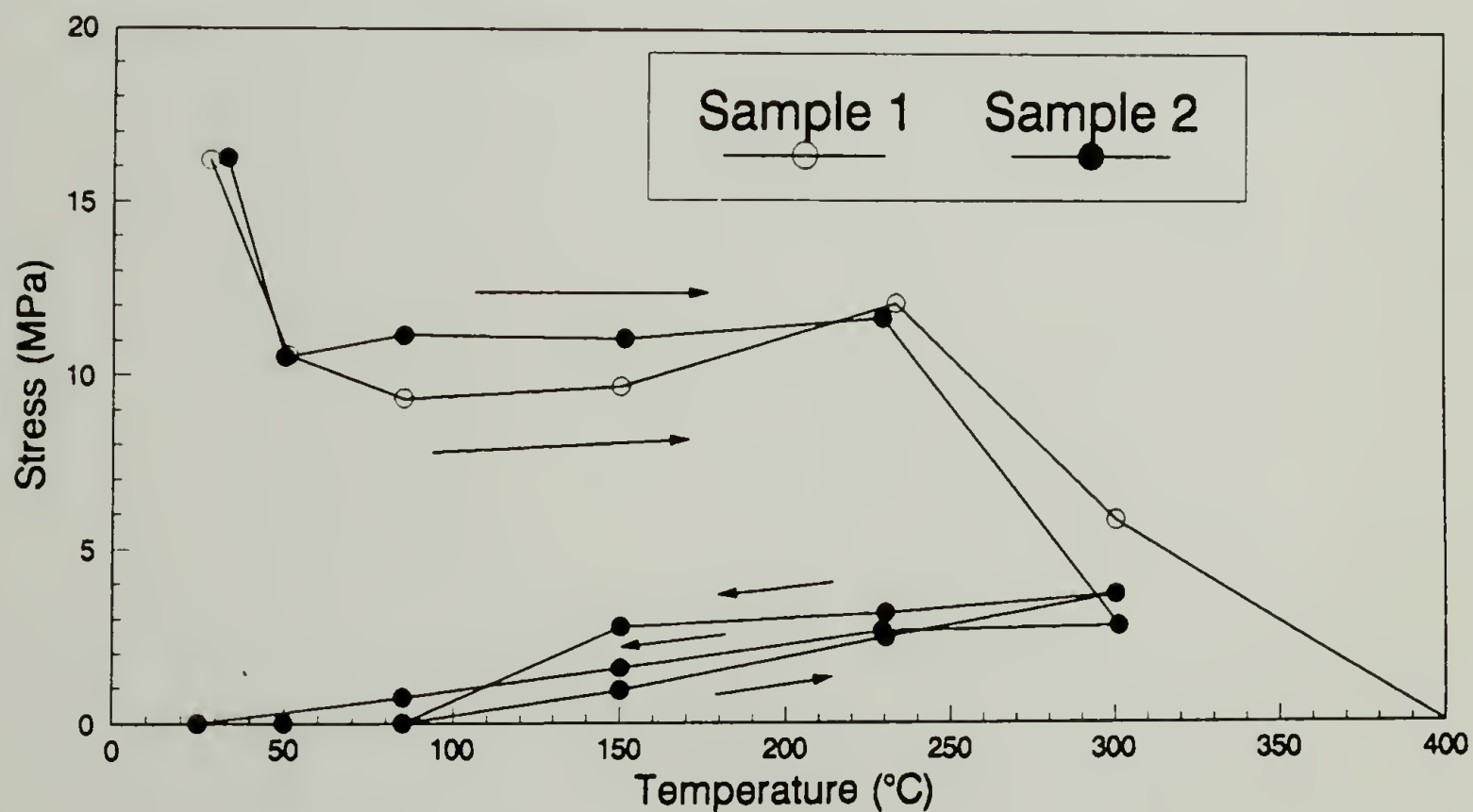
Figure 4.7.b   Plot of stress vs temperature for a BPDA-PDA membrane, heated in large vacuum chamber.

4.4   Discussion

We have succeeded where others have failed, in designing and building an environmental chamber for holographic interferometry experiments which will operate at very high (400°C) and very low (-65°C) temperatures. The chamber is also designed so that different atmospheres can be introduced to study the effects of humidity on the stresses in coatings. The chamber is light enough and small enough so that the entire chamber can be mounted onto the piezoelectric shaker, and will transmit vibration to a sample mounted inside.

The first stress vs temperature experiments done in the original vacuum chamber shown in Figure 4.1 demonstrated that stresses can be measured using holographic interferometry at high temperatures using the technique developed in this work. The effects of curing on the stresses in PMDA-ODA samples and BPDA-PDA samples were studied. The first attempts to study stresses at high temperatures were not successful due to degradation of the high temperature epoxy used to mount the coatings to the washers. The samples which were mounted between clamped washers as described above gave interesting information about the cure cycle. The original stress in the membranes is induced during mounting and is perhaps due to some residual solvent loss before testing while the sample is clamped between the steel washers at room temperature.

Initially, at room temperature, the stress in the PMDA-ODA membrane has a value of about 18.5 MPa. Upon heating the PMDA-ODA sample from room temperature to 85°C (the initial cure temperature) the stress drops to about 10 MPa. The steep slope indicates a very high coefficient of thermal expansion of $48.5 \times 10^{-6}/°C$, using equation (4.1) and taking into account the coefficient of thermal expansion of the steel washer ($12 \times 10^{-6}/°C$). The Poisson's ratio of the material is taken to be 0.42 and the Young's modulus as 2 GPa as reported by Bauer [2]. As the sample cures further, the stress in the film increases due to imidization reactions that occur above 100 °C, stabilizes between

200 and 250 °C, and decreases upon curing to its final temperature of 400 °C. This result confirms studies that find that the imidization reactions of these materials are complete above 200 °C [3]. After the sample is fully cured, the stress vs temperature upon heating and cooling follows a straight line with an average slope ($\Delta\sigma/\Delta T$) of -0.031. If we take the Young's modulus and the Poisson's ratio of the PMDA-ODA to be 3 GPa and 0.34 respectively, this gives a CTE value of $18.8 \times 10^{-6}/°C$ which closely matches that reported in the literature ($18.0 \times 10^{-6}/°C$ [4]).

Similar results are shown for the BPDA-PDA material in Figure 4.6.b. Results from two different samples are shown on this figure. Sample number 1 (open circles) was heated to 400 °C at which point the sample began to degrade. Further experiments could not be done with this sample. The second sample was only taken up to 300 °C to avoid degradation of the sample so that subsequent cooling and heating could be done. The heating and cooling lines are indicated by arrows on the plot of stress vs temperature. The final slope of the stress vs temperature plots is positive indicating that the coefficient of thermal expansion of the polyimide is lower than that of the steel washers, and gives a CTE of BPDA-PDA of $11.3 \times 10^{-6}/°C$ (assuming a Poisson's ratio of 0.34 and a Young's Modulus of 8.8 GPa as reported in the product literature [5]). This is about 40 % higher than the reported value of $8 \times 10^{-6}/°C$. The CTE is very close to that of the steel washers, and at low temperatures < 85°C the stress changes from tensile to compressive, causing the samples to buckle.

This work has shown that the environmental chamber can be used to study the effects of curing temperature on the stresses in membranes, and that we can conduct holographic interferometry experiments at high temperatures. This is the first time that work of this nature has been done for polyimide films. It should prove to be useful for studying humidity effects on moisture sensitive materials as well.

REFERENCES

1. P. Buchwalter, personal communication, IBM T. J. Watson Research Center, Yorktown Heights, NY, April 1991.

2. C. L. Bauer, *The Determination of the Mechanical Behavior of Polyamic Acid/Polyimide Coatings*, Ph.D. diss., University of Massachusetts, 1987, (Amherst, MA: 1987).

3. I. C. Noyan, and L. T. Nguyen, "Residual Stresses in Polymeric Passivation and Encapsulation Materials," *Polymer Engineering and Science*, **28**(16), 1026 (1988).

4. *Kapton Polyimide Film: Summary of Properties*, (Wilmington: DuPont Company, 1986).

5. *Upilex Polyimide Films: Technical Data*, (Wilmington: ICI Americas, Inc., 1989).

CHAPTER 5

ORTHOTROPIC MATERIAL PROPERTIES OF POLYMER FILMS

5.1   Introduction

As the electronics industry moves to greater levels of device miniaturization, and the behavior of composite systems is examined on a microstructural level, the need for new testing methods to address the unique behavior of materials in these systems has become apparent. It is crucial, in the prediction of thin film reliability to know the material properties and to be able to quantify the biaxial stresses and strains present in films due to processing. The approaches taken to determine the material properties and behavior of thin polymer coatings are by necessity much different than those used with bulk samples. It is not necessarily accurate to assume that the properties of a thin film are the same as those in the bulk. This chapter introduces a holographic technique to measure biaxial stresses [1, 2] and several complementary mechanical tests developed in our lab which may be used in a comprehensive study of constitutive behavior of thin orthotropic coatings. This method enables the identification of the orthotropic axes of a film. The material properties which can be determined include all nine orthotropic elasticity coefficients for a variety of commercial polymer films which are thought to possess orthotropic symmetry due to processing.

5.2   Orthotropic Materials

Commercially available films develop residual orientation in the plane due to complicated stress fields during processing [3, 4, 5, 6]. The principal directions of orientation do not necessarily correspond to the machine and transverse directions of the

122

film processing line and can vary across the width [7]. In order to fully characterize these anisotropic films, it is desirable to be able to identify the orthotropic axes. This allows the determination of the nine elasticity coefficients of the film by measurements on samples cut from the film along the orthotropic axes. These elasticity coefficients are necessary to accurately model film behavior near holes, at edges, under thermal cycling, and when stresses in the thickness direction are important. An orthotropic material, of unidentified orthotropic axes is fully characterized by twenty one elasticity coefficients. If the orthotropic axes are known, the matrix of coefficients reduces to nine material properties. The methods are well established for measuring these properties for large samples with easily identified orthotropic axes (i.e. wood and composite materials) [8,9]. Work has also been done on materials which form single crystals with well known planes of symmetry [10,11,12]. The experimental techniques used in these measurements rely heavily on sonic reflectance methods [13,14,15]. Such methods are well suited for cases where fluctuations in atomic packing are not large. For non-crystalline polymers however, potential limitations include imperfections in the material which make it difficult to record sonic reflectance and the problem of applying electrodes to the edge of a thin film [12].

5.3   Principal Direction Determination

It has been established that the in-plane tensile stresses in coatings can be measured using holographic interferometry [16,17,18,19]. This method combines classical membrane vibration theory with holographic interferometry used to identify the resonant frequencies of a membrane. A coating can be made into a stretched membrane by removing a portion of the substrate and will maintain its original state of stress based on the premise that the interface between a substrate and a coating is completely stress free away from the edges. Previous stress measurement techniques have dealt primarily

with films in a state of planar isotropic stress [20,21,22,23,24,25,26,27,28]. The ability to completely characterize a state of biaxial stress by obtaining the two principal directions and principal stresses has been studied by coworkers [1, 2], and is presented here as a means for determining the orthotropic axes of polymer films.

5.3.1 Method

Holographic interferometry can be used as a tool to determine the principal directions of stress in an orthotropic material. If the axes of the principal thermal expansion coefficients coincide with the orthotropic axes of a material, then the principal directions of stress (caused by constrained heating and cooling) also correspond to the orthotropic axes in the plane of the film. The material properties such as shear moduli, Poisson's ratio's and Young's moduli in these directions can then be measured to obtain the nine elastic constants for a material oriented along the principal axes.

The holographic technique offers several advantages over currently used methods for isotropic plane stress determination. The primary advantage is that no material constants (aside from the density) are necessary to obtain the stress in the coating. This allows a simple analysis of the behavior of new or developmental materials. Another equally important advantage is that the holographic interferometry method can be used to determine the biaxial stresses for a non-uniformly stressed material. The principal axes of stress can be identified easily in non-uniformly stressed circular membranes. Certain resonant vibration patterns exhibit "splitting" behavior whereby a pattern appears rotated 90° with respect to a second identical pattern. These patterns occur at two distinct frequencies. The direction of the nodal line of the pattern indicates the principal direction of stress. For circularly symmetric modes of vibration (no diametric nodes) the pattern occurs at a frequency which is the average of the two principal stresses [1, 2]. Beam bending methods and wafer curvature techniques currently used assume a uniform

curvature due to the uniform stress in the film. This would not be the case however for an anisotropically stressed material, and could cause erroneous interpretation of results.

Simple variations on the membrane vibration scheme, e.g. cutting the membrane to create a uniaxially tensioned ribbon, enable one to determine the in-plane Poisson's ratio and shear modulus. This, combined with free and axially constrained compressibility experiments enables all of the Poisson's ratios and elastic moduli for an orthotropic material (nine elastic constants) to be measured. Determination of the state of stress and the elastic constants are required to predict the stress behavior in more complex coating geometries. These methods will be discussed in detail in section 5.4.

5.3.2 Biaxial Stress Theory

The initial work done in the area of stress measurement using holographic interferometry focused on the measurement of isotropic stresses. Classical membrane vibration theory was combined with holographic interferometry to measure a redundant value of stress in a coating at each of its resonant frequencies. The theory for the vibration of an isotropic membrane and the extension of this theory to stress analysis has been discussed in previous chapters and in the literature [11-14]. Here, the focus is on the determination of material constants of orthotropic films under anisotropic states of stress.

The equation for determining the biaxial stresses in a coating has been derived in detail elsewhere [1, 2]. The resulting expression for a square membrane is as follows:

$$\sigma_1 = \frac{4\rho \, L^2 \, \upsilon_{mn}^2}{(m^2 + \delta n^2)} \qquad (5.1)$$

where σ_1 and σ_2 are the principal stresses, ρ is the density of the material, υ is the resonant frequency of vibration, and m and n are the mode numbers of the vibration. The constant $\delta = \sigma_2/\sigma_1$ can be calculated by averaging the frequency data from different modes of vibration:

$$\delta = \frac{(\upsilon'^2 m^2 - \upsilon^2 m'^2)}{(\upsilon^2 n'^2 - \upsilon'^2 n^2)} \tag{5.2}$$

Where υ, m, n and υ', m', and n' represent the natural frequencies and the corresponding mode numbers for two different vibration modes.

5.4   Material Property Determination

During the processing of free-standing thin films, different material properties may develop in different directions in the film. For example, in making some commercial polymer films, the film is held on each side by tenterhooks and is held taut as the film is pulled from the front, orienting the film to different degrees across its transverse direction. This causes the film to have different properties in different orthogonal directions. The principal directions of stress do not necessarily coincide with the machine and transverse directions. The out-of-plane properties will also be quite different than those in the in-plane transverse and machine directions.

The relationship between stress and strain in matrix notation for a linearly elastic and thermally orthotropic material is as follows:

$$
\begin{vmatrix}
\varepsilon_{11} - \alpha_1 \Delta T \\
\varepsilon_{22} - \alpha_2 \Delta T \\
\varepsilon_{33} - \alpha_3 \Delta T \\
2\varepsilon_{12} \\
2\varepsilon_{13} \\
2\varepsilon_{23}
\end{vmatrix}
=
\begin{vmatrix}
C_{11} & C_{12} & C_{13} & 0 & 0 & 0 \\
C_{21} & C_{22} & C_{23} & 0 & 0 & 0 \\
C_{31} & C_{32} & C_{33} & 0 & 0 & 0 \\
0 & 0 & 0 & C_{44} & 0 & 0 \\
0 & 0 & 0 & 0 & C_{55} & 0 \\
0 & 0 & 0 & 0 & 0 & C_{66}
\end{vmatrix}
\cdot
\begin{vmatrix}
\sigma_{11} \\
\sigma_{22} \\
\sigma_{33} \\
\sigma_{12} \\
\sigma_{13} \\
\sigma_{23}
\end{vmatrix}
\qquad (5.3)
$$

where $[C_{ij}]$ is the compliance matrix relating the strains to known stresses, ε_{ij} are the normal and shear strains, α_i are the coefficients of thermal expansion, and σ_{ij} are the normal and shear stresses. The constants C_{ij} represent the following values:

$$C_{11} = 1/E_{11} \qquad\qquad C_{44} = 1/G_{12}$$

$$C_{22} = 1/E_{22} \qquad\qquad C_{55} = 1/G_{13}$$

$$C_{33} = 1/E_{33} \qquad\qquad C_{66} = 1/G_{23}$$

$$(5.4)$$

$$C_{12} = C_{21} = -v_{12}/E_{11} = -v_{21}/E_{22}$$

$$C_{13} = C_{31} = -v_{13}/E_{11} = -v_{31}/E_{33}$$

$$C_{23} = C_{32} = -v_{23}/E_{22} = -v_{32}/E_{33}$$

where v_{ij} are the Poisson's ratios, E_{ij} are the orthogonal Young's moduli, and G_{ij} are the shear moduli. One can then rewrite the most general form of Hooke's law for an orthotropic material in component form as,

$$\varepsilon_{11} - \alpha_1 \Delta T = \frac{1}{E_{11}} (\sigma_{11} - \nu_{12}\sigma_{22} - \nu_{13}\sigma_{33}) \qquad (5.5.a)$$

$$\varepsilon_{22} - \alpha_2 \Delta T = \frac{1}{E_{22}} (\sigma_{22} - \nu_{21}\sigma_{11} - \nu_{23}\sigma_{33}) \qquad (5.5.b)$$

$$\varepsilon_{33} - \alpha_3 \Delta T = \frac{1}{E_{33}} (\sigma_{33} - \nu_{31}\sigma_{11} - \nu_{32}\sigma_{22}) \qquad (5.5.c)$$

$$2\varepsilon_{12} = \frac{1}{G_{12}} \sigma_{12} \qquad (5.5.d)$$

$$2\varepsilon_{13} = \frac{1}{G_{13}} \sigma_{13} \qquad (5.5.e)$$

$$2\varepsilon_{23} = \frac{1}{G_{23}} \sigma_{23} \qquad (5.5.f)$$

The subscripts 1, 2, 3, refer to the two in-plane and one out-of-plane principal directions respectively. The principal directions of stress are determined using the holographic interferometry technique described earlier.

The following sections outline the sample preparation and stress measurement techniques followed by the theory and experimental methods for determining all nine orthotropic elasticity coefficients. The order of the sections follows the order of constants from the upper left-hand corner of the compliance matrix, to the lower right hand corner of the matrix.

5.4.1   Sample Preparation and Stress Measurement

The samples used for the orthotropic material property measurements are made by mounting a circular washer with epoxy onto a sheet of commercially made polymer

film. The machine and transverse directions are marked on the washer to give a frame of reference for determining the principal directions of stress. When the sample is heated to cure the epoxy, differences in coefficient of thermal expansion between the film and the washer, cause a "self-loaded" state of stress in the film as it is cooled and is constrained by the epoxy and the metal washer. The stress in the film (provided the film has anisotropic in-plane coefficients of thermal expansion - indicative of an orthotropic material) will be anisotropic. The principal directions are determined by observing the nodes of the vibration patterns using holographic interferometry as described above. Once the principal directions are known, a square washer is mounted to the sample with its sides parallel to the principal directions of stress. These samples are then used to determine the magnitudes of the principal stresses. Two samples must be made from the center of each sheet of film so that two ribbon samples can be cut (one from each membrane) in each of the principal directions. The ribbon samples are used for in-plane Poisson's ratio measurements in each of the principal directions. The specifics of the Possion's ratio measurements are given below in section 5.4.3.

For materials under anisotropic stress, the principal directions are identified directly from the symmetry of the holographic interference patterns. A pattern which appears at a given frequency with its symmetric axis parallel to one of the principal stress directions will appear again, perpendicular to the first pattern at a higher frequency corresponding to the other higher principal stress (see Figure 5.1). The axes of the vibration patterns correspond to the principal directions of stress. A circular sample is used to determine the principal directions, then a square membrane is made by mounting washer with a square opening inside the circular one (see Figure 5.2). The principal stresses in the square membrane are then measured using the holographic interferometry technique and the analysis described in section 5.4. The square sample is used to solve for the principal stresses because the boundary conditions are simpler than those for the vibration of a circular membrane. For an orthotropic material that is under stress due to

Angle: 22°

Resonant Frequency: 2353 hz

Angle: 111.5°

Resonant Frequency: 2216 hz

Figure 5.1   Photographs of real-time holograms of a vibrating circular membrane used to determine the principal directions of stress in a membrane of Upilex R film. The resonant frequencies and angle with respect to the transverse direction (0°) are given below each photograph.
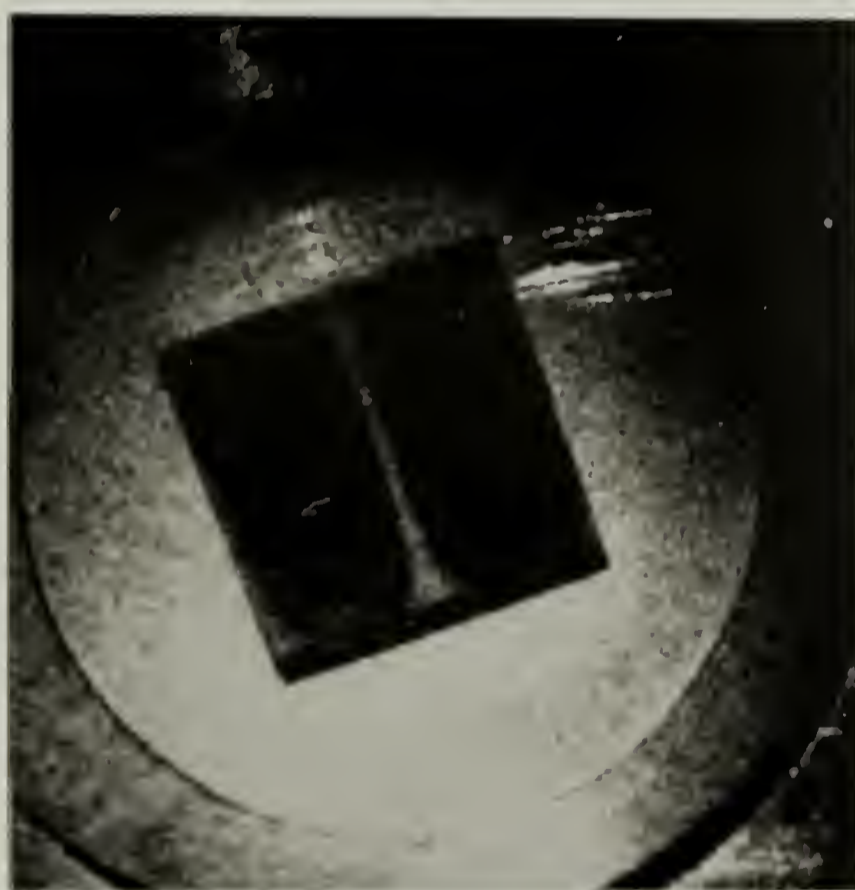
Figure 5.2   Photographs of real-time holograms of vibrating square membrane used to determine the principal stresses in the same Upilex R membrane pictured above, σ_1 = 6.44 MPa, σ_2 = 5.97 MPa.

constrained thermal contraction, the axes of principal stress and the orthotropic axes coincide.

5.4.2   In-plane Young's Moduli

The first element of the compliance matrix is $C_{11} = 1/E_{11}$, the reciprocal of Young's modulus in the 11 direction, which is also the denominator in the constants C_{12} and C_{23}. The other orthogonal Young's modulus in the plane of the film is E_{22}, and is the denominator in the constants C_{21} and C_{23} (see equation (5.4)). The measurement of the in-plane Young's moduli for films is performed using a standardized tensile test [29].

For a linearly elastic film under uniaxial tension, the stress is related to the Young's modulus by the equation,

$$E_{11} = \frac{\sigma_{11}}{\varepsilon_{11}}$$

(5.6)

The tensile samples (10 cm long x 0.5 cm wide) are cut along the directions of the orthotropic axes of the film which are determined as described in the previous section. The stress and the strain are measured by monitoring the amount of force needed to strain a sample at a constant rate in an Instron machine.

5.4.3 Poisson's Ratio

The isotropic Poisson's ratio of a material is defined as the ratio of the absolute value of strain in the lateral direction to an applied strain in the axial direction for a uniaxial stress state [30]. This is most commonly written as

$$v = -\frac{\varepsilon_{22}}{\varepsilon_{11}} = -\frac{\varepsilon_{33}}{\varepsilon_{11}} \tag{5.7}$$

where v is Poisson's ratio, ε_{22} and ε_{33} are lateral strains, and ε_{11} is the axial strain. For thin films this quantity is difficult to measure because both the in-plane and out-of-plane strains are generally too small to be measured using conventional strain gage techniques which are used on bulk samples. Extensions of the holographic interferometry technique for measuring the biaxial stress in a vibrating membrane can be used to measure the in-plane Poisson's ratios of coatings. The following sections describe new methods for obtaining the in-plane and the out-of-plane Poisson's ratios for isotropic and orthotropic materials. A description of the isotropic case is given first to introduce the technique. It is then extended to the case of an orthotropic material.

5.4.3.1   Isotropic Materials

For an isotropic linearly elastic material, the equation for the two dimensional stress is

$$\sigma_{2D} = \frac{\varepsilon E}{1 - v} \tag{5.8.a}$$

or in terms of vibrational measurements,

$$\sigma_{2D} = \frac{\rho \omega^2 R^2}{Z_{mn}^2} \tag{5.8.b}$$

where all terms have been defined previously. The equation for stress in a one dimensionally constrained sample (such as a string) is simply,

$$\sigma_{1D} = \varepsilon E \tag{5.9.a}$$

or in terms of vibrational measurements,

$$\sigma_{1D} = \frac{\rho \omega^2 L^2}{\pi^2 n^2} \tag{5.9.b}$$

where L is the length of the ribbon. Substituting equation (5.9.a) into (5.8.a) and rearranging, we obtain,

$$\nu = \frac{\sigma_{2D} - \sigma_{1D}}{\sigma_{2D}} \tag{5.10}$$

For isotropic materials, the relationship between Poisson's ratio, the two dimensional (biaxial) stress and the one dimensional (uniaxial) stress is straightforward as shown in equation (5.10). The measurements are conducted (in vacuum) using the holographic interferometry technique described in chapter 2 to measure the two-dimensional stress in an isotropic circular membrane (under tension and constrained at the circumference). This sample is then removed from the chamber and two semi-circular portions of the membrane are cut away leaving only a thin (~ 0.5 - 1.0 mm wide) ribbon constrained at each end by the washer. A state of uniaxial stress now exists in the ribbon, as the constraint in one direction has been removed but the axial strain is preserved. The ribbon is returned to the vacuum chamber, a hologram of the stationary ribbon is made, and the resonant frequencies are determined as it is shaken at a steadily increasing frequency (in the same manner as for the membrane samples). The vibration patterns for a ribbon appear as dark lines running perpendicular to the length of the ribbon. The order of the vibration, n, is determined by the number of segments observed

between the nodal points (dark lines). The one dimensional stress is calculated using equation 5.9.a and is combined with the value of the two dimensional stress to obtain v.

5.4.3.2   In-plane Poisson's Ratio - Orthotropic Materials

For an orthotropic film, two independent Poisson's ratios exist, v_{12} and v_{21}. These are the numerators of the compliance matrix elements C_{12} and C_{21} respectively. They can be determined using the general form of Hooke's law (equations 5.5.a - 5.5.f) where the stress in the 3 (out-of-plane) direction, σ_{33}, is zero because the film is only constrained in the plane of the film. The equations reduce to,

$$\varepsilon_{11} = \frac{1}{E_{11}}(\sigma_{11} - v_{12}\sigma_{22}) \qquad (5.11.a)$$

$$\varepsilon_{22} = \frac{1}{E_{22}}(\sigma_{22} - v_{21}\sigma_{11}) \qquad (5.11.b)$$

where $v_{12} \neq v_{21}$ for an orthotropic material.

Equations (5.11) represent the state of stress in a biaxially constrained square membrane with edges parallel to the orthotropic axes (and principal directions of stress). The strain in the membrane is induced by heating the sample and bonding it to a holder with high temperature epoxy while at an elevated temperature as described above.

The terms σ_{11} and σ_{22} are the stresses in the 1 and 2 principal directions respectively. The first term on the right hand side of each equation represents the one dimensional state of stress present when one cuts a ribbon sample from a square membrane in the 1 or 2 direction where the strain ε_{11} (or ε_{22}) remains the same and the stress across the width of the ribbon, σ_{22} (or σ_{11}) goes to zero (see Figure 5.3). The one
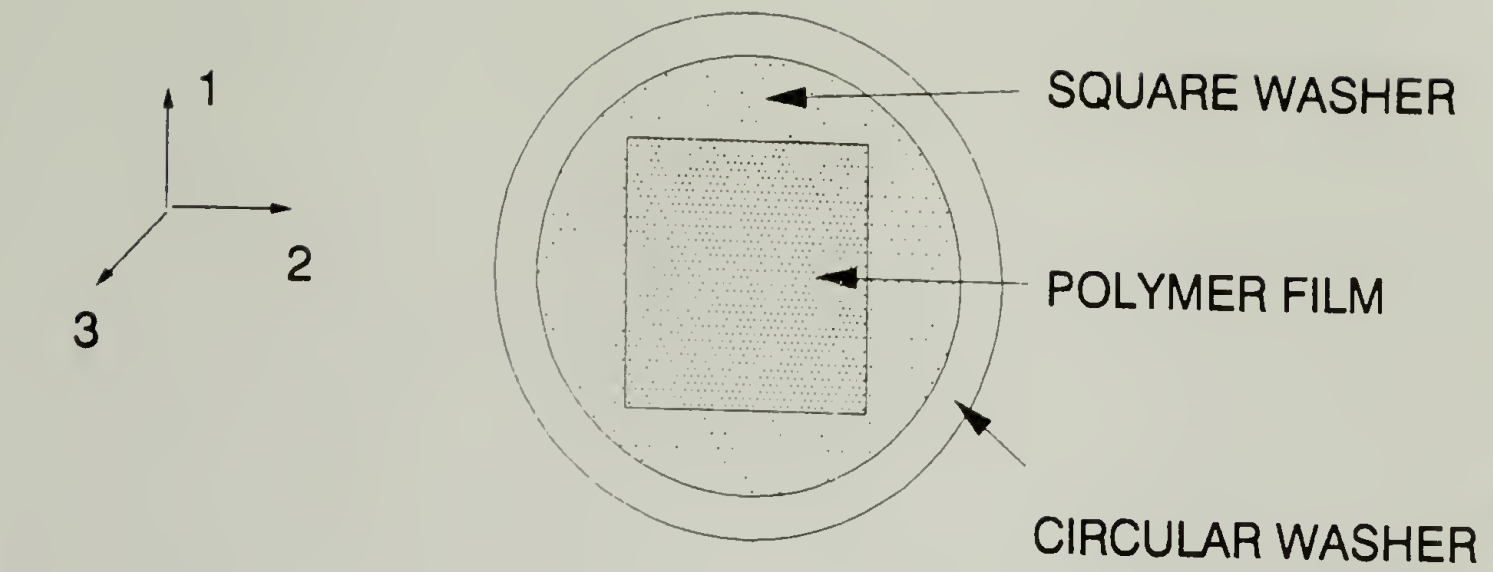
$$\sigma_{11}^{2D}, \ \sigma_{22}^{2D} \neq 0 \qquad\qquad \varepsilon_{11}^{2D}, \ \varepsilon_{22}^{2D} \neq 0$$

$$\sigma_{33} = 0$$
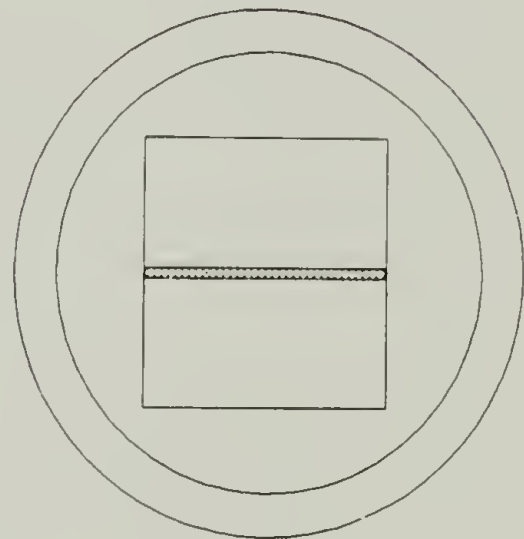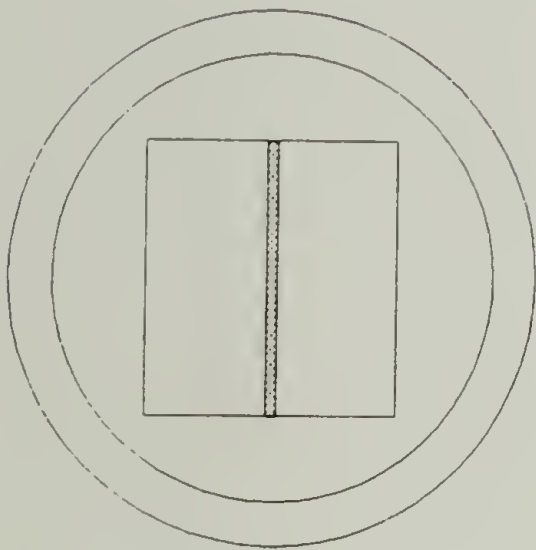
$$\sigma_{11}^{1D} \neq 0, \ \sigma_{22} = 0 \qquad\qquad \sigma_{22}^{1D} \neq 0, \ \sigma_{11} = 0$$

$$\varepsilon_{11}^{1D} = \varepsilon_{11}^{2D} \qquad\qquad \varepsilon_{22}^{1D} = \varepsilon_{22}^{2D}$$

Figure 5.3   Illustration of how ribbon samples are made from membrane samples and the state of stress and strain in each case.

dimensional stress can is measured using a ribbon sample, constrained in either of the principal directions. The equation for the one-dimensional stress in a vibrating string is given above in equation 5.8.b. The one dimensional stress is measured in the same manner as for the isotropic case described above in section 5.4.3.1. The nodes of vibration of a ribbon are observed on a real time hologram as the ribbon is being vibrated at its resonant frequency. The one dimensional stress in the 22 direction can be obtained by performing the same experiment on a ribbon cut perpendicular to the 11 direction. The uniaxial stress in each of the principal directions is used in conjunction with the biaxial stress measurements to obtain Poisson's ratio (v_{12} and v_{21}) in the film using equations (5.10.a) and (5.10.b).

5.4.3.3   Out-of-plane Poisson's Ratios - Orthotropic Materials

The Poisson's ratio in the out-of-plane (33) direction is one of the most difficult to obtain for thin films, as it is difficult to measure the minute changes in thicknesses which occur as the film is stretched. It is proposed (based on work by Bauer [31]) that dilatometric measurements on a thin film sample can be used to measure this quantity. Using this method both v_{13} and v_{23} can be obtained by using samples cut in the principal directions. Given a sample held at constant strain in the 1 direction and under hydrostatic pressure,

$$\varepsilon_{11} = c_{11}\sigma_{11} + c_{12}\sigma_{22} + c_{13}\sigma_{33} \tag{5.12}$$

The dilatometer used for these experiments has a load cell which is located inside the pressure chamber so that the only force differential it senses is the change in axial stress in the specimen (see Figure 5.4). The stresses in each of the principal directions can be described as functions of the hydrostatic pressure as follows:

$$\sigma_{22} = \sigma_{33} = -P \tag{5.13.a}$$

$$\sigma_{11} = (\sigma - P) \tag{5.13.b}$$

where P is the applied hydrostatic pressure and σ is the stress resulting from the constant applied strain. Substituting (5.13.a) and (5.13.b) into (5.12), and dividing by c_{11}, gives

$$\frac{\varepsilon_{11}}{c_{11}} = \sigma - P\left[1 + \frac{c_{12}}{c_{11}} + \frac{c_{13}}{c_{11}}\right]. \tag{5.14}$$

If the elements of the compliance matrix, c_{ij}, as defined in (5.4) are substituted into (5.14), an equation in terms of v_{12} and v_{13} is obtained.

$$\varepsilon_{11}E_{11} = \sigma - P(1 - v_{12} - v_{13}) \tag{5.15}$$

By plotting the measured stress, versus the pressure, a line of slope

$$\left(\frac{\partial\sigma}{\partial P}\right)_{\varepsilon_{11}} = 1 - v_{12} - v_{13} \tag{5.16}$$

is obtained where v_{12} is known from previous in-plane Poisson's ratio measurements, thus one can determine v_{13}. In a similar way, v_{23} can be determined by the same measurement on a sample cut in the 22 direction.

The out-of-plane Poisson's ratios (v_{23} and v_{13}) can be measured using dilatometric experiments on samples cut in the principal directions of stress. The sample
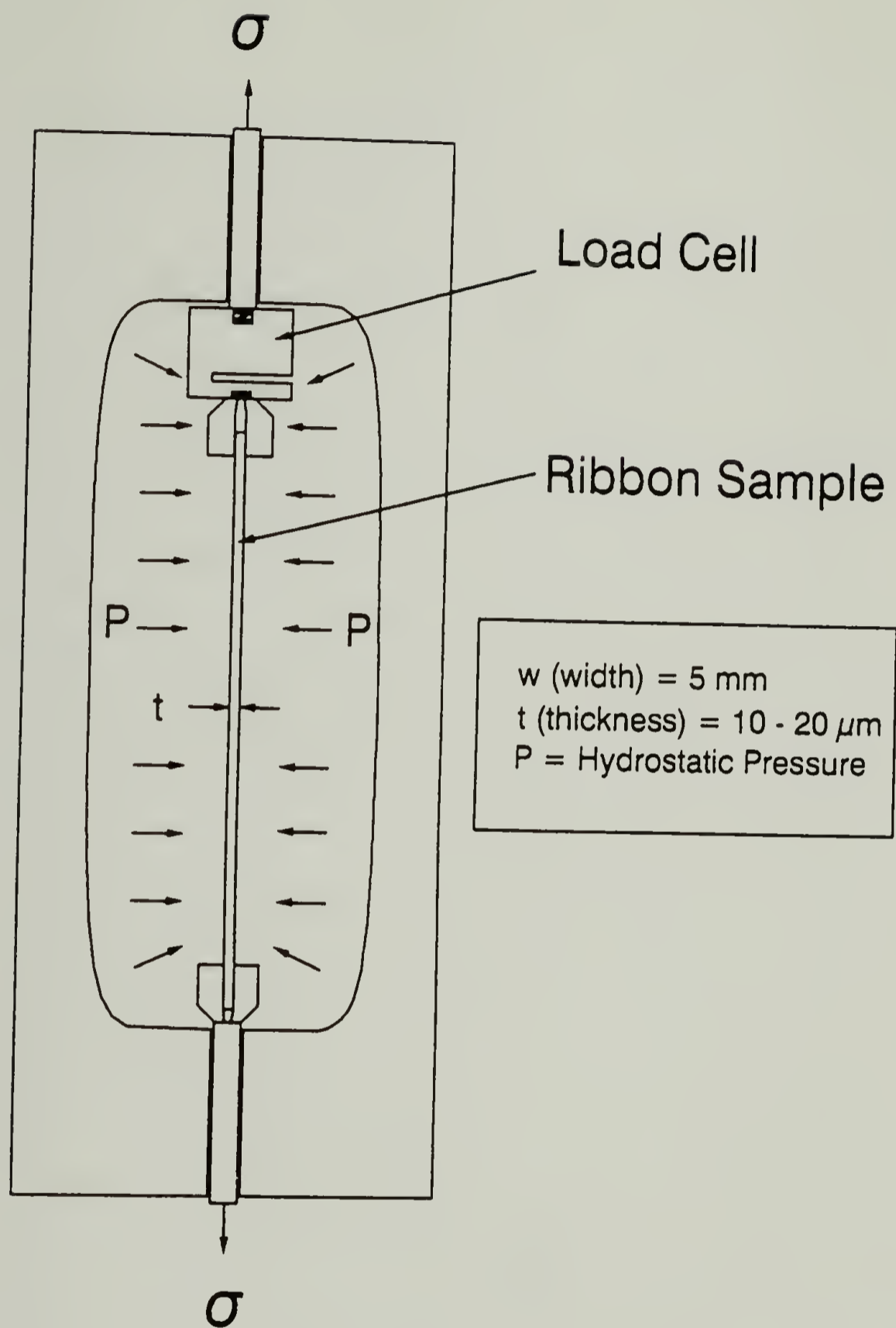
Figure 5.4   Schematic of High Pressure Gas Dilatometer made by Farris Instruments which can be used for out-of-plane Poisson's ratio measurements.

is held under constant strain and the chamber is pressurized (up to 2000 psi (14 MPa)).
The change in stress is measured as a function of the change in hydrostatic pressure in
the chamber, and the out of plane Poisson's ratios can be obtained using equation (5.16).

5.4.4 Out-of-Plane Young's Modulus (E_{33})

The out of plane Young's modulus may be determined once five of the six
material properties in the upper (3 x 3) corner of the compliance matrix are known. This
is done by measuring the volume change of a sample under applied pressure at constant
temperature. The hydrostatic (dilatometric) strain, $\dfrac{\Delta V}{V_0}$, is equal to the sum of the strains
in the principal directions, $\varepsilon_1 + \varepsilon_2 + \varepsilon_3$, which equals the product of the hydrostatic
pressure, P, and the sum of the coefficients of the compliance matrix, Σc_{ij}, where i and j
equal 1,2,3 (shear moduli do not enter into this analysis). The equations are given below.

$$\frac{\Delta V}{V_0} = \varepsilon_1 + \varepsilon_2 + \varepsilon_3 = P \sum_{i\,j=1}^{3} c_{ij} \tag{5.17}$$

or

$$\frac{1}{P}\frac{\Delta V}{V_0} = \sum_{i\,j=1}^{3} c_{ij} \tag{5.18}$$

where

$$\sum_{i\,j=1}^{3} c_{ij} = c_{11} + c_{22} + c_{33} + 2(c_{12} + c_{23} + c_{13}) \tag{5.19}$$

The out-of-plane Young's modulus may be obtained, knowing all of the above elements of the compliance matrix, by doing a dilatational experiment in a PVT (Pressure-Volume-Temperature) apparatus at constant temperature. This will yield a measure of $\Delta V/V_o$ as a function of hydrostatic pressure, P. They are related by the equation

$$\frac{(\sigma_{11} + \sigma_{22} + \sigma_{33})}{3K} = \left(\frac{\Delta V}{V_o}\right) = (\varepsilon_1 + \varepsilon_2 + \varepsilon_3) = -P \Sigma c_{ij} \qquad (5.20)$$

where K is the bulk modulus, ΔV is the change in volume of a sample, and V_o is the original volume of the sample.

The out of plane modulus of a film, is probably the most difficult to determine using mechanical testing methods. The thickness of the film is so small, that it would be hard to measure the modulus in tension, and even with a compression experiment, the small changes in thickness with pressure would be nearly impossible to determine and the state of stress would not be conserved. This leads us to use the constitutive equations, and a technique which is sensitive to small changes in volume with pressure to obtain E_{33}. The Pressure-Volume-Temperature apparatus used in these experiments is made by Gnomix Corp. First, the volume of a sample of polymer film is measured, and then the film is cut into strips which may be rolled and put into the sample chamber in the instrument. The weight should be between 1 - 2 grams for the best results. The sample chamber is then evacuated and filled with mercury under vacuum. Once the sample cell is mounted in the chamber, a steadily increasing pressure (10 -200 MPa) is applied at constant temperature and the change in volume is recorded. The change in volume with pressure can then be related to the sum of the compliances of the material as described in equations (5.17) - (5.20).

5.4.5 Shear Moduli

The shear moduli for an orthotropic material are denoted by the reciprocals of C_{44}, C_{55}, C_{66} in the compliance matrix (5.4). It is relatively straightforward to obtain the in-plane shear modulus, however, the out-of-plane modulii prove less direct to measure.

5.4.5.1 In-plane, $(G_{12} = G_{21})$

The in-plane modulus, G_{12} ($= G_{21}$), may be obtained by cutting a ribbon at some angle, θ, to the principal directions and measuring the Young's modulus in this direction, xx. This value can be related to the shear modulus using the following tensor transformation equation for an orthotropic material [8]:

$$\frac{1}{E_{xx}} = \frac{\cos^4 \theta}{E_{11}} + \frac{\sin^4 \theta}{E_{22}} + \frac{1}{4}\left[\frac{1}{G_{12}} - \frac{2\nu_{12}}{E_{11}}\right]\sin^2 2\theta \qquad (5.21)$$

Since E_{11}, E_{22}, ν_{12} are easily measurable and E_{xx}, the Young's modulus at some angle θ to the principal directions, can be measured, the value of G_{12} can be determined.

The in-plane shear modulus is determined by doing tensile experiments in an Instron on samples cut at 45 degrees to the principal directions. The length of the samples between the grips is 10.0 cm +/- 0.1 cm, the width is 0.5 cm +/- 0.05 cm, and the thickness depends on which commercial film is used (ranging from 7 - 25 µm). Five samples in each direction are measured, and an average value of E_{xx} is used in the calculation of G_{12}.

5.4.5.2 Out-of-Plane, (G$_{31}$ and G$_{32}$)

Applying a torsion pendulum technique, described by Allen [32] for a cylindrically orthotropic fiber, to thin ribbon samples cut in the 11 and 22 directions, the shear moduli, G$_{31}$ and G$_{32}$ can be determined. The analysis for this problem has been solved by Lekhnitskii [33]. The result only is presented here. For a ribbon with length, L, in the 22 direction (see Figure 5.5),

$$\text{Torsional rigidity} = \frac{TL}{\theta} = \frac{4\pi^2 IL}{p^2} = G_{12}\,ab^3 \left[\left(\frac{32a^2 G_{32}}{\pi^4 b^2 G_{12}}\right) \sum_{m=1}^{\infty} \frac{1}{m^4}\left(1 - \frac{1}{Q_m}\tanh Q_m\right)\right] \quad (5.22)$$

where

L = Length of ribbon (m)

T = Torque

θ = Angle of rotation

I = Polar moment of inertia of pendulum.

p = Period of oscillation (sec)

G$_{12}$ = Shear modulus on 1 face in 2 direction (in plane modulus),

G$_{32}$ = Shear modulus on 3 face in 2 direction.

and
$$Q_m = \frac{\pi bm \sqrt{G_{12}/G_{32}}}{2a} \quad (5.23)$$

where m = 1, 2, 3, ..., b is the thickness of the ribbon, and a is the width and a/b > 0. The period of oscillation and the shear moduli are related as follows:

$$p^{-2} = \left[\frac{8a^3 \, bG_{32}}{\pi^6 \, IL}\right] \sum_{m=1}^{\infty} \frac{1}{m^4} \left[1 - \frac{1}{Q_m} \tanh Q_m\right] \tag{5.24}$$

Therefore, one can measure the period of oscillation of a ribbon and write a program which calculates the period, p, for different values of G_{12} and G_{32}, and match this value to the experimentally measured value. The out of plane shear modulus, G_{31} is determined using samples with their long axis in the 11 direction.

The torsion pendulum experiment is done on seven fiber-like samples cut in each principal direction. Each ribbon sample is mounted with tabs at each end with which it is held in the apparatus. One end of the sample is held fixed (no rotation possible) and a circular disk, of moment of inertia, I, is attached to the other end. A schematic of the torsion pendulum experiment is shown in Figure 5.6. The samples are about 5 cm long and range from 250 μm to 500 μm wide, the thickness depends on the type of film used. Each sample is cut using a new razor blade. It is important to have edges free from nicks and or jagged edges, because edge effects can affect the results. The pendulum is displaced by some angle θ about the long axis of the ribbon, and released. The period of oscillation is measured by watching the movement of a mark on the pendulum past a mark on the lower platform. Several periods are measured and an average period is used in the calculations. The shear moduli are determined by using a program to find the moduli values which yield a value of p which is identical to the one measured experimentally.

145
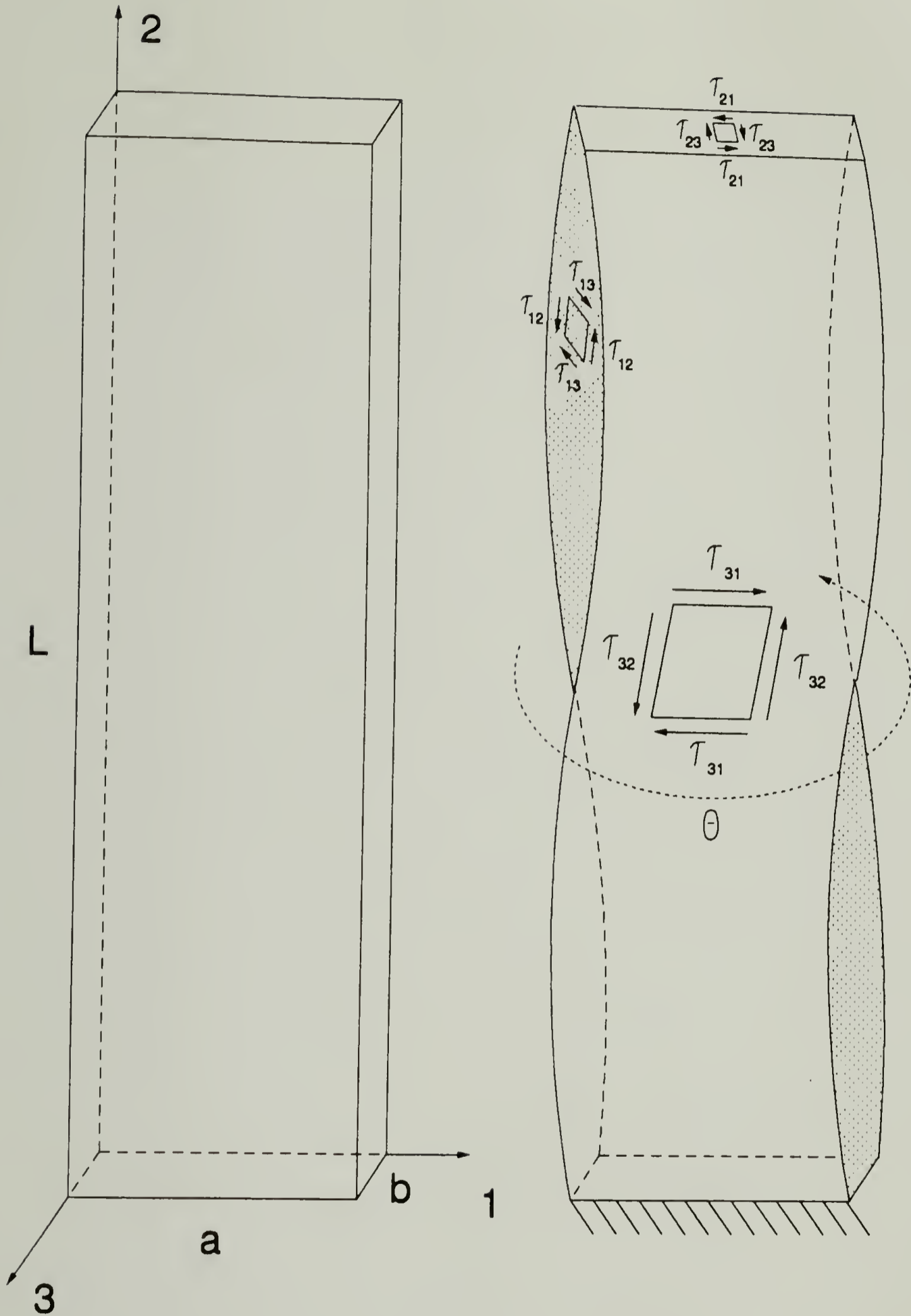
Figure 5.5   Schematic diagram of the torsion of an anisotropic ribbon.

Table 5.1   Stress values for isotropic Poisson's ratio measurement.

Sample	Biaxial Stress (MPa)	Uniaxial Stress (MPa)	Poisson's Ratio
1	8.22 +/- 0.46	4.75 +/- 0.02	0.42(0.38 - 0.46)
2	8.55 +/- 0.16	4.91 +/- 0.02	0.43(0.41 - 0.44)
3	7.97 +/- 0.18	4.32 +/- 0.30	0.46(0.41 - 0.50)
			$v_{ave} = 0.44$

The results from measurements made on the slightly orthotropic Upilex R (Ube Corp.) material are shown below in Table 5.2. The Young's moduli measured in our lab on Upilex R (12.5 μm thick) are about 7 % higher than those reported in the manufacturer's literature (measured in the machine direction on 25 μm thick films). A comparative study was done on Kapton 30H film supplied by E. I. DuPont de Nemours, Inc. Measurements of anisotropic properties were also made on a film of oriented poly(vinyl alcohol) which was elongated by a factor of 3.9:1 in one direction from the isotropic state. This material was supplied by Polaroid Corporation. Samples were made by mounting washers to the poly(vinyl alcohol) film with epoxy and cured at 60 °C.

The angle noted in the second column of Table 5.2 is the angle of the orthotropic axes with respect to the transverse direction (across the width of the film line). The sense of the angle is shown in Figure 5.7. The Poisson's ratios in the plane range from 0.26 to 0.58. For isotropic materials, the values of Poisson's ratio may only have values between -1.0 and 0.5, however for anisotropic materials this is not necessarily the case. The only limit placed on the value of Poisson's ratio is that the compliance matrix be positive definite, meaning that the determinate of the matrix and all of its subdeterminants must be greater that zero [34]. The sub-determinant for which we have data (the upper left hand elements of the compliance matrix) meets this requirement for all samples. Noted

below Table 5.2 are the calculated values of the off diagonal elements of the compliance matrix.

Other experiments were also done to test the extent of anisotropy of the properties of the polymer films. Tensile measurements were made on samples taken at various angles from Upilex R film. The results are shown in Figure 5.8. Each point represents the average Young's modulus of three samples. Based on these measurements, the
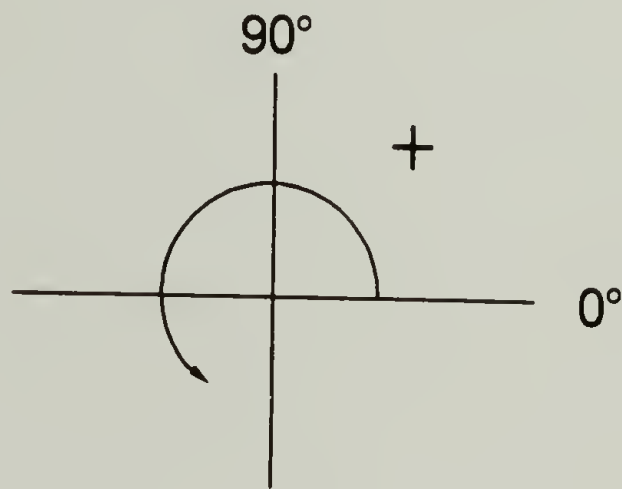
Figure 5.7   Schematic of the identification of angles for commercially made films. The transverse direction is at 0° and the machine direction is at 90°.

Table 5.2   Material properties of some orthotropic polymer films.

Sample	Angle	E_{11} (GPa)	E_{22} (GPa)	ν_{12}	ν_{21}	G_{12} (GPa)
PVOH[a]	25°	6.0	4.4	0.26	0.58	1.6
Upilex R[b]	20°	4.0	3.9	0.36	0.23	1.7
Kapton 30H[c]	20°	3.8	4.5	0.39	0.52	1.4

a: $-\nu_{21}/E_{11} = 0.04$; $-\nu_{21}/E_{22} = 0.13$

b: $-\nu_{21}/E_{11} = 0.09$; $-\nu_{21}/E_{22} = 0.06$

c: $-\nu_{21}/E_{11} = 0.10$; $-\nu_{21}/E_{22} = 0.11$

materials are not highly orthotropic. However, there is some degree of anisotropy as indicated in the vibration experiments. Measurements of the coefficient of thermal expansion for Kapton H films also did not show a strong degree of anisotropy for measurements made on samples taken at various angles from these films. These experiments were done on a TA Instruments Thermal Mechanical Analysis Instrument, where the change in length was monitored as a function of temperature. A polar plot of these experiments is shown in Figure 5.9.

Torsion measurements done on Upilex R samples yielded values of G_{32} = 1.5 GPa (+/- 0.27) and G_{31} = 1.4 GPa (+/- 0.27). The value of G_{12} (= G_{21}) is 2.9 GPa (+/- 0.15) which is inconsistent with that measured using the tensile measurements at 45° to the principal directions. (This will be discussed further in the next section.) The error reported is the standard deviation of the averages of ten measurements.

There are several factors which can affect the accuracy of these measurements. Simulations done by Leitzau [35] indicate that there is an effect of the width of the ribbon sample on the calculation of the moduli for samples in which a > 3b. A plot of modulus ($G_{12} = G_{21}$) vs the width of a ribbon is shown in Figure 5.10. Even when the width becomes very small, the value for the modulus approaches, but is still about 20 % higher than the value measured using the tensile test method.

A sample calculation for the out of plane Young's Modulus (E_{33}) is given below for Kapton 30H (PMDA-ODA) material. For the sake of illustration, assume that $v_{13} \approx v_{23} \approx 0.34$ (from work done by Bauer on spin coated PMDA-ODA films). The matrix is symmetric, therefore, $- v_{12}/E_{11} = - v_{21}/E_{22}$, $-v_{13}/E_{11} = -v_{31}/E_{33}$, and $- v_{23}/E_{22} = - v_{32}/E_{33}$.

$$
\begin{pmatrix}
\dfrac{1}{E_{11}} & \dfrac{-v_{12}}{E_{11}} & \dfrac{-v_{13}}{E_{11}} \\[2ex]
\dfrac{-v_{21}}{E_{22}} & \dfrac{1}{E_{22}} & \dfrac{-v_{23}}{E_{22}} \\[2ex]
\dfrac{-v_{31}}{E_{33}} & \dfrac{-v_{32}}{E_{33}} & \dfrac{1}{E_{33}}
\end{pmatrix}
=
\begin{pmatrix}
\dfrac{1}{3.8} & \dfrac{-0.39}{3.8} & \dfrac{-v_{13}}{3.8} \\[2ex]
\dfrac{-0.52}{4.5} & \dfrac{1}{4.5} & \dfrac{-v_{23}}{4.5} \\[2ex]
\dfrac{-v_{31}}{E_{33}} & \dfrac{-v_{32}}{E_{33}} & \dfrac{1}{E_{33}}
\end{pmatrix}
$$

$$
=
\begin{pmatrix}
0.263 & -0.103 & -0.090 \\
-0.116 & 0.22 & -0.076 \\
-0.090 & -0.076 & 1/E_{33}
\end{pmatrix}
$$

$$
\sum_{i,j=1}^{3} c_{ij} = \frac{1}{P}\frac{\Delta V}{V} = 0.263 + 0.222 + \frac{1}{E_{33}} - 0.219 - 0.180 - 0.152 = 0.21
$$

$\therefore$ if v_{13} and v_{23} are $\cong$ 0.34, as determined by Bauer for spin cast PMDA-ODA films, then E_{33} = 3.6 GPa.

The values for $\dfrac{1}{P}\dfrac{\Delta V}{V_o}$ Upilex R film and oriented poly(vinyl alcohol) films are

0.19 and 0.16 GPa^{-1}, respectively. Assuming out of plane Poisson's ratios of between 0.25 and 0.35 for these materials would yield E_{33} values between 5.3 to 11.8 GPa for Upilex and between 4.6 and 7.2 GPa for poly(vinyl alcohol). A sample plot of the data from a PVT experiment is shown in Figure 5.11.

The polyvinyl alcohol sample (PVOH) was mechanically oriented as received in a 3.6:1 draw ratio in one direction. This material shows considerable orthotropic behavior, both in its values for Young's modulus and for the Poisson's ratio. The Upilex™ and Kapton™ materials do not show very strong orthotropic character based upon the modulus behavior, however the Poisson's ratio values are considerably different. It would be interesting to know from which section across the width of the film line these samples were taken to give more insight into their behavior.
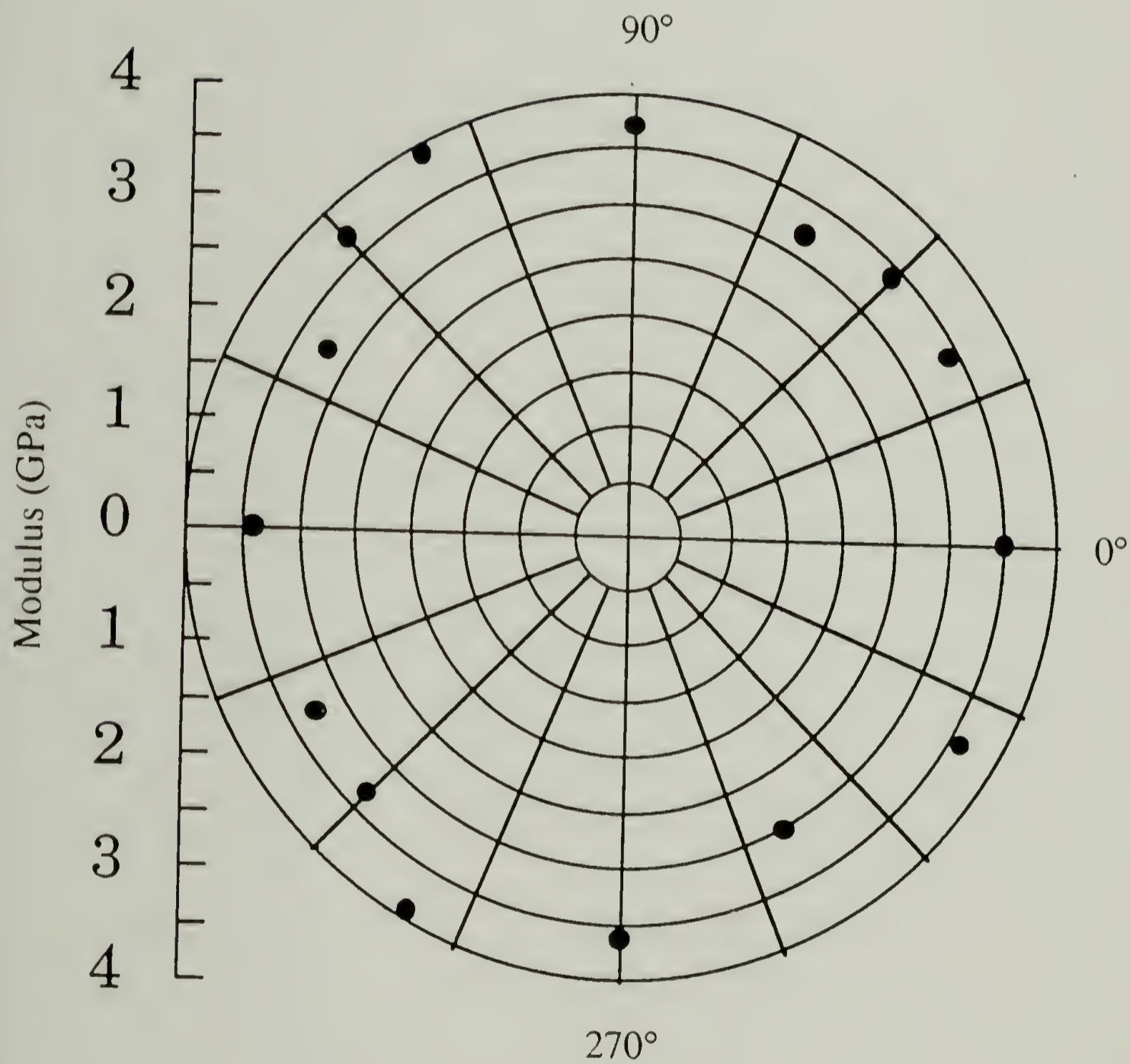
Figure 5.8   Young's modulus vs. angle for Upilex R film. The transverse direction is at 0°.
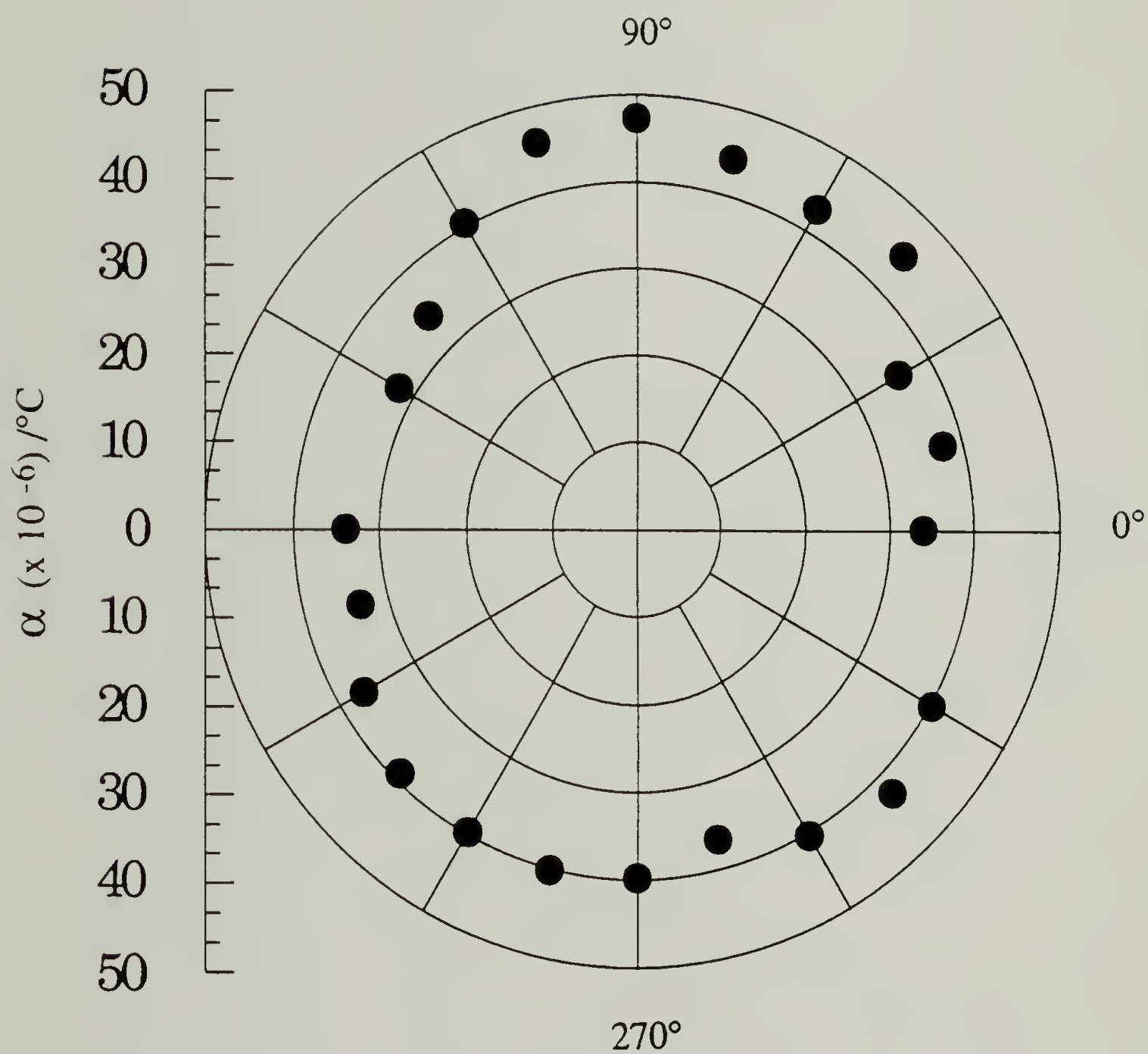
Figure 5.9   Coefficient of thermal expansion for Kapton H film vs angle. The transverse direction is at 0°.
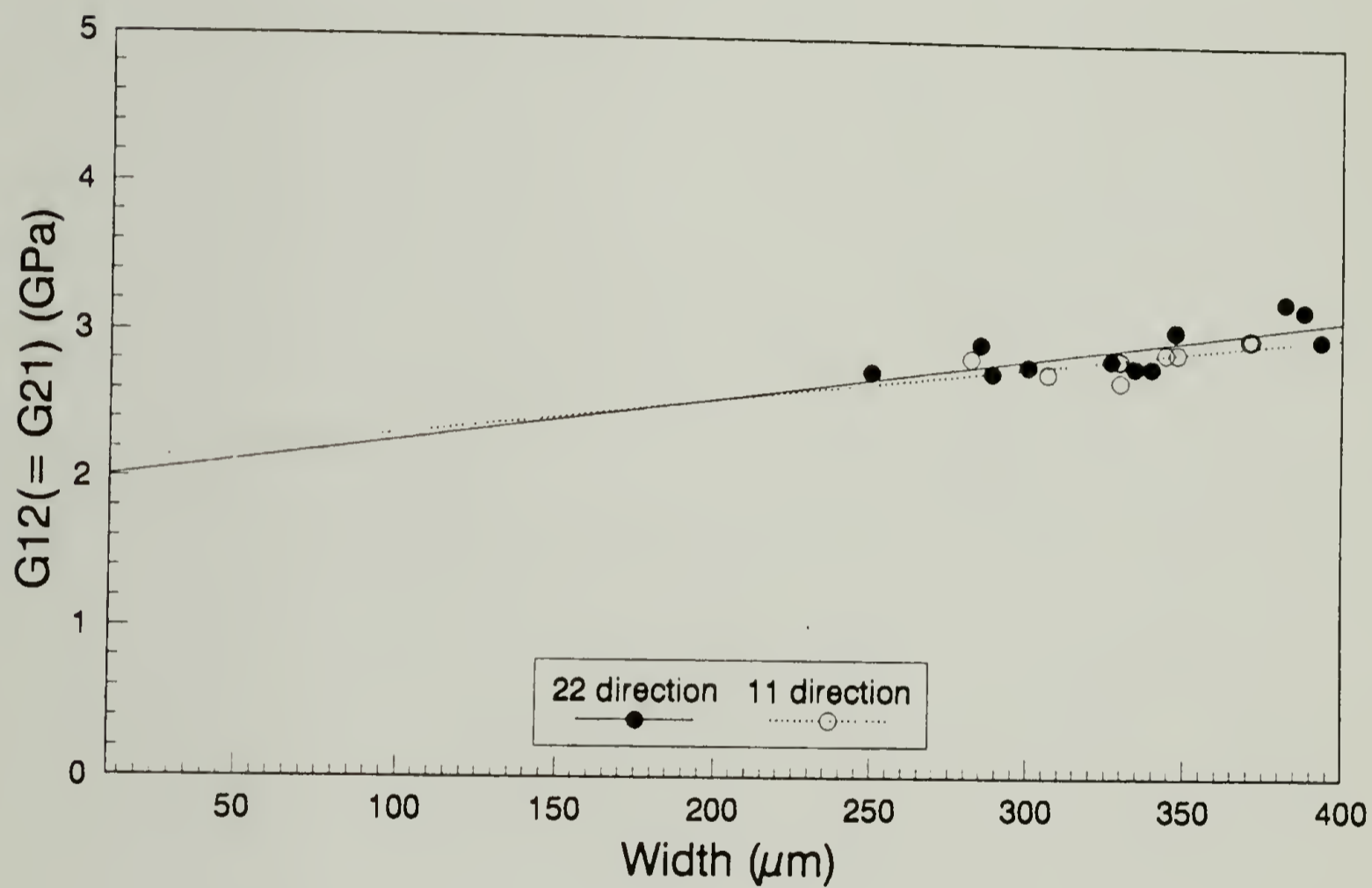
Figure 5.10 Plot of shear modulus, G_{12} (G_{21}) vs ribbon width for sample made from Upilex R film. The film thickness is 12.5 μm.
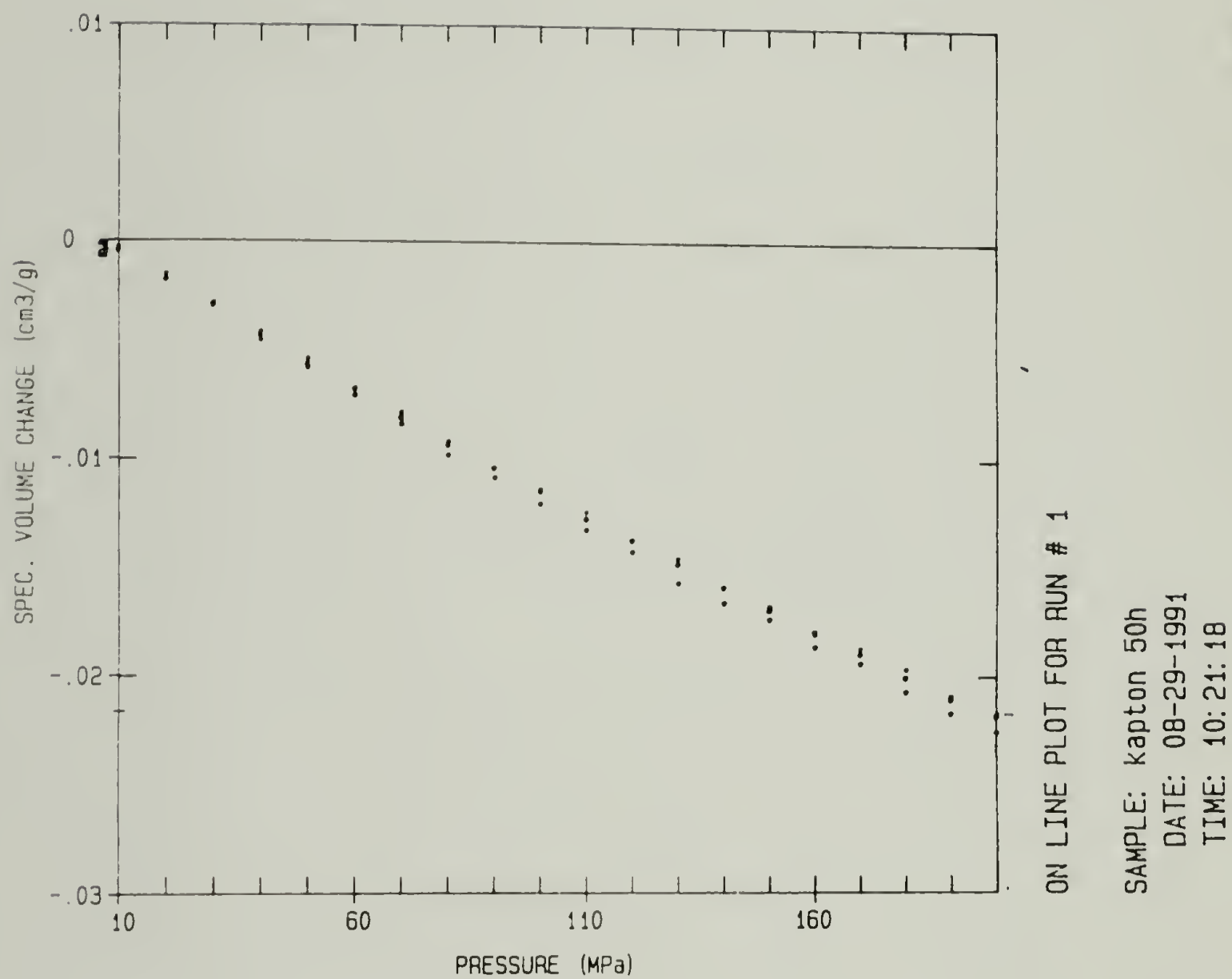
Figure 5.11 Plot of change in volume vs applied pressure for a Kapton 50H film. This experiment was done on a Gnomix PVT apparatus.

The methods described here are an effort to provide a comprehensive set of mechanical tests for orthotropic material property measurement. Unfortunately there is a dearth of data available on orthotropic properties of polymers of any sort with which to compare these results. Most notable is the work done on polydiacetylene crystals[8]. Other work done in the area of orthotropic material property measurement of films has been limited to metal/ceramic composites and paper sheet. There is also no way of knowing if these materials are orthotropic. It is definitely known that they are not isotropic and this is the best approximation that can be made.

5.7   Discussion

We have shown that using real time holographic interferometry we can fully characterize the state of stress in a film. This technique has universal applications for measuring stresses in any coating in a state of tension. These experiments have been done on metal films, paint coatings, and using environmentally controlled chambers, the effects of humidity and temperature can be analyzed [7]. Using the holographic technique to determine the principal stress directions also allows us to determine the orthotropic material properties of thin films. This work shows that we can obtain several of the orthotropic elastic constants which satisfy the requirement of positive definiteness for the part of the compliance matrix which has been determined. A combination of proven methods for material property measurement have also been proposed to completely characterize the nine orthotropic elasticity coefficients of commercially made polymeric films.

Some preliminary torsion experiments on Upilex ribbons indicate that the width to thickness ratio plays a role in that one of the shear moduli dominates the results for a large width to thickness ratio (40:1). Attempts are in progress to minimize this effect by

cutting ribbons with a ratio of 5:1. This would allow us to obtain an independent value for each out of plane modulus, G_{31} and G_{32}.

REFERENCES

1. Q. K. Tong and R. J. Farris, "Measurement of Two-Dimensional Stresses in Thin Polymer Films Using Holographic Interferometry," submitted for publication, (1990).

2. Q. K. Tong, M. A. Maden, A. Jagota, and R. J. Farris, "Vibrational Techniques for Stress Measurement in Films - 2. Extensions and Complicating Effects," *Journal of Materials Research,* submitted for publication (1991).

3. E. M. Berg, D. C. Sun, and J. H. Magill, "3-D Structure-Property Relationships in Rolltruded Polymers. Part 1: Mechanical Property Enhancement in Three Directions," *Polymer Engineering and Science,* **29**(11), 715 (1989).

4. D. C. Sun, E. M. Berg, and J. H. Magill, "3-D Structure-Property Relationships in Rolltruded Polymers. Part 2: Anisotropic Yielding and Deformation in Triaxially Oriented Polymers," *Polymer Engineering and Science,* **30**(11), 635 (1990).

5. T. W. D. Chan, and L. J. Lee, "Analysis of Molecular Orientation and Internal Stress in Extruded Plastic Sheets," *Polymer Engineering and Science,* **29**(3), 163 (1989).

6. S. Osaki, "Explanation of Orientation Patterns Determined for Sheet Materials by Means of Microwaves," *Journal of Applied Physics,* **67**(10), 6513 (1990).

7. R. M. Jennings and R. J. Farris, "Analysis of Stresses Arising During the Processing of Polymeric Films on Tentering Frames," in press, *Polymer Science and Engineering,* (1992).

8. S.W. Tsai and H.T. Hahn, *Introduction to Composite Materials* (Wesport, CT: Technomic, 1980).

9. R.F.S. Hearmon, *An Introduction to Applied Anisotropic Elasticity* (London: Oxford University Press, 1961).

10. W. Voight, *Lehrbuch der Kristallphysik* (Leipzig: Teubner, 1928) 716 -761.

11. O.L. Blakslee, D.G. Proctor, E. J. Seldin, G. B. Spence and T. Weng, "Elastic Constants of Compression-Annealed Pyrolytic Graphite," *Journal of Applied Physics* **41**(8), 3373, (1970).

12. H. B. Huntington, "The Elastic Constants of Crystals," *Solid State Physics: Advances in Research and Applications*, vol. 7, ed. F. Seitz and D. Turnbull, (New York: Academic Press, Inc., 1958) 213 - 351.

13. W. Rehwald, A. Vonlanthen and W. Meyer, "Single Crystal 2,4-Hexadiynylene-Bis(p-Toluenesulfonate): Elastic Properties and Phase Transitions in the Monomer and Polymer," *Physical Statistics of Solids (A)* **75**, 219 (1983).

14. R. J. Young, "Polymer Single Crystal Fibres," *Developments in Oriented Polymers II*, ed. E. M. Ward, (New York: Elsevier Applied Science Publishers, 1987).

15. H.M. Ledbetter, "Orthotropic Elastic Stiffness of a Boron-Aluminum Composite," *Journal of Applied Physics*, **50**(12), 8247 (1979).

16. M. A. Maden and R. J. Farris, "Stress Measurement in Spin Coated Polyimide Films Using Time Average Holographic Interferometry," *Electronic Packaging Materials Science*, Materials Research Society Symposium Proceedings (Pittsburgh, PA: Materials Research Society, 1989).

17. M.A. Maden, Kun Tong, and R. J. Farris, "Measurement of Stresses in Thin Films Using Holographic Interferometry: Dependence on Atmospheric Conditions," *Thin Films: Stresses and Mechanical Properties II*, Materials Research Society Symposium Proceedings, vol. 188 (Pittsburgh, PA: Materials Research Society, 1990).

18. M. A. Maden, and R. J. Farris, "Stress Analysis Of Thin Polyimide Films Using Holographic Interferometry," *Journal of Experimental Mechanics*, Accepted for Publication (1991).

19. M. A. Maden, R. J. Farris, A. Jagota, and S. Mazur, "Vibrational Techniques for Stress Measurement in Films - 1. Ideal Membrane Behavior," *Journal of Materials Research*, Submitted for Publication (1991).

20. R. W. Hoffman, "The Mechanical Properties of Thin Condensed Films", *Physics of Thin Films: Advances in Research and Development*, Vol. 3, ed. G. Haas and R. Thun (New York: Academic Press, 1966).

21. B. Ya. Pines, V. M. Andronov, and V. B. Rabushkin, "Device for Investigating the Mechanical Properties of Whiskers and Thin Films", *Zavod. Laborat.* (translated from Russian), **35**(6), 741 (1969).

22. D. S. Campbell, "Mechanical Properties of Thin FIlms," *Handbook of Thin Film Technology*, ed. L. I. Maissel and R. Glang (New York: McGraw-Hill Book Company, 1970).

23. S. G. Croll, "Internal Stress In Solvent-Cast Thermoplastic Coating," *Journal of Coatings Technology*, **50**(638), 33 (1978).

24. C. Goldsmith, P. Geldermans, F. Bedetti, and G. A. Walker, "Measurement of Stresses Generated In Cured Polyimide Films," *Journal of Vacuum Science and Technology*, **A1**(2), 407 (1983).

25. M. Karnezos, "Effects of Stress on the Stability of X-Ray Masks," *Journal of Vacuum Science and Technology*, **B4**(1), 226 (1986).

26. J. T. Pan, and S. Poon, "Film Stress in High Density Thin Film Interconnects," *Electronic Packaging Materials Science*, Materials Research Society Symposium Proceedings (Pittsburgh, PA: Materials Research Society, 1989).

27. P. Lin, and S. D. Senturia, "The In-Situ Measurement of Biaxial Modulus and Residual Stress of Multi-layer Polymeric Thin Films," *Thin Films: Stresses and Mechanical Properties II*, Materials Research Society Symposium Proceedings, vol. 188 (Pittsburgh, PA: Materials Research Society, 1990).

28. P. A. Flinn, D. S. Gardner, and W. D. Nix, "Measurement and Interpretation of Stress in Aluminum-Based Metallization as a Function of Thermal History," *Transactions of Electron Devices*, **ED-34**(3), 689 (1987).

29. American Society for Testing Materials Test Method D882-88.

30. E. P. Popov, *Introduction to the Mechanics of Solids* (Englewood Cliffs, NJ: Prentice-Hall, Inc., 1968).

31. C. L. Bauer, *The Determination of the Mechanical Behavior of Polyamic Acid/Polyimide Coatings*, Ph.D. diss., University of Massachusetts, Amherst, MA, (1988).

32. Allen, S. R., "Stress-coupling Phenomena in Anisotropic Fibres," *Polymer*, **29**(6), 1091 (1988).

33. Lekhnitskii, S. G., *Theory of Elasticity of an Anisotropic Body*, English translation, (Moscow: MIR Publishers, 1981).

34. R. J. Farris, R. Falabella and Y. D. Tsai, "The Influence of Vacuole Formation and Growth on the Mechanical Behavior of Polymers," *Durability of Macromolecular Materials*, ACS Symposium 95, ed. R. K. Eby, (American Chemical Society, 1979).

35. C. Leitzau, personal communication, 1991.

CHAPTER 6

SUMMARY

6.1   Conclusions

The development of biaxial stresses in polyimide coatings during processing
poses a serious reliability problem for the microelectronics industry. The subsequent
exposure of these coatings to temperature cycling and solvents causes significant stress
changes in the materials, which leads to device failure via cracking and/or blistering of
the coating. Work has been done to study the changes in uniaxial stress in PMDA-ODA
under various processing conditions [1], however, it is always desirable to test materials
under conditions which most closely resemble those to which a coating will be exposed
in service. Therefore a technique which is able to measure the biaxial stresses in a
coating without changing its state of stress is required. The technique developed in this
work is our response to a need for reliable stress measurement techniques for polymer
coatings which do not invoke linear elastic assumptions and do not rely on prior
knowledge of many material constants for the solution.

The primary goal of this work was to establish a new technique for measuring the
stresses in coatings which meets the following requirements:

- little or no previous knowledge of coating material properties

- does not disrupt the state of stress in an applied coating

- requires no linear elastic assumptions, as do other stress measurement
  techniques currently used

- can be used to study the stress in a material at different temperatures and
  environments.

160

The technique which we have developed to accomplish this is a unique combination of several concepts from the areas of mechanics of materials, acoustics, and optics. We begin with the idea proposed by Hess and others [2, 3] that the shear and normal tractions between a thin coating and a rigid substrate go to zero away from the edges of the coating (at a distance of about three film thicknesses from the edge). This suggests that an internal portion of the substrate may be removed without disturbing the state of stress in the coating. The removal of a portion of the substrate results in a membrane (the coating material) under tension, supported on its edges by a rigid substrate. Classical vibration theory [4] states that the stress in a vibrating membrane is directly proportional to the square of its resonant frequencies and inversely proportional to the square of the mth zero of the nth order Bessel function which describes the corresponding mode of vibration. The membrane is vibrated using a piezoelectric transducer, and the vibration patterns of the resonant frequencies recorded using real-time holographic interferometry.

We have shown that for measurements conducted in vacuum, each resonant frequency yields a repeatable measure of the stress in a coating. Up to thirty five different resonant modes of vibration have been resolved using the holographic interferometry technique which provides a high degree of redundancy for each stress measurement for a given film. This technique was applied to a variety of different materials with consistent success, providing the samples were under uniform tension and supported uniformly at the circumference.

Measurements conducted in air showed that the resonant frequencies of vibration are lowered due to an air damping effect described before by both Lax and Gottleib and Aebischer for large drumheads [5, 6]. In order to do measurements in different environments it is necessary to be able to quantify the effect of air damping on a given sample. Application of corrections proposed by the Lax to our data from samples measured in air showed that the air damping effect can be accounted for, giving the

value of stress which would be measured in vacuum (to within 5%) of the measured value.

The air damping correction depends strongly on the parameter β, the ratio of the density of the medium times the radius of the membrane, to the density of the membrane times the thickness of the membrane. Lax suggested that if β was below a critical value of 1 then air damping would not be important for his systems. Our results indicate a much lower critical β value of about 0.05 for both epoxy and silver samples.

If one accounts for both the value of β and of C (the stiffness parameter) for a given material it should be possible to design samples with geometries which can be tested in air without the complications of air damping corrections. This is especially true for polymeric samples that have, in general, very small values of C for a wide range of sample geometries. The corrections and tables given by Gottleib and Aebischer can be used to give a good indication of the true stress values in a membrane.

To perform experiments in different atmospheres and at different temperatures it was necessary to design a special environmental chamber which was small enough to fit on the holographic bench and light enough to be shaken by the piezoelectric transducer. Attempts have been made in the past to design an environmental chamber for use in holography experiments by others [7] without success. Our chamber was designed to operate at high and low temperatures, under different atmospheres and under vacuum for holography experiments. The chamber is capable of holding samples up to 5 inches in diameter and can heat to 400 °C and cool to -65 °C. The chamber is controlled by a programmable temperature controller.

The second part of the work showed that the orthotropic axes of stress can be identified using real-time holographic interferometry, thereby simplifying the task of characterizing the material properties of an orthotropic material which are reduced to nine elasticity coefficients. (If the orthotropic axes are unknown, the compliance matrix contains 21 variables.) Membrane samples of commercially made polymer films were

made by mounting a washer to the film with epoxy, and curing the epoxy at an elevated temperature. Upon cooling, the membrane is under a state of self induced tension (due to restricted thermal contraction). The orthotropic axes are identified as the directions of the nodes of a vibration pattern which occurs at two distinct resonant frequencies rotated by 90 °.

The material properties are then measured using a series of mechanical tests - some standard, and some developed in our lab or used in new ways. For example, the Young's moduli are measured using standard tensile tests in an Instron according to ASTM Standard D882-88. The in- and out-of-plane Poisson's ratios can be measured using the holographic technique and a dilatometric technique both developed in our lab. The out-of-plane shear moduli are measured using a modified analysis of a torsion pendulum experiment and the pressure-volume-temperature apparatus is put to new use as an aid in determining the out-of-plane Young's modulus. In the past, orthotropic materials have been tested using sonic reflectance methods, however, these methods are very difficult to apply to thin polymeric films. The experiments proposed and carried out in this work take a mechanical measurement approach to this same problem.

6.2   Future Studies

Research in our lab is currently continuing with the use of the techniques pioneered in this work. Extensions of this work that are currently in progress and proposed for future research projects include, 1.) the use of holographic interferometry to measure swelling and thermal expansion of polymeric materials; 2.) the study of stresses in thick photoresist coatings due to various thermal and ultraviolet curing cycles; 3.) a study of bending effects and biaxial stresses in thick polymer coatings and 4.) studies of stress build-up in gels used in the photographic industry, as functions of temperature and humidity. Future work will include the measurement of stresses in

composite coating systems, and in other photo-polymerizable polymers. Hopefully some of the insights into the preparation of samples which are not affected by air damping will be useful to people who undertake this work in the future.

Future upgrades to the equipment will also include the ability to digitally analyze the holographic images to obtain more exact out-of-plane displacement measurements which are important in swelling and temperature studies, the modification of the system to enable in-plane displacement of materials to be monitored using moire analysis, and perhaps even the digitization of the holographic pattern on the recording plate which could be connected directly to a computer for analysis.

We believe that this technique has proven itself quite useful among a field of other stress measurement techniques currently in use, and has advantages for those interested in new material screening and/or people who need to conduct experiments under environmentally controlled conditions. The applications are only limited to the imagination of the user.

REFERENCES

1.   S. T. Sackinger, *The Determination of Swelling Stresses in Polyimide Films*, Ph.D. diss., University of Massachusetts, (1990).

2.   M. S. Hess, "The End Problem for a Laminated Elastic Strip - II. Differential Expansion Stresses," *Journal of Composite Materials*, **3**(10), 630 (1969).

3.   B. J. Aleck, "Thermal Stresses in a Rectangular Plate Clamped Along an Edge," *Journal of Applied Mechanics*, **16**, 118 (1949).

4.   J. W. Strutt, 3rd Baron Rayleigh, *The Theory of Sound*, (New York: Dover Publications, 1945) (First published, 1877).

5.   Lax, M. "The Effect of Radiation on the Vibrations of a Circular Diaphragm," *The Journal of the Acoustical Society of America*, **16**(1), 5 (1944).

6.   H. P. W. Gottlieb, and H. A. Aebischer, "Eigenfrequency Shifts of a Baffled Circular Membrane in a Fluid Medium," *Acustica*, **61**(4), 223 (1986).

7.   *Newport Catalog*, (Fountain View, CA: Newport Corporation, 1989).

APPENDIX

PROGRAM "CORRECTION"

*** Sample and Environmental Parameters

REAL DENAIR, C0, R, THICK, DENS, PI, ARLDEN, BETA

*** DENAIR = density of air
*** C0 = speed of sound in air
*** R = radius of membrane
*** THICK = thickness of coating
*** DENS = density of coating
*** PI = 3.1415
*** ARLDEN = Areal density of membrane
*** BETA = DENAIR*R/ARLDEN

*** Values associated with the 1 - 4th modes of vibration

REAL FAIR(4), OMEGA(4), K(4), ZERO(4), KTH(4)

*** Values which are read from the look-up tables m(k,n,i), and the b(n,i) values
*** calculated in the summation terms. RAT1 and RAT2 are the values for the
*** ratios of the frequency parameter in vacuum to that in air, quantity squared.

REAL M0(100,4,4), M(4,4), B(4,4), RAT1(4), RAT2(4,4)

*** Temporary storage variables

REAL BSUM, DUM(4,4), IDIOT(4)

*** Counters for reading from lookup table

INTEGER I, J, L

*** Truncated K(N) value and search counters

INTEGER KTRUNC(4), LOW, HIGH, MIDDLE

*** Subscript variables

INTEGER P, S, N

166

*** Truncated differences between iterations for m and b (to see how close value is
*** to previous iteration.

```
      INTEGER DIFFB(4,4), DIFFR(4)
```

*** Identify file TABLE as a character string

```
      CHARACTER*10 TABLE
```

*** Beginning of program code
*** Prompt user for experimental parameters

```
      WRITE(*,*) 'Density of air = '
      READ(*,20) DENAIR
      WRITE(*,*) 'Speed of Sound = '
      READ(*,25) C0
      WRITE(*,*) 'Radius of Membrane = '
      READ(*,30) R
      WRITE(*,*) 'Thickness of Membrane = '
      READ(*,30) THICK
      WRITE(*,*) 'Density of Membrane = '
      READ(*,25) DENS
20    FORMAT(F5.2)
25    FORMAT(F6.1)
30    FORMAT(E9.2)
```

*** Calculate Areal Density of Membrane and the Value of Beta.

```
      ARLDEN = DENS*THICK
```

```
      BETA = (DENAIR*R)/ARLDEN
```

*** Read in M(J,L,I) values from look-up tables in file = TABLE

```
      OPEN(3,FILE=TABLE)
      DO 70  L = 1,100
      DO   60 J = 1,4
      DO    50 I = 1,4
      READ(16,40) M0(L,J,I)
40    FORMAT(16F10.4)
50    CONTINUE
60    CONTINUE
70    CONTINUE
```

```
*** Prompt user to enter frequencies measured in air for FAIR(0,N), and
*** calculate associated frequency parameter, K(N) values then multiply K(N) by ten
*** and truncate to an integer value to use for matching with the K values in the look-
*** up tables.

      PI = 3.1415
      DO 220 N = 1,4
      WRITE(*,80) N
 80   FORMAT('Frequency in air for n = ',I1,':'F8.1)
      READ(*,80) FAIR(N)

      OMEGA(N) = FAIR(N)*2*PI

      K(N) = OMEGA(N)*R/C0

 90   KTRUNC(N) = (10.0*K(N))

*** Set the index, L, equal to the truncated value of K(N)

      L = KTRUNC(N)

*** For each N, (each time through the n = 1 - 4 loop), calculate the values of m(p,s)
*** and print them to the screen (*).
*** M(P,S) is calculated by interpolating between L and L+1.
*** P and S also vary from 1 to 4.

      DO 150  P = 1,4
      DO   140  S = 1,4
      L0 = FLOAT(L)
      M(P,S) = ABS(((L0 + 1)-(10.0*K(N)))*(M0(L,P,S) -
MO((L+1),P,S))+M0((L+1),P,S))
      WRITE(*,130)P,S,M(P,S)
130  FORMAT('M('I1','I1') ='F8.4)
140  CONTINUE
150  CONTINUE

*** Assign values to first four zeros of Bessel Functions

      ZERO(1) = 2.405
      ZERO(2) = 5.520
      ZERO(3) = 8.654
      ZERO(4) = 11.792

*** Initialize Summation Terms to zero
      B(P,N) = 0
      BSUM = 0
```

```
      IDIOT(N) = 0
      IF (P .NE. N) GOTO 160
160   DUM(P,N) = 0


***   Calculate the ratio of freq parameter in vacuum to that in air squared (1st time
***   through B(P,N) = 0 because it hasn't been calculated yet.

      RAT1(N) = 1 + BETA*(M(N,N)) +B(P,N)


***   Calculate the theoretical value for k (the frequency parameter in vacuum) from the
***   above ratio

      KTH(N) = RAT1(N)**0.5*K(N)


***   Calculate the values of (kTH(S)/K(N))^2 for S not equal to N.

      DO 190  S = 1,4
         WRITE(3,168)P,S
168   FORMAT(' P = 'I1' S  = 'I1)
      WRITE(3,169) P,N,B(P,N)
169   FORMAT(' B('I1','I1') = 'F8.4)
      WRITE(3,170)


IF (S .NE. N) GOTO 170
170   KTH(S) = KTH(N)*ZERO(S)/ZERO(N)
      RAT2(S,N) = (KTH(S)/K(N)**2


***
```

BIBLIOGRAPHY

Aleck, B. J. "Thermal Stresses in a Rectangular Plate Clamped Along an Edge." *Journal of Applied Mechanics* **16** 118 (1949).

Allen, M. G., M. Mehregany, R. T. Howe, and S. D. Senturia. "Microfabricated Structures for the in-situ Measurement of Residual Stress, Young's Modulus, and Ultimate Strain in Thin Films." *Applied Physics Letters* **51**(4) 241 (1987).

Allen, M. G. *Measurement of Adhesion and Mechanical Properties of Thin Films Using Microfabricated Structures*. Ph.D. Dissertation, Massachusetts Institute of Technology, (1989).

Allen, S. R. "Stress-coupling Phenomena in Anisotropic Fibres" *Polymer* **29**(6) 1091 (1988).

Arfken, G. "Bessel Functions." *Mathematical Methods for Physicists, 3rd ed..* Chapter 11. p. 572. New York: Academic Press, 1985.

Baum, G. A., D. C. Brennan, and C. C. Habeger. "Orthotropic Elastic Constants of Paper." *Tappi* **64**(8) 97 (1981).

Bauer, C. L. *The Determination of the Mechanical Behavior of Polyamic Acid/Polyimide Coatings*. Ph.D. Diss. University of Massachusetts. Amherst, MA, (1988).

Berg, E. M., D. C. Sun and J. H. Magill. "3-D Structure-Property Relationships in Rolltruded Polymers. Part 1: Mechanical Property Enhancement in Three Directions." *Polymer Engineering and Science* **29**(11) 715 (1989).

Berry, B. S., W. C. Pritchet, and C. E. Uzoh. "Dynamical Method for the Thermomechanical Study of Thin Membranes." *Journal of Vacuum Science Technology* **B7**(6) 1565 (1989).

Berry, B. S., and W. C. Pritchet. "Internal Stress and Internal Friction in Thin-Layer Microelectronic Materials." *Journal of Applied Physics* **67**(8) 3661 (1990).

Blakslee, O.L., D.G. Proctor, E. J. Seldin, G. B. Spence and T. Weng, "Elastic Constants of Compression-Annealed Pyrolytic Graphite." *Journal of Applied Physics* **41**(8) 3373 (1970).

Bourget, M. J. "Memoire sur le Mouvement Vibratoire des Membranes Circulaires." *Annales Scientifiques d'Ecole Normale Superieure.* **III** 55 (1866).

Buchwalter, P., private communication, IBM T. J. Watson Research Center, Yorktown Heights, NY, April 1991.

171

Campbell, D. S. "Mechanical Properties of Thin Films." *Handbook of Thin Film Technology.* Chapter 12. L. I. Maissel and R. Glang, Eds. New York: McGraw-Hill Book Co., 1970.

Chan, T. W. D. and L. J. Lee. "Analysis of Molecular Orientation and Internal Stress in Extruded Plastic Sheets." *Polymer Engineering and Science* 29(3) 163 (1989).

Chladni, E. F. F. *Die Akustik.* Leipzig: Breitkopf & Hartel, 1802.

Clebsch, R. F. A. *Theorie der Elasticität Fester Körper.* Leipzig: B. F. Teubner, 1862. from R. B. Lindsay. "The Story of Acoustics." *Journal of the Acoustical Society of America* 39(4) 629 (1966).

Croll, S. G. "Internal Stress in a Solvent-Cast Thermoplastic Coating." *Journal of Coatings Technology* 50 (638) 33 (1978).

Croll, S. G. "The Origin of Residual Internal Stress in Solvent-Cast Thermoplastic Coatings." *Journal of Applied Polymer Science* 23(3) 847 (1979).

Croll, S. G. "Internal Strain in Solvent-Cast Coatings." *Journal of Coatings Technology* 51(648) 64 (1979).

Cuthrell, R. E., F. P. Gerstle, Jr., and D. M. Mattox. "Measurement of Residual Stresses in Films of Unknown Elastic Modulus." *Review of Scientific Instruments* 60(6) 1018 (1989).

DeGreef-Sasst, A. private communication, Rogers Corporation, Rogers, CT, (1992).

Elsner, G. "Residual Stress and Thermal Expansion of Spun-on Polyimide Films." *Journal of Applied Polymer Science* 34(2) 815 (1987).

Engelstad, M. J., Chambless, D. A., Swinson, W. F., and Turner, J. L. "Hybrid Stress Analysis of Vibrating Plates Using Holographic Interferometry and Finite Elements," *Experimental Mechanics,* 27(1) 23 (1987).

Farris, R. J., R. Falabella and Y. D. Tsai. "The Influence of Vacuole Formation and Growth on the Mechanical Behavior of Polymers." *Durability of Macromolecular Materials.* ACS Symposium 95 Ed. R. K. Eby. American Chemical Society, (1979).

Faupel, F., C. H. Yang, S. T. Chen, and P. S. Ho. "Adhesion and Deformation of Metal/Polyimide Layered Structures." *Journal of Applied Physics* 65(5) 1911 (1991).

Flinn, P. A., D. S. Gardner, and W. D. Nix. "Measurement and Interpretation of Stress in Aluminum-Based Metallization as a Function of Thermal History." *Transactions of Electron Devices* ED-34(3) 689 (1987).

Gabor, D. "A New Microscopic Principle." *Nature* 161(4098) 777 (1948).

Gabor, D. "Holography, 1948-1971." *Science* **177**(4046) 299 (1972).

Galilei, G. *Dialogues Concerning Two New Sciences*. (1638). in *Acoustics: Historical and Philosophical Development*. Ed. R. B. Lindsay. Stroudsburg, PA: Dowden, Hutchinson and Ross, Inc., 1966.

Garza, R. and B. Sharpe. "Holography for Non-Contact Structural Analysis." *Sensors* September 1986.

Ghandhi, S. K. *VLSI Fabrication Principles: Silicon and Gallium Arsenide*. New York: John Wiley and Sons, (1983).

Gilbert, J. A., and J. W. Herrick, "Dual-beam Holographic Deflection Measurement." *Experimental Mechanics* **21**(9) 349 (1981).

Gilbert, J. A., and J. W. Herrick. "Holographic Displacement Analysis with Multimode-fiber Optics." *Experimental Mechanics* **21**(8) 316 (1981).

Gilbert, J. A., and G. A. Exner. "Holographic Displacement Analysis Using Image-plane Techniques." *Experimental Mechanics* **18**(10) 382 (1982).

Goldsmith, C., P. Geldermans, F. Bedetti, and G. A. Walker. "Measurement of Stresses Generated in Cured Polyimide Films." *Journal of Vacuum Science Technology* **A1**(2) 407 (1983).

Gottlieb, H. P. W. "Hearing the Shape of an Annular Drum." *Journal of the Australian Mathematical Society, B* **24**(4) 435 (1983).

Gottlieb, H. P. W., and H. A. Aebischer. "Eigenfrequency Shifts of a Baffled Circular Membrane in a Fluid Medium." *Acustica* **61**(4) 223 (1986).

Gruninger, M. F., B. R. Lawn, E. N. Farabaugh, J. B. Wachtman, Jr. "Measurement of Residual Stresses in Coatings on Brittle Substates by Indentation Fracture." *Journal of the American Ceramic Society* **70**(5) 344 (1987).

Handbook of Chemistry and Physics. 64th Edition. Ed. R. C. Weast. Boca Raton: CRC Press, 1983.

Handbook of Plastics and Elastomers. Ed. C. H. Harper. New York: McGraw-Hill Book Co., 1975.

Hearmon, R.F.S. *An Introduction to Applied Anisotropic Elasticity* London: Oxford University Press, (1961).

Heflinger, L. O., R. F. Wuerker, and R. E. Brooks. "Holographic Interferometry." *Journal of Applied Physics* **37**(2) 642 (1966).

Hess, M. S. "The End Problem for a Laminated Elastic Strip - II. Differential Expansion Stresses." *Journal of Composite Materials* 3(10) 630 (1969).

Hoffman, R. W. "The Mechanical Properties of Thin Condensed Films." *Physics of Thin Films: Advances in Research and Development*, Vol. 3, p. 211 G. Haas, and R. Thun, Eds. New York: Academic Press, 1966.

Huntington, H. B. "The Elastic Constants of Crystals." *Solid State Physics: Advances in Research and Applications* vol. 7. Ed. F. Seitz and D. Turnbull. New York: Academic Press, Inc., (1958).

Ito, A., and T. Kashiwagi. "Measurement Technique for Determining the Temperature Distribution in a Transparent Solid Using Holographic Interferometry." *Applied Optics* 26(5) 954 (1987).

Jagota, A., and C. Y. Hui, "Mechanics of Sintering Thin Films - I. Formulation and Analytical Results." *Mechanics of Materials* 9 107 (1990).

Jennings, R. M., and R. J. Farris. "Analysis of Stresses Arising During the Processing of Polymeric Films on Tentering Frames." in press *Polymer Engineering and Science* (1992).

Kak, M. "Can One Hear the Shape of a Drum?" *American Mathematics Monthly* 73, 1 (1966).

Kapton Polyimide Film: Summary of Properties. Wilmington: DuPont Company. 1986.

Karnezos, M. "Effects of Stress on the Stability of X-ray Masks." *Journal of Vacuum Science and Technology* B4(1) 226 (1986).

Kaufman, G. H., and C. M. Vest. "Thermal Waves Visualized by Holographic Interferometry." *Applied Optics* 26(14) 2799 (1987).

Kimoto, M., I. Nagata, A. Minowa, K. Moriwaki, and T. Watanabe. "Evaluation of Disbondings and Measurement of Poisson's Ratio for Plastic Composites Using Holographic Interferometry." *Journal of Applied Polymer Science* 40(7) 1085 (1990).

Klokholm, E. "Delamination and Fracture of Thin Films." *IBM Journal of Research and Development* 31(5) 585 (1987).

Lax, M. "The Effect of Radiation on the Vibrations of a Circular Diaphragm." *The Journal of the Acoustical Society of America* 16(1) 5 (1944).

Ledbetter, H.M. "Orthotropic Elastic Stiffness of a Boron-Aluminum Composite." *Journal of Applied Physics*, 50(12) 8247 (1979).

Leissa, A. W. *Vibration of Thin Plates*. NASA Publication SP-160, Washington, D. C.: 1969.

Leith, E. N., and Upatnieks, J. "Photography by Laser," *Scientific American*, **212**(6) 24 (1965).

Leitzau, C. personal communication (1991).

Lekhnitskii, S. G. *Theory of Elasticity of an Anisotropic Body* English translation, Moscow: MIR Publishers, (1981).

Lewis, C. F. "What's Wrong in This Picture?" *Materials Engineering* **106**(1) 49 (1989).

Lin, P and Senturia, S. "The In-situ Measurement of Biaxial Modulus and Residual Stress of Multi-Layer Polymeric Thin Films." *Thin Films: Stresses and Mechanical Properties II*, Philadelphia: Materials Research Society, 1990.

Lindsay, R. B. Preface. *The Theory of Sound.* by J. W. Strutt, 3rd Baron Rayleigh. New York: Dover Publications, 1945.

Lindsay, R. B. *Acoustics: Historical and Philosophical Development.* Stroudsburg, PA: Dowden, Hutchinson and Ross, Inc., 1966.

Maden, M. A., Jagota, A., Farris, R. J., Tong, Q. and Mazur, S. "Vibrational Technique for Stress Measurement in Films - 1. Ideal Membrane Behavior," Submitted for publication, *Journal of Materials Research*, (1991).

Maden, M. A. and R. J. Farris. "Stress Measurement in Spin Coated Polyimide Films Using Time Average Holographic Interferometry." *Electronic Packaging Materials Science* Materials Research Society Symposium Proceedings. Pittsburgh, PA: Materials Research Society, (1989).

Maden, M.A., Kun Tong, and R. J. Farris, "Measurement of Stresses in Thin Films Using Holographic Interferometry: Dependence on Atmospheric Conditions." *Thin Films: Stresses and Mechanical Properties II* Materials Research Society Symposium Proceedings, vol. 188. Pittsburgh, PA: Materials Research Society, (1990).

Maden, M. A. and R. J. Farris. "Stress Analysis Of Thin Polyimide Films Using Holographic Interferometry." *Journal of Experimental Mechanics* Accepted for Publication (1991).

Mann, R. W., Baum, G. A. and Habeger, C.C. "Determination of All Nine Orthotropic Elastic Constants for Machine-Made Paper." *Tappi* 63(2) (1980).

Newport Catalog, Fountain View, CA: Newport Corporation, (1989).

Nkansah, M. A., and K. E. Evans. "Thermal Stresses in Multilayer Optical Storage Media." *Journal of Applied Physics* **66**(1) 50 (1989).

Noyan, I. C., and L. T. Nguyen. "Residual Stresses in Polymeric Passivation and Encapsulation Materials." *Polymer Engineering and Science* **28**(16) 1026 (1988).

O'Regan, R., and T. D. Dudderar. "A New Holographic Interferometer for Stress Analysis." *Experimental Mechanics* **9**(6) 241 (1971).

Osaki, S. "Explanation of Orientation Patterns Determined for Sheet Materials by Means of Microwaves." *Journal of Applied Physics* **67**(10) 6513 (1990).

Pan, J. T. and S. Poon. "Film Stress in High Density Thin Film Interconnects." *Electronic Packaging Materials Science* Materials Research Society Symposium Proceedings Pittsburgh, PA: Materials Research Society, (1989).

Parker, R. J., and D. G. Jones. "Holography in an Industrial Environment." *Optical Engineering* **27**(1) 55 (1988).

Pennington, K. S. "Advances in Holography." *Scientific American* **218**(2) 40 (1968).

Perera, D. Y. "Internal Stress in Latex Coatings." *Journal of Coatings Technology* **56**(716) 111 (1984).

Perera, D. Y., and D. V. Eynde. "Moisture and Temperature Induced Stresses (Hygrothermal Stresses) in Organic Coatings." *Journal of Coatings Technology.* **59**(748) 55 (1987).

Pines, B. Ya., V. M. Andronov, and V. B. Rabukhin. "Device For Investigating the Mechanical Properties of Whiskers and Thin Films." *Zavodskaya Laboratoriya* **35**(6) 741 (1969).

Pirodda, L. "Conjugate Wave Holographic Interferometry for the Measurement of In-plane Deformations," *Applied Optics,* **28**(10) 1842 (1989).

Plepys, A. *A Study of the Evolution of Residual Stresses in Three Dimensionally Constrained Epoxy Resins.* Ph.D. Diss. University of Massachusetts. (1992).

Poisson, S. D. "Mémoire sur L'équilibre et le Mouvement des Corps Élastiques." *Mémoires de L'Academie de la Royale Institute des Sciences du France.* **8** 357 (1829), from R. B. Lindsay, "The Story of Acoustics." *Journal of the Acoustical Society of America,* **39**(4) 629 (1966).

Popov, E. P. *Introduction to the Mechanics of Solids* Englewood Cliffs, NJ: Prentice-Hall, Inc., (1968).

Powell, R. L., and K. A. Stetson. "Interferometric Vibration Ananlysis by Wavefront Reconstruction." *Journal of the Optical Society of America* **55**(12) 1593 (1965).

Protter, M. H. "Can One Hear the Shape of a Drum?: Revisited." *SIAM Review* **29**(2) 185 (1987).

Pryputniewicz, R. J. "Time Average Holography in Vibration Analysis." *Optical Engineering* **24**(5) 843 (1985).

Rehwald, W., A. Vonlanthen, and W. Meyer. "Single Crystal 2,4-Hexadiynylene-Bis(p-Toluenesulfonate): Elastic Properties and Phase Transitions in the Monomer and Polymer." *Physica Status Solidi (A)* **75**(1) 219 (1983).

Röll, K. "Analysis of Stress and Strain Distribution in Thin Films and Substrates," *Journal of Applied Physics,* **47**(7) 3224 (1976).

Sackinger, S. T. *The Determination of Swelling Stresses in Polyimide Films.* Ph. D. Diss. University of Massachusetts. (1990).

Sanford, R. J. "Differential Stress-Holo-Interferometry." *Experimental Mechanics* **11**(8) 330 (1973).

Sanford, R. J. "Photoelastic Holography - A Modern Tool for Stress Analysis." *Experimental Mechanics* **20**(12) 427 (1980)

Sato, K. "The Internal Stress of Coating Films." *Progress in Organic Coatings* **8**(2) 143 (1980).

Sciammarella, C. A., and Gilbert, J. A. "A Holographic-moiré Technique to Obtain Separate Patterns for Components of Displacement." *Experimental Mechanics* **14**(6) 215 (1976).

Sharpe, B. "Fringe Benefits of Hologram Views." *Industrial Photography* **36**(8) A28 (1987).

Soane, D. S. "Stresses In Packaged Semiconductor Devices." *Solid State Technology* **32**(5) 165 (1989).

Stewartson, K., and R. T. Waechter. "On Hearing the Shape of a Drum: Further Results." *Proceedings of the Cambridge Philosophical Society.* **69**(2) 353 (1971).

Strutt, J. W., 3rd Baron Rayleigh. *The Theory of Sound.* New York: Dover Publications, 1945. London: 1867.

Suhir, E. "An Approximate Analysis of Stresses in Multilayered Elastic Thin Films." *Journal of Applied Mechanics* **55**(3) 143 (1988).

Sun, D. C., E. M. Berg and J. H. Magill. "3-D Structure-Property Relationships in Rolltruded Polymers. Part 2: Anisotropic Yielding and Deformation in Triaxially Oriented Polymers." *Polymer Engineering and Science* **30**(11) 635 (1990).

Taylor, B. "De Motu Nervi Tensi." *Philosophical Transactions of the Royal Society.* **28**, 11 (1713). in *Acoustics: Historical and Philosophical Development.* Ed. R. B. Lindsay. Stroudsburg, PA: Dowden, Hutchinson and Ross, Inc., 1966.

Taylor, C. E. "Holography." *Experimental Mechanics* **19**(9) 339 (1979).

Taylor, J. F., Jennings, R. M., and Farris, R. J. "A Deflection Technique for the Determination of Residual Stresses in Coatings." in preparation (1992).

Taylor, M. E. "Estimate on the Fundamental Frequency of a Drum." *Duke Mathematical Journal* **46**(2) 447 (1979).

Tentori, D., and M. Celaya. "Film Deposit Assessment with Hologram Interferometry," *Applied Optics* **25**(16) 2707 (1986).

Tiitto, S. "Magnetoelastic Testing of Biaxial Stresses." *Experimental Techniques* **15**(1) 17 (1991).

Timoshenko, S. "Analysis of Bi-Metal Thermostats." *Journal of the Optical Society of America* **11**(9) 233 (1925).

Tong, Q. K., and R. J. Farris. "Measurement of Two-Dimensional Stresses in Thin Polymer Films Using Holographic Interferometry." *submitted for publication*: 1990.

Tong, Q. K., M. A. Maden, A. Jagota and R. J. Farris, "Vibrational Techniques for Stress Measurement in Films - 2. Extensions and Complicating Effects," *Journal of Materials Research,* submitted for publication (1991).

Tong, Q. K. *Characterization of Processing Stress and Structure-Property Relationships on a Polyacrylate Photoresist Coating.* Ph.D. diss. University of Massachusetts. (1992).

Trolinger, J. D. "Outlook for Holography Strong as Applications Achieve Success." *Laser Focus/Electro-Optics* **22**(7) 82 (1986).

Tsai, S.W. and H.T. Hahn. *Introduction to Composite Materials* Wesport, CT: Technomic (1980).

Upilex Polyimide Films: Technical Data. Wilmington: ICI Americas, Inc., (1989).

Voight, W. *Lehrbuch der Kristallphysik* Leipzig: Teubner, (1928).

Wiley, R. IBM Endicott. Endicott, NY. telephone conversation, (1990).

Williams, D. and J. Spangler, *Physics for Science and Engineering*. New York: D. Van Nostrand Company, (1981).

Wilson, A. D., and D. H. Strope. "Time-Average Holographic Interferometry of a Circular Plate Vibrating Simultaneously in Two Rationally Related Modes." *Journal of the Optical Society of America* **60**(9) 1162 (1970).

Yamaguchi, I., and H. Saito. "Application of Holographic Interferometry to the Measurement of Poisson's Ratio." *Japanese Journal of Applied Physics* **8**(6) 768 (1969).

Yaseen M. and H. E. Ashton. "Effect of Free Film Preparation Method on Physical Properties of Organic Coatings." *Journal of Coatings Technology* **49**(629) 50 (1977).

Young, R. J. "Polymer Single Crystal Fibres." *Developments in Oriented Polymers II*. Ed. E. M. Ward. New York: Elsevier Applied Science Publishers, 1987.

Yu, Y. H., and J. K. Kittleson. "Measuring Flow by Holographic Interferometry." *NASA Technical Briefs* July/August, 60 (1988).